

UNIVERSITA' DI PISA



CORSO DI LAUREA MAGISTRALE IN CHIMICA INDUSTRIALE

Curriculum Materiali

CLASSE: LM 71 (Scienze e Tecnologie Chimiche)

Valency effects in the formation of supramolecular nanoparticles

Relatori:

Dott. Andrea Pucci

Prof. Jurriaan Huskens

Controrelatore:

Prof. Valter Castelvetro

Candidato:

Eugenio Staltari Ferraro

Anno Accademico: 2013/2014

*To my parents,
my family
and Laura*

Abstract

Supramolecular materials hold great promise as they allow the development of a versatile toolbox combined with properties such as responsiveness, exchange, uptake and delivery, size control, and many others. Supramolecular nanoparticles (SNPs) are of huge interest because of their high potential for biomedical applications, for example as in-vivo imaging and drug delivery vehicles. Here, SNPs based on the ternary-complex formation among cucurbit[8]uril (CB[8]), a methyl viologen polyethylene imine (MV-PEI) and novel multivalent naphthol-functionalized moieties, were assembled and the influence of the multivalency over the size-tunability was studied.

A bivalent PEG-based stopper and a more intense grafted PAMAM dendrimer, named Np₂-PEG and Np₁₆-PAMAM, were synthesized, functionalized with the naphthol moieties and then separately employed as recognition units in the nanoparticles self-assembling. The effects of their greater valency over the SNPs size-tunability were investigated through Dynamic Light Scattering (DLS) and Scanning Electron Microscopy (SEM). Particles assembled with the bivalent stopper revealed that the increased valency of the stopper induces the formation of more stable ternary complexes. Hence, the dynamic disassembly and reassembly processes, required for the formation of well-defined and size-tunable SNPs, are disfavored unless the temperature increases and well-defined nanoparticles are shaped. In contrast, the studies about the increased valency in the core of the nanoparticles showed that by respecting the 1:1:1 ratio among MV²⁺:CB[8]:Np-PEG/Np₁₆-PAMAM, required for the formation of the ternary complex, the amount of the stopper is not enough to control the intermolecular network formation caused by the more intense grafted dendrimer. However, a control over the size of the SNPs was possible when the ratio among the supramolecular recognition units was changed from the traditional 1:1:1 to the newly 1:1:1:X, where X represents the amount of Np₁₆-PAMAM.

Contents

Abstract	3
1 Introduction	6
1.1 Supramolecular chemistry.....	6
1.2 Multivalency and its working principles	10
1.3 Cucurbit[n]uril as supramolecular hosts.....	15
1.4 Charge transfer interactions: driving force for CB[8]-based supramolecular nanoparticles formation.....	17
1.5 Size-controlled supramolecular nanoparticles as drug-delivery vectors.....	18
2 Aim of the project	24
3 Experimental	26
3.1 Chemicals	26
3.2 Equipment.....	26
3.3 Synthesis of the molecules	27
3.3.1 Synthesis of N-(3,5-bis(2-(2-(2-(naphthalen-2-yloxy)ethoxy)ethoxy)ethoxy)benzyl)-3-(methoxypolyethylene glycol)propanamide (Np ₂ -PEG)	27
3.3.2 Synthesis of Np ₁₆ -PAMAM	31
3.4 Supramolecular Nanoparticles assembling	32
3.4.1 Size tunable supramolecular nanoparticles assembled with Np ₂ -PEG.....	32
3.4.2 Size tunable supramolecular nanoparticles assembled with Np ₁₆ -PAMAM	32
4 Results and discussion	34
4.1 Synthesis of Np ₂ -PEG.....	34
4.1.1 Synthesis of 2-(2-(2-(naphthalen-2-yloxy)ethoxy)ethoxy)ethanol	35
4.1.2 Synthesis of 2-(2-(2-(2-bromoethoxy)ethoxy)ethoxy)naphthalene	36
4.1.3 Synthesis of 3,5-bis(2-(2-(2-(naphthalen-2-yloxy)ethoxy)ethoxy)ethoxy)benzotrile.	38
4.1.4 Synthesis of (3,5-bis(2-(2-(2-(naphthalen-2-yloxy)ethoxy)ethoxy)ethoxy)phenyl)methanamine.....	39
4.1.5 N-(3,5-bis(2-(2-(2-(naphthalen-2-yloxy)ethoxy)ethoxy)ethoxy)benzyl)-3-(methoxypolyethylene glycol)propanamide (Np ₂ -PEG)	41
4.2 Synthesis of Np ₁₆ -PAMAM	44
4.3 Preparation of supramolecular nanoparticles through the assembling with the multivalent Np ₂ -PEG.....	46

4.3.1	Size control given by the relative concentration of Np ₂ -PEG.....	48
4.3.2	Size control obtainable by altering the external condition	51
4.3.3	Influence of the impurities present in the Np ₂ -PEG on the nanoparticles formation ...	56
4.4	Supramolecular nanoparticles assembled with Np ₁₆ -PAMAM.....	59
4.4.1	Size control through the relative concentration of Np ₁₆ -PAMAM	60
4.4.2	Size control by adjusting the ratio among the supramolecular recognition units.....	64
5	CONCLUSIONS AND OUTLOOK.....	73
	REFERENCES	76

1 Introduction

1.1 Supramolecular chemistry

Supramolecular chemistry was defined by Lehn as the “chemistry beyond the molecules”.¹ It examines the non-covalent inter and/or intramolecular interactions between two or more molecules which lead to the formation of stable and well-defined structures. This new branch of chemistry got tremendous attendance in recent years and is inspired by the formation of nanostructured systems in nature.

Self-assembly is an important procedure, used by supramolecular chemists, to obtain complex structures by simplifying the synthetic procedure.² Whitesides defined the self-assembly as “the spontaneous association of molecules under equilibrium condition into stable, structurally well-defined aggregates joined by non-covalent bonds”.³ These well-defined structures are obtained by carefully design the binding sites present on the supramolecular building blocks. The key-point of the self-assembling lies on the recognition and interaction of two or more complementary binding sites. The interactions between these complementary binding sites are governed by thermodynamics. Thanks to the non-covalent bonds, supramolecular building blocks are able to assemble and disassemble, thus forming stable yet reversible supramolecular structures. The reversibility leads to systems able to self-correct errors eventually present in the self-assembled structure³ and this is possible because molecules tend to adjust their own position in order to find a thermodynamic minimum.

One of the most famous biological self-assembled supramolecular system is certainly DNA. The typical double-helix structure of DNA originates from the secondary interactions between the purine and pyrimidine bases present on the individual filament. This highly organized structure is obtained through the triple hydrogen bond formed between guanine (G) and cytosine (C) and the double hydrogen bond of the adenine (A) with the thymine (T) (figure 1.1), which held together the two filaments of the DNA. These bases also present a high selectivity in the formation of complexes. In fact, guanine selectively interacts with cytosine and not with thymine because the complex G-C is much more thermodynamically stable than the G-T complex, which gives the formation of a single hydrogen bond instead of three.

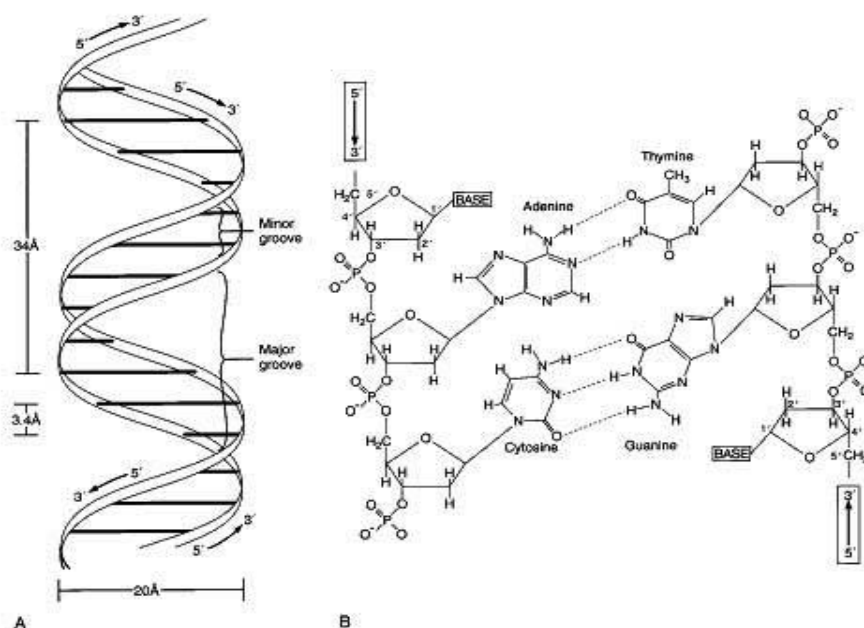


Figure 1.1: a) DNA double-helix structure. b) purine and pyrimidine bases interaction through hydrogen bond formation.

The biological example earlier reported demonstrates how it is possible to obtain structures with highly defined geometries while using simple hydrogen bonds. While the highly defined structure of DNA is just based on simple hydrogen bonding interactions, supramolecular chemistry offer a full toolbox of different interactions to assemble supramolecular structures. Therefore, an overview over the main types of the non-covalent interactions is given below.

These non-covalent bonds range from weak Van der Waals interactions (few $\text{kJ}\cdot\text{mol}^{-1}$) to stronger ion-ion bonds (hundreds of $\text{kJ}\cdot\text{mol}^{-1}$) and they can be divided into categories. Van der Waals interactions ($0.1\text{-}10 \text{ kJ}\cdot\text{mol}^{-1}$) involve both polar and non-polar molecules and they act within a short range through the polarization of an electron cloud by the proximity of an adjacent nucleus, resulting in a weak electrostatic interaction.⁴ Other important non-covalent interactions are those involving the π -systems. These intermolecular interactions are achieved through the overlap of the π -orbitals in π -conjugated systems.⁵ Another interesting system originates from the interaction between a cation and a π -system. The aromatic rings, such as benzene, present a quadrupole moment where a σ -scaffold, partially positively charged, is surrounded above and below by a π -cloud. Consequently, the cationic species may interact with this cloud forming complexes with binding energy in the order of $5\text{-}80 \text{ kJ}\cdot\text{mol}^{-1}$.⁶ Another important interaction is that between π -

donors and π -acceptors aromatic systems. The electron-rich aromatic compound donates its electrons to the electron-withdrawing thus forming a complex particularly stable called “charge-transfer complex”.⁷ Other non-covalent interactions certainly important, especially in biological systems, are hydrogen bonds. In supramolecular chemistry they play an important role as they are very directional bonds. They allow a control over the geometry of the complex through a careful design of the interacting molecules. This bond occurs when the hydrogen binds to a highly electronegative atom like nitrogen, oxygen or fluorine. Depending on the distance at which it is located, the hydrogen bond can be strong, moderate or weak.⁴ Strong hydrogen bonds have binding energy in the range of 60-120 $\text{kJ}\cdot\text{mol}^{-1}$ and a heteroatom-heteroatom distances between 2.2 and 2.4 Å. Moderate hydrogen bond has energy between 15 and 60 $\text{kJ}\cdot\text{mol}^{-1}$ and distance between the heteroatoms of 2.5-3.2 Å. Whereas, weak hydrogen bond has a distance between donor and acceptor of up to 4 Å therefore binding energy drop to $< 12 \text{ kJ}\cdot\text{mol}^{-1}$.⁴

The strongest non-covalent interactions are the ion-ion interaction. It occur between charged particles and presents a binding energy in the range of 100 to 350 $\text{kJ}\cdot\text{mol}^{-1}$.⁴ Another strong bond, but weaker than ion-ion, is the ion-dipole interaction. This non covalent bond takes place when charged molecules interact. It presents a binding energy in the range between 50-200 $\text{kJ}\cdot\text{mol}^{-1}$.⁴ Finally, a particular case which recently has taken lot of attention, especially in host-guest chemistry, is represented by the hydrophobic interactions. They are of fundamental importance for the formation of micelles and membranes. These interactions are based on the incompatibility of polar/nonpolar molecule to stay in a nonpolar/polar solvents which tend to minimize the energetically unfavorable surface.⁸ Their binding energy has been estimated to be about 0.2 $\text{kJ}\cdot\text{mol}^{-1}$ per Å².⁹

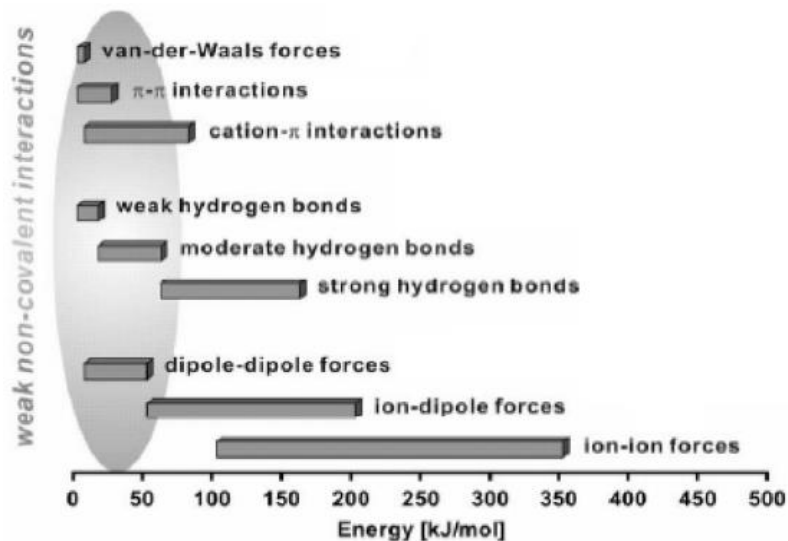


Figure 1.2: Energies of the typical non-covalent interactions.

Plenty impressive supramolecular structures were obtained through the application of these non-covalent bonds. One of these was obtained by Loeb and his coworker.¹⁰ They showed the synthesis of a [2]pseudorotaxanes by self-assembly of a bispyridinium salt (1,2-bis(pyridinium)ethanedication) in the presence of a crown ether (dibenzo-24-crown-8, figure 1.3a). The X-ray structure of the pseudorotaxanes revealed that the complex is stabilized by eight $N^+ \cdots O$ bonds and eight $C-H \cdots O$ hydrogen bonds. In contrast, 1H -NMR revealed that in solution π -stacking is also present between the electron rich catechol rings of the crown ether and the electron poor aromatic rings of the bispyridinium salt. The multiplicity of the non-covalent bonds lead to a very stable complexes with an association constant up to $1200 M^{-1}$.¹⁰

Another supramolecular system which presents some interesting non-covalent bonds is obtained by the interaction between cyclodextrins (CD) and non-polar molecules. Bonds present in these CD-based complexes are also of interest as they inspired the formation of the non-covalent interactions used for the assembling of the supramolecular system described in this thesis. In these complexes a guest molecule is hold inside the CD cavity (host) by a combination of non-covalent bonds. Depending on the guest molecule, the driving forces for the formation of inclusion complexes may be the hydrophobic interactions,¹¹ electrostatic interactions, Van der Waals interactions and/or hydrogen-bond formation¹² between the host and the guest. Moreover, if these host-guest complexes are assembled in water the release of the water from the cavity gives an overall entropy gain.⁸ The combination of these bonds lead to the formation of stable complexes, for example the complex between 1-adamantanecarboxylic acid and β -CD presents association constants of $501 M^{-1}$.¹³

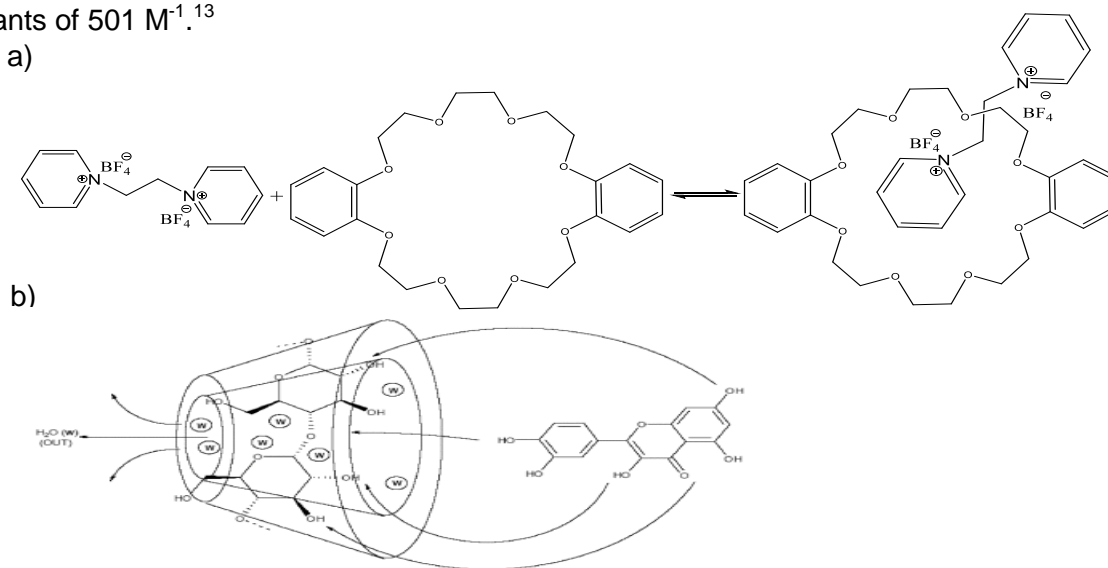


Figure 1.3: a) formation of [2]pseudorotaxanes by the self-assembly of a bispyridinium salt (1,2-bis(pyridinium)ethanedication) and dibenzo-24-crown-8 (DB24C8). b) Inclusion complex formation between β -cyclodextrine and quercetin.¹⁴

1.2 Multivalency and its working principles

Multivalency plays an important role in the molecular self-assembly. Multivalency describes the binding between two or more molecules through multiple interactions of complementary groups present on these molecules. This concept has been a topic of extensive investigation over the last decades, especially in the field of biochemistry, since it regulates many biological processes. One of these processes might be, for instance, the adhesion of a virus on the cell surface (Figure 1.4).¹¹

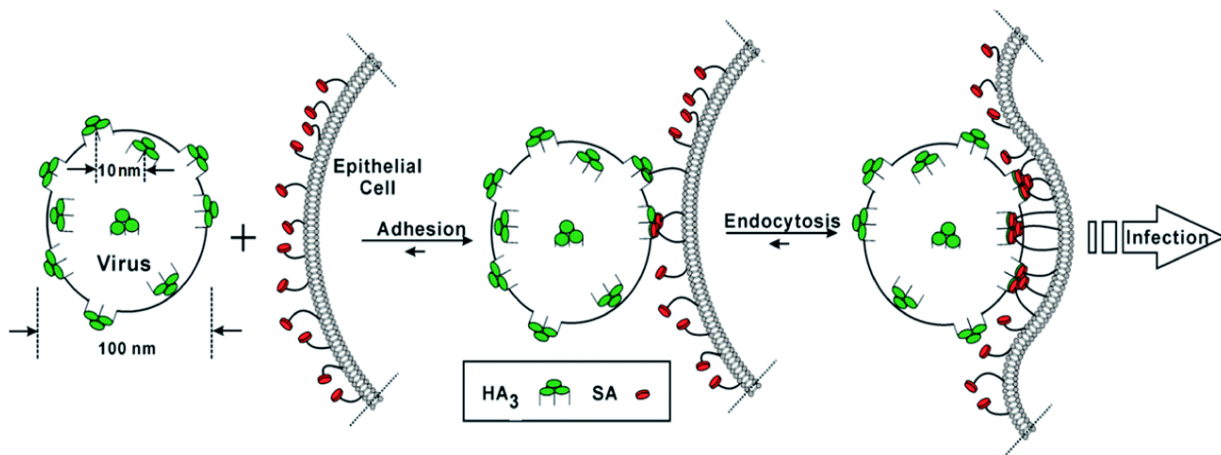


Figure 1.4: Virus adhesion over cell surface through multivalent interaction between the trimeric hemmagglutinin (HA₃) groups present on the virus with the salicylic acid (SA) of the cell.¹⁵

Before proceeding with the illustration of the rules which govern multivalency, it is important to understand what the valency of a molecule is. Reinhoudt *et al.* defined the valency of an entity as "the number of separate connections of the same kind that it can form through host-guest interactions with entities bearing the complementary functionality".¹⁶ These multivalent hosts and guests are able to interact in different ways. In fact, binding may occur in *intra* or *intermolecular* ways. Well-defined supramolecular structures may arise when multivalent interactions take place in an intramolecular fashion. On the contrary, if intermolecular binding are favored the formation of larger aggregates is preferred. The achieving of multivalent intramolecular interactions is possible through the combination of two important features. One of these is related to the architecture of the multivalent self-recognizing molecules. It was proved that the geometry of these molecules has a strong influence on the mode of binding.¹⁷ Structures which present high bond directionality and mobility of the interacting functionalities are inclined to the formation of intramolecular multivalent interaction, like supramolecular assembled monolayers.¹⁶ Whereas intermolecular binding are favored by small, three-dimensional and relatively rigid structures like dendrimers.¹⁸ This is

understandable by taking into account the molecular pre-organization.¹⁹ The first stage of an host-guest interaction regards the activation and rearrangement stage in which the binding sites, present on the host, pre-organized for the interaction with the guest. This stage is thermodynamically unfavorable, so energy is required for the rearrangement. However, when the binding between the host and the guest moieties occurs energy is released by the enthalpy of binding. If the energy released exceed the energy paid for the rearrangement, complex formation is enabled. The easier the pre-organization step between the host and the guest, the higher the stability of such complexes.¹⁹ Therefore the mobility of the binding sites is of fundamental importance as rigid structures require high energies for their preorganization to give adequate architectures for the formation of intramolecular interactions.

The other fundamental feature, which was marginally introduced above, regards the thermodynamic aspects of the multivalent complex formation. These aspects may be described by using a general approach based on the Gibbs free energies of multivalent binding (ΔG_{multi}) as shown in equation 1:

$$\Delta G_{multi} = n\Delta G_{mono} + \Delta G_{interaction} \quad \text{Equation 1}$$

Where ΔG_{mono} is the standard free energy for the monovalent interaction, n is the valency of the complex and $\Delta G_{interaction}$ corresponds to the energetic balance between favorable and unfavorable interactions.²⁰

The Gibbs free energy can also be written as a function of the binding constant K_{multi} (equation 2). It represents the strength of multivalent interactions of a multivalent complex.

$$\Delta G_{multi} = -RT \ln K_{multi} \quad \text{Equation 2}$$

The contributions of the enthalpy and the entropy to the Gibbs free energy have been described by Whitesides *et al*, (equation 3).²¹

$$\Delta G_{multi} = \Delta H_{multi} - T\Delta S_{multi} \quad \text{Equation 3}$$

They assert that the variation of the enthalpy for a multivalent binding may be approximate to the sum of the enthalpy for a monovalent binding, e.g. a divalent binding is expected to have an enthalpy of binding that is twice of a monovalent one. However, they also take into account that the interactions around the active site may alter this sum. Two cases are considered. The first involves

an enhancement of the enthalpy of binding. In some circumstances the binding of a first ligand may favor the binding of the following ligands by altering the architecture of the receptor. This is the case of the hemoglobin when binds oxygen, or the pentameric cholera toxin when binds to the cell surface.²² The second case regards a diminishing of the enthalpy of binding. Once again, it is related to the architecture of the two interacting entities. In fact, if the bond of the first ligand interferes somehow with the next binding events, the enthalpy of the multivalent interaction is less favorable than that expected for n monovalent interactions.²¹

They also affirm that entropy is the driving force of the multivalent binding.^{20, 21} They define the entropy of binding for a multivalent system as the sum of the contributions from the changing in translational, rotational and conformational entropy (equation 4).

$$\Delta S_{multi} = \Delta S_{Trans}^{Multi} + \Delta S_{Rot}^{Multi} + \Delta S_{Conf}^{Multi} \quad \text{Equation 4}$$

In equation 4 ΔS_{Trans}^{Multi} represents the translational entropy, which symbolizes the freedom of an entity to translate through the space. ΔS_{Rot}^{Multi} describes the rotational entropy of an entity, and it represents the freedom of the entity to rotate around its three main axes. The other important parameter is ΔS_{Conf}^{Multi} . It expresses the cost that needs to be paid to re-shape an entity. In this approach the mode of binding is mainly determined by the entropy, in particular by the conformational entropy. When the sum of the translational and rotational entropy cost gained exceeds the cost of the conformational entropy intramolecular binding are achievable. However, when the conformational costs exceeds the translational and rotational cost the formation of intermolecular binding are favoured. If the conformational cost is equal to the sum of the translational and rotational entropy there is no preference between an intramolecular or intermolecular pathways.²¹

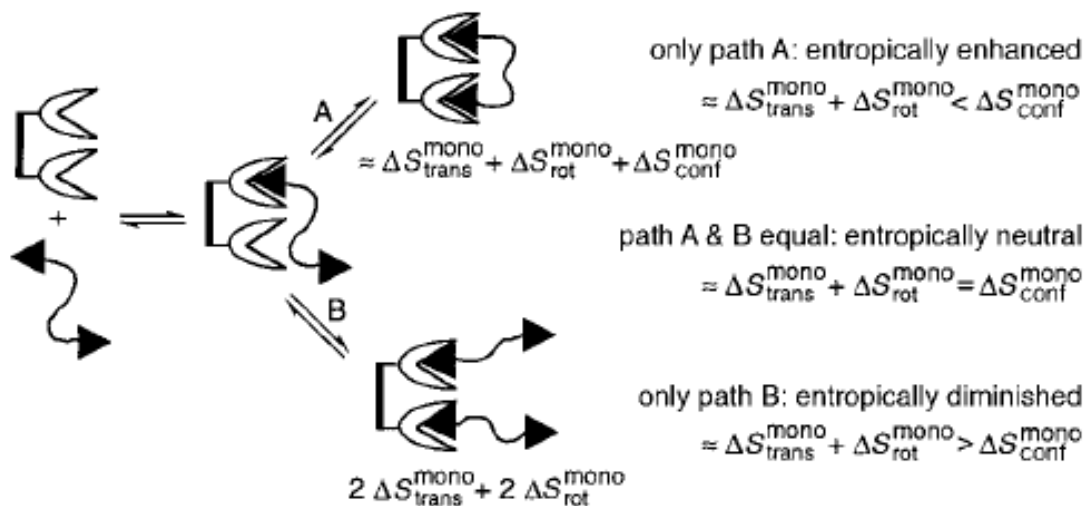


Figure 1.5: Relationship among translational, rotational and conformational entropy for a divalent system¹⁹

This approach envisages that the entropy associated to the formation of multivalent binding is more favorable than that associated to multiples monovalent binding, which is in discordance with the large negatively entropies usually found for multivalent interaction, therefore it should not be taken too seriously¹⁶. An alternative approach which allows a more understandable relation between the length and flexibility of the linker and the energy of binding is given by the effective concentration (C_{eff}). Reinhoudt and Huskens defined C_{eff} as the "probability of interaction between two reactive or complementary interlinked entities and symbolizes a physically real concentration of one of the reacting or interacting functionalities as experienced by its complementary counterpart."¹⁶ Formally it is expressed as shown in equation 5:

$$K_{\text{multi}} = \gamma (K_{\text{mono}})^n (C_{\text{eff}})^{n-1} \quad \text{Equation 5}$$

Where γ represents all the statistical factors determined by the number of the possible association/dissociation pathways in subsequent interaction steps.

The first interaction of a multivalent guest with a multivalent host modifies the guest concentration noticed by the adjacent free host site. Therefore, the effective concentration gives rise to a concentration-dependent binding mode. When the effective concentration of the guest is higher than its concentration in solution, intramolecular binding are favoured. However, when the C_{eff} is lower than the concentration of the guest in solution intermolecular connections can take place.

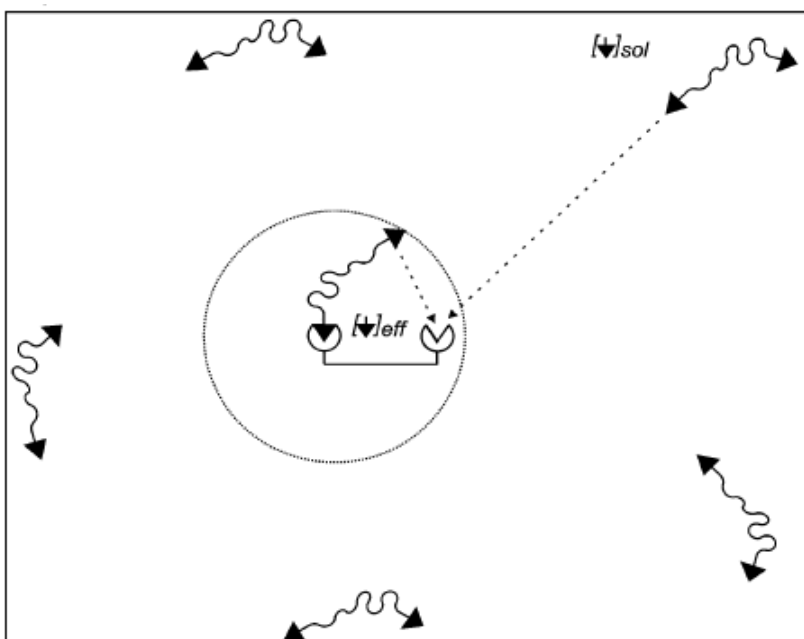


Figure 1.6: Schematic representation of effective concentration. In this scheme a free host site notices an effective concentration (C_{eff}) of the guest which is higher in comparison to the concentration of the guest in solution. Therefore, intramolecular binding are favored.¹⁶

C_{eff} is difficult to determine, as it is based on concentration calculated from physical geometries of the complex, like the rigidity of the spacer and its length. Effective molarity (EM)²³ is conceptually similar to effective concentration and it is commonly used for the estimation of the intramolecular efficiency. It represents the ratio between intra and intermolecular binding association constants (equation 6).¹⁶

$$EM = \left[\frac{K_{\text{multi}}}{\gamma K_{\text{mono}}} \right]^{\frac{n}{n-1}} = \frac{K_{\text{intra}}}{K_{\text{inter}}} \quad \text{Equation 6}$$

EM is more utilised than C_{eff} because it could be determined experimentally, as shown by Hunter *et al.*^{24, 25} The knowledge of the EM value is of great interest for the estimation of multivalency effects. In fact, high values of EM come out when intramolecular processes are favored over intermolecular one.

1.3 Cucurbit[n]uril as supramolecular hosts.

The class of macrocyclic glycoluril compounds was firstly introduced by Behrend *et al.* in 1905.²⁶ They noted that the condensation of glycoluril (acetyleneurea) with formaldehyde, in concentrated HCl, led to the formation of an amorphous, insoluble, polymeric substance. They also saw that, after recrystallization of this substance with concentrated H₂SO₄ followed by a dilution in water, a crystalline compound was formed. This compound had the capability to complex some substances like KMnO₄ or AgNO₃. However, no structures were explained until Mock and co-worker, in 1981, defined the spatial-conformation of these macrocyclic compounds. Due to the characteristic shape of these compounds (figure 1.7), which resemble to a pumpkin, they called these class of compounds with the name of cucurbituril (CB[n]).²⁷ CB[n] are cyclic methylene-bridged glycoluril oligomers. Depending on the number of glycoluril units (n=5,6,7,8,10,11), the size of this molecule change. In particular the equatorial width, and therefore the internal volume, increases by increasing the number *n* of glycoluril units. On the contrary the depth is constant (9.1 Å) and the portals width is approximately 2 Å narrower than the equatorial width.²⁸ Since the characterization of the architecture of the CB[6] and the first innovative works of Mock, the host-guest chemistry, based on CB[n], saw an increased interest, especially in the last two decades thanks to the developing of CB[5], CB[7], CB[8] and CB[10].²⁹

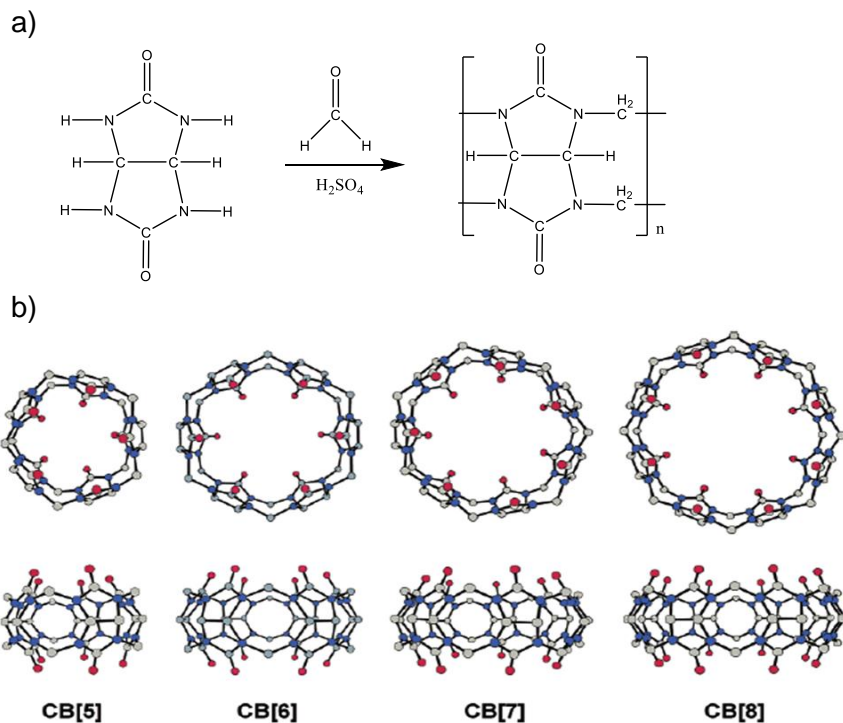


Figure 1.7: a) synthesis of CB[n]. b) X-ray crystal structures of CB[n] (n=5-8)²⁹

The special host behavior of the cucurbituril is possible thanks to its particular structure. In comparison with the commonly used cyclodextrin (CD), CB[n] presents an average binding affinity which is almost an order of magnitude higher ($K_a=10^{3.8} \pm 1.5$ vs. $10^{2.5} \pm 1.1$).^{30, 31} This is possible thanks to a cooperation of non-covalent interactions which take place during the host-guest complexation. While the hydroxyl groups on the CD allows only hydrogen bonds, the carbonyl groups present on the portals of the CB[n] allow ion-dipole interactions as well as hydrogen bonding³². Figure 1.8a shows the differences between β -CD and CB[7] visualized by the electrostatic potential (ESP). The blue-colored area around the carbonyl region in the cucurbituril points out a region negatively charged. Due to the presence of this charge, CBs prefer a binding formation with molecules positively charged. Furthermore, the rigidity of the CB[n], in comparison with CD, and its hydrophobic cavity allow an higher selectivity and stability of the complexes thus formed.³¹ Moreover, as in CDs hydrophobic effects play an important role. This is due to the release of “high-entropy” water molecules replaced by non-polar organic molecules thus forming a complex much more thermodynamically stable.⁸ Of particular interest for the research described in this thesis is the cucurbit[8]uril (CB[8]). The property previously described for this class of hosts are completely transferable on the CB[8]. It is constituted of 8 glycoluril units with an inner diameter of 8.8 Å. Its inner volume is 479 Å.²⁸ As for the other homologues, CB[8] prefers to bind with positively charged molecules by ion-dipole interaction.²⁸ However, in contrast to CB[5]-CB[7] the larger cavity of CB[8] allows the inclusion of even two different aromatic molecules to give a ternary complex through the formation of a charge-transfer complex.³³

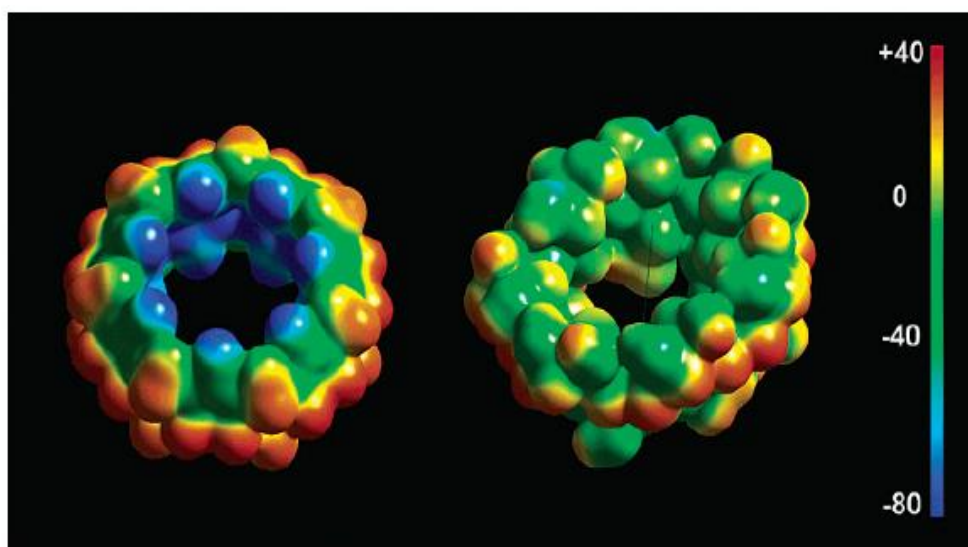


Figure 1.8: Electrostatic potential surface of CB[7] (left) and β -CD (right).²⁸

1.4 Charge transfer interactions: driving force for CB[8]-based supramolecular nanoparticles formation.

The large and negatively charged cavity of the CB[8] allows the inclusion of two molecules, an electron-deficient and an electron-rich molecule, giving rise to a formation of a 1:1:1 complex. One of the most representative examples is the interaction between the CB[8] with the electron deficient methyl viologen (MV^{2+}) and the electron rich naphthol. The driving force for the formation of this ternary complex is the charge transfer (CT) interaction between the two guest molecules inside the host cavity. Kim and co-worker reported that when 1 equivalent of 2,6-dihydroxynaphthalene (HN), an electron-rich species able to donate its electrons from its high energy filled orbitals, was added to the 1:1 solution of CB[8] and methylviologen (MV^{2+}), an electron-poor species able to withdraw electrons from the HN, an instantaneous and quantitative formation of a charge-transfer complex takes place (figure 1.9a). They proved the complex formation through UV/Vis analysis (figure 1.9b). While the only HN in water presents no absorption in the UV/Vis spectra, the ternary complex formation leads to an absorption band at 580 nm, which is red shifted (≈ 100 nm) and with a concomitant increasing in the intensity compared to the binary complex between HN and MV^{2+} . The higher intensity and the red-shifted band indicates that the highly enhanced charge-transfer interaction strength is due to the close contact of the two guests inside the cavity of the CB[8]. Furthermore, they also observed that the absence of the electron-poor methyl viologen moieties implies no complex formation.³⁴ This is due to the abundance of electrons in the HN which do not allow its inclusion in the negatively charged CB[8].

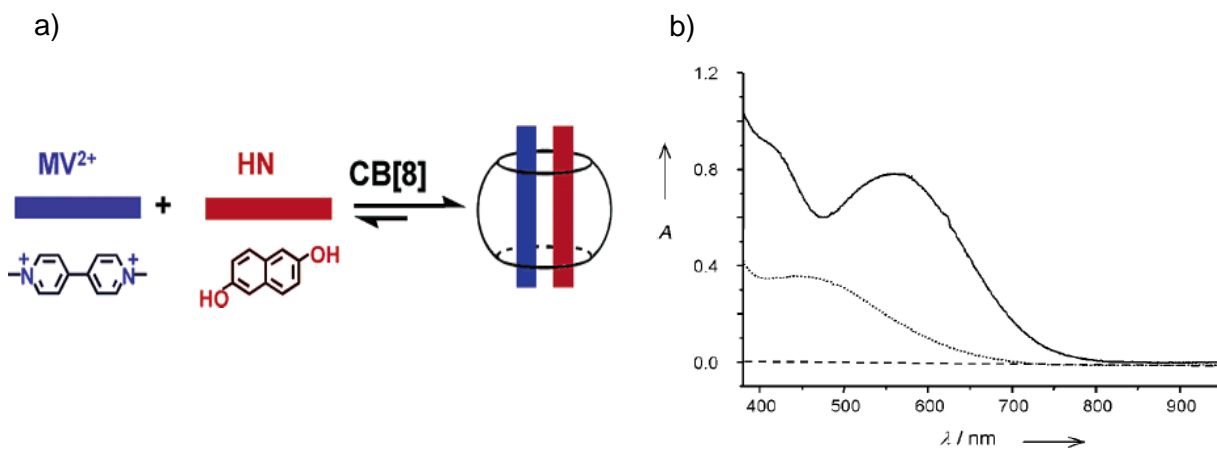


Figure 1.9: a) Inclusion of methyl viologen (MV^{2+}) and 2,6-dihydroxynaphthalene (HN) into CB[8] cavity through charge-transfer complex formation^[28]. b) Absorption spectra obtained in H₂O of HN(dashed line); a 1:1 mixture of HN and MV^{2+} (dotted line) and the 1:1:1 ternary complex among HN, MV^{2+} and CB[8] (solid line).³⁴

The interaction of a single guest molecule of MV^{2+} with CB[8] leads to the formation of a complex with an association constant of $1.1 \cdot 10^5 \text{ M}^{-1}$. The charge-transfer interactions between the electron-poor MV^{2+} and the electron-rich HN lead to a formation of a more stable ternary complexes with binding constant estimated to be $(5.9 \pm 0.5) \cdot 10^5 \text{ M}^{-1}$.³⁵ Of particular interest for the future applications of supramolecular system based on this kind of non-covalent interaction, is the possibility to control the stoichiometry of the 1:1:1 complexes. Kim and co-worker observed that the reduction of MV^{2+} to MV^+ , in the presence of CB[8], readily leads to a formation of a 2:1 inclusion complex. This complex presents a binding constant of $2 \cdot 10^7 \text{ M}^{-1}$, which is almost 10^5 times larger than that of the MV^{2+} alone.³⁶ They also recognized that if to a 1:1:1 complex was added one equivalent of free MV^{2+} and a reducing agent, such as sodium dithionate ($\text{Na}_2\text{S}_2\text{O}_4$), the hetero-ternary complex disassembles. The naphthol is removed from the CB[8] cavity and it is replaced by another molecule of MV^+ , thus giving the formation of a 2:1 homo-ternary complex. However, this guest exchange is completely reversible by a simple oxidation which reinstates the 1:1:1 hetero-guest ternary complex.⁷

1.5 Size-controlled supramolecular nanoparticles as drug-delivery vectors

The interest of nanotechnology applied to medicine relies on the property of these sub-micron systems to deliver drugs, proteins, peptides or even genes directly to the target site, protecting them from the enzymatic degradation mechanism and increasing the selectivity of these therapeutic agents towards a certain tissues.³⁷ Significant efforts have been done during the past decades in order to improve and develop highly efficient nanoparticles. Nevertheless, some issues still need to be taken into account during the design of the nanoparticles. Due to the unique size of NPs the enhanced-permeability-and-retention (EPR) effect is utilized for drug delivery purposes in oncology. This effect describes accumulation of macromolecules into tumor tissue caused by vascular hyper permeability and impaired lymphatic drainage.³⁸ However, when nanoparticles are injected into the body, different immune defense mechanism can get induced. Serum proteins can bind to nanoparticles making them recognizable to macrophages, thus leading to reduction of nanoparticles present in the body. Therefore, it is essential to hide nanoparticles from macrophages. This is possible by preventing the protein binding on the surface of the particles. A commonly used method involves the coating of the nanoparticles with polyethylene glycol (PEG). This inert polymer binds to the surface of the nanoparticles, generating a steric hindrance capable to prevents protein binding.³⁹ It was proved that nanoparticles coated with PEG increase their half-

life, reducing their uptake by the mononuclear phagocyte system (MPS), the macrophages responsible of the degradation of the particles.⁴⁰ Sadzuka *et al.* compared the uptake of non-PEGylated and PEGylated particles by the MPS in the liver. It was demonstrated that the degradation of non-PEGylated nanoparticles was three times higher than the PEGylated one,⁴¹ thus resulting in an increase of nanoparticles uptake by the tumor tissue. Therefore, the employment of PEG is a smart solution to hide nanoparticles from the degradation mechanism and to enhance the solubility in water of the particles thanks to its hydrophilic property.³⁹ Furthermore, the size of the nanoparticles is a crucial design parameter which has to be taken into account. For example, solid tumors have a vascular pore cutoff in the range between 100 and 780 nm, depending on the type of tumor.⁴² Consequently, it is important to design nanoparticles smaller than the vascular pore in order to allow their penetration. However, these nanoparticles should not be too small otherwise they are removed from the body by the renal capillary walls (figure 1.10). For example, Allen and co-workers showed that for lung cancer, liposomes with sizes of almost 120 nm may be absorbed 10-20 times more than liposomes having sizes of 170 nm.⁴³ Hence, it is important to be able to tune the size of the nanoparticles as a function of the target site.

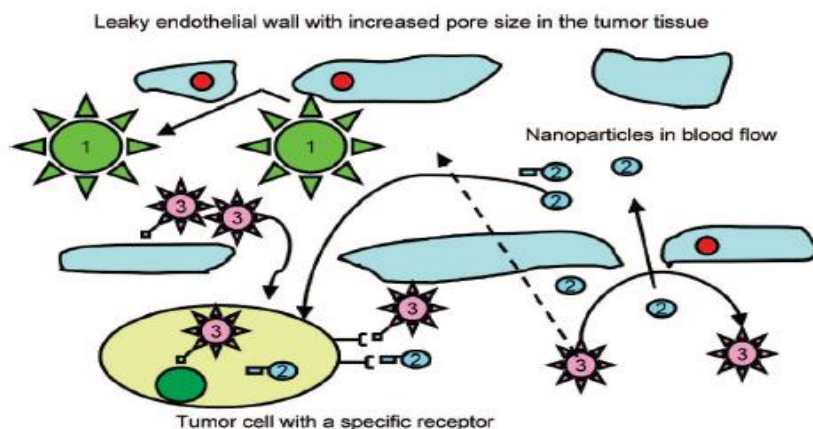


Figure 1.10: Schematic representation of the effect of nanoparticles size on tumor accumulation and uptake. (1) Nanoparticles larger than the pore cutoff cannot be accumulated into the tumor. (2) Too much smaller nanoparticles show little accumulation because they can easily come out from the tumor tissue. (3) represents particles with optimal size which exhibit an enhanced permeability and retention (EPR).³⁹

Another issue that comes out during the design of nanoparticles regards the therapeutic agent release once they reach the target site. An important example is given by Doxil.⁴⁴ Doxil are pegylated liposomal particles containing doxorubicin as anticancer drug, used for the refractory ovarian cancer and metastatic breast cancer.^{45, 46} These liposomes showed a great accumulation in solid tumors. However, Laginha and colleagues demonstrated that even if the accumulation of the Doxil in breast cancer was good, the bioavailability of the doxorubicin was only the 40-50%, thus the overall antitumor activity was modest in comparison with the real potential of the system.⁴⁷

Besides the stealth property and size of the nanoparticles, is also important to take care about the release mechanisms involved for the drugs delivery. For that reason externally-triggered nanoparticles degradation is gaining an increasing interest. An answer to these issues can be the employment of supramolecular nanoparticles as they are stable, but the reversible origin of their binding motifs make them perfect candidates as drug delivery vectors.

The group of Tseng developed a fascinating highly adaptable system for the delivery of drugs, and especially genes.⁴⁸ These nanoparticles are based on a supramolecular complex formation established on the host-guest interaction between β -cyclodextrin (β -CD) and adamantane (Ad). They used a multivalent poly(amidoamine) "generation 1" (PAMAM) dendrimer functionalized with 8 Ad units in combination with a monovalent Ad-PEG as guests, and β -CD grafted to a polyethylene imine (PEI) as host.

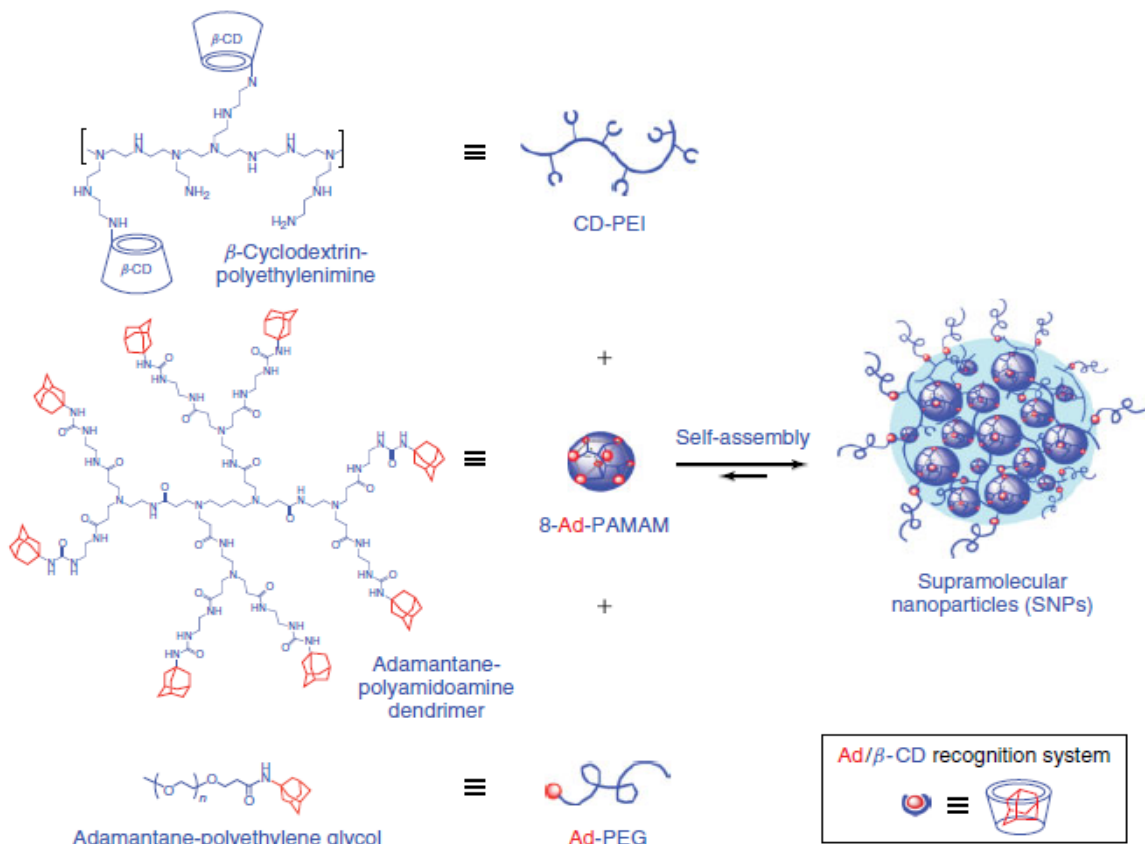


Figure 1.11: Schematic representation of CD-based nanoparticles.⁴⁹

An important role is played by both PEG and PAMAM. The presence of a multivalent dendrimer in the core of the nanoparticles promotes intermolecular interactions, which thanks to its

functionalized branch gives a continuous propagation of the cross-linked network. On the contrary, Ad-PEG acts as a supramolecular stopper, disfavoring interlinking connections among particles, thus enabling a control over the proliferation of the intermolecular network. Moreover, PEG ensures the stealth effects necessary to hide these particles from the serum proteins, allowing higher retention time in the body, as well as an enhanced solubility in water. The interplay between the monovalent PEG with the multivalent dendrimer has been shown to allow the tunability over the size of the nanoparticles. Therefore, a control over the dimension of these particles was possible by simply controlling the monovalency and multivalency of the system, thus obtaining particles with sizes in a range between 30 and 450 nm.⁴⁸ The presence of the PEI bearing β -CD units plays a pivotal role in the formation of these nanoparticles and in the encapsulation efficiency of drugs and DNA. On one hand β -CD, as stated in chapter 1.3, works as a host allowing the inclusion of a hydrophobic guest, in this particular case the Ad moieties, into its hydrophobic cavity.⁵⁰ On the other hand, it has been demonstrated that the presence of the cationic CD-PEI polymer allows the formation of electrostatic interaction with the anionic DNA.⁵¹ Therefore, Tseng and co-workers were able to create self-assembled nanoparticles having good stealth property, high stability, size-tunability and with the capability to incorporate genes through non-covalent interactions. Additionally, by playing on the exchange of monovalent and multivalent adamantane guests, they were able to insert RGD-targeting ligands on the outer shell of the nanoparticles in order to increase their affinity with the target site (figure 1.11).

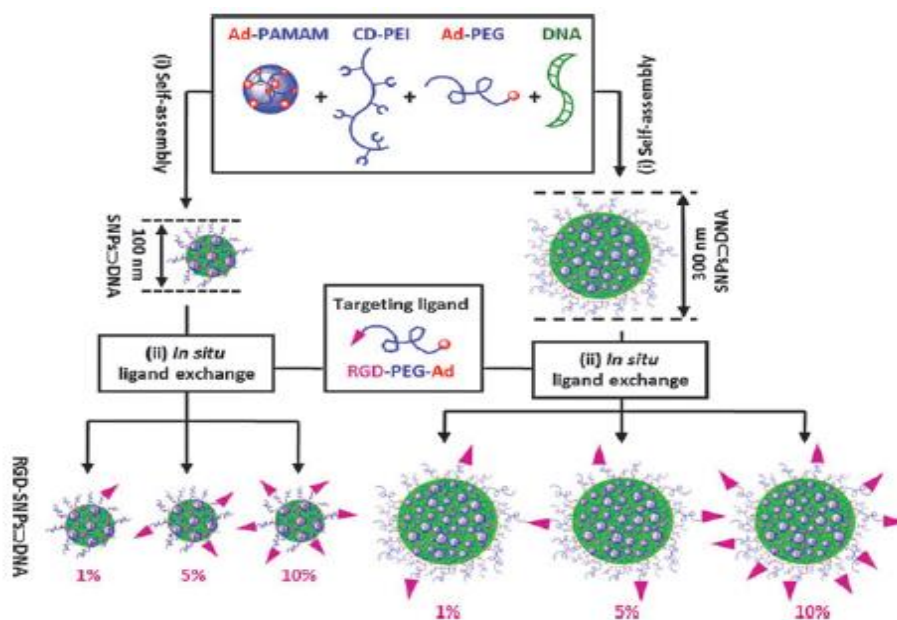


Figure 1.12: A two-step preparation of supramolecular self-assembled nanoparticles. First step encapsulation of DNA into the self-assembled nanoparticles. Substitution of the monovalent stopper with the target-ligand in the outer shell.⁵⁰

Inspired by these supramolecular nanoparticles (SNPs), Huskens and co-worker developed a supramolecular complex based on the ternary complex among CB[8], methylviologen and naphthol building blocks.⁵² As for the Tseng's system, intermolecular interactions between the multivalent PAMAM "generation 1" dendrimer, bearing 8 units of naphthol, and PEI, functionalized with 5 MV units per polymer chain, guarantee the formation of the NP core. On the contrary, the monovalent PEG functionalized with naphthol allows the control over the proliferation of the multivalent interactions, while ensuring a high solubility in water and the incognito properties necessary for a long residence into the body. The MV²⁺ units, grafted onto the PEI, permits the formation of the charge-transfer complexes with the naphthol units and the CB[8].

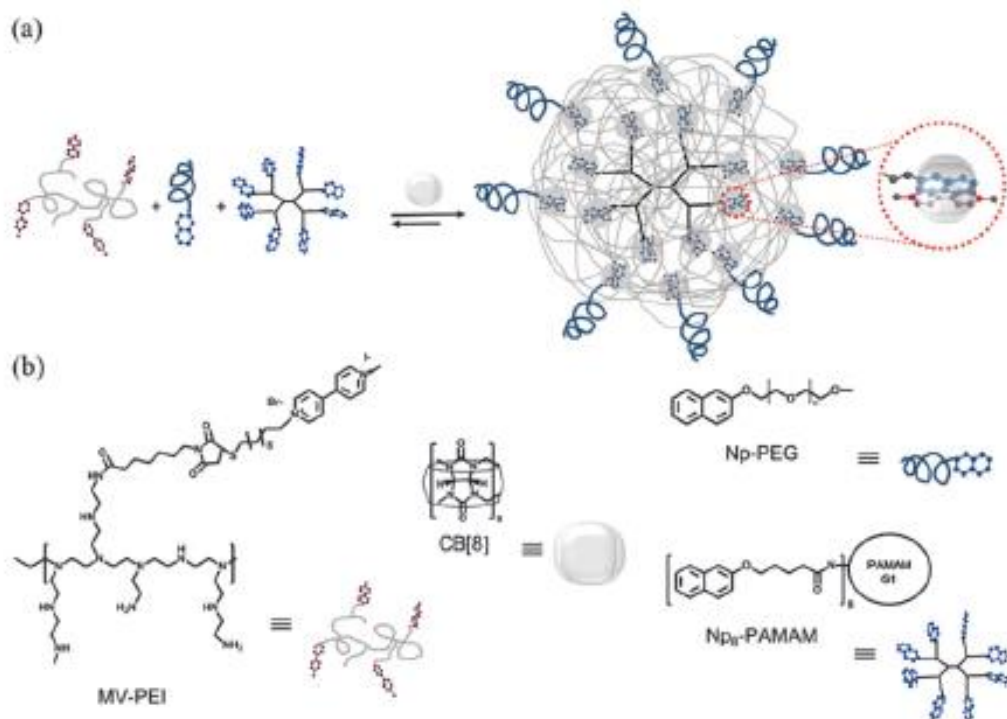


Figure 1.13: a) Supramolecular nanoparticles formation between cucurbit[8]uril (CB[8]), methyl viologen (MV), and naphthol moieties. b) Supramolecular building blocks: methyl viologen-poly(ethylene imine) (MV-PEI), cucurbit[8]uril (CB[8]), naphthol-poly(ethylene glycol) (Np-PEG) and naphthol₈-poly(amidoamine) (Np₈-PAMAM).⁵²

Like the CD-based nanoparticles, these particles possess the property to adjust their size depending on the ratio between the monovalent stopper and multivalent dendrimer assembling in the core. In particular, by increasing the amount of naphthol derived from the dendrimer, while keeping constant the ratio between the supramolecular building block, the size of nanoparticles increased from 51 to 137 nm. These CB[8]-based particles also showed slower assembly thermodynamics and an increased stability, in comparison with the CD-based system, thanks to the presence of the more stable charge-transfer complex. The real advantage for the use of this system

lies in its responsive character. As stated in chapter 1.4, in the presence of a reductant MV^{2+} reduces to MV^+ , thus leading to nanoparticles disassembly. This step is of fundamental importance for biomedical applications since it can facilitate the release of drugs eventually carried within these nanoparticles. Recently, Huskens and colleagues also announced the formation of another CB[8]-based SNPs system, in which the naphthol units were replaced by photoresponsive azobenzene moieties (Azo).⁵³ Such as the naphthol, Azo is an electron rich molecule able to give ion-dipole interaction in presence of the methyl viologen cation. As a consequence, azobenzene in the presence of MV^{2+} and CB[8] leads to the formation of the ternary complex, giving the opportunity to shape supramolecular nanoparticles.⁵⁴ The real innovation is due to its reversible structure. Azobenzene may exist in the *trans* or *cis* form. In particular, when subjected to irradiation at a wavelength shorter than 350 nm it converts into the bulkier and less stable *cis* form. This bulkier structure cannot be part of the host anymore in the CB[8] cavity, thus the ternary complex disassemble as both guests cannot fit in the cavity after azobenzene isomerization. Whereas, when the smaller *trans* form is restored the 1:1:1 complex form again. By exploiting this property of the azobenzene is therefore possible to create nanoparticles that can be assembled and disassemble in a completely reversible fashion by simply employing UV light, or irreversibly by the chemical reduction of the methylviologen (figure 1.12).

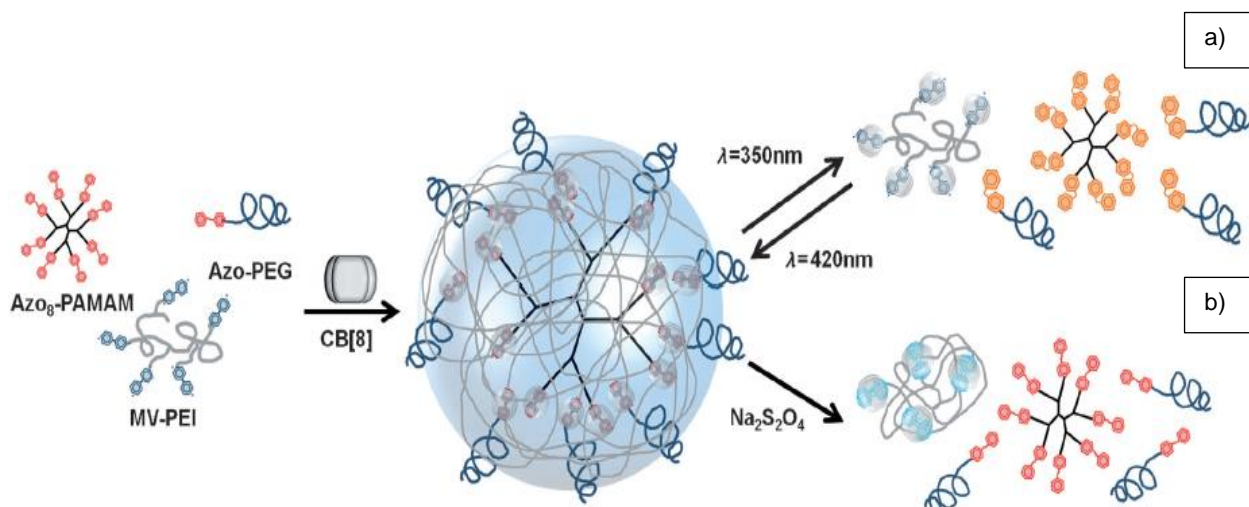


Figure 1.14: Self-assembled of supramolecular nanoparticles and subsequently disassemble. a) UV/light-mediated reversible disassemble. b) Irreversible disassemble through chemical reduction of MV^{2+} .⁵³

2 Aim of the project

The research described in this master thesis is focused on the investigation about the effect of multivalency on the CB[8]-based supramolecular nanoparticles. These effects were investigated by changing the nature of the stopping unit and the type of nanoparticles core. On this purpose, a core and a stopper agent with a greater valency, than that reported in literature, were employed with the aim to obtain particles which present an enhanced stability with time. Since the last decade these nanoparticles have gained an increasing interest in the field of biomedical sciences, especially as drug delivery systems. Thanks to their stability and their ability to be easily triggered is possible to obtain nanoparticles with specific size. It is known that depending on their size nanoparticles could be absorbed by different organs or, if too small, rejected by the body.⁵⁵ Consequently size and stability of nanoparticles are important to ensure the achievement of the target site without being degraded or rejected. Therefore, of particular interest are the implications involved on the use of these new supramolecular recognition units on the stability and size-tunability of the nanoparticles thus formed. While supramolecular CB[8]-based systems have been already known as highly size-tunable nanoparticles by simply controlling the ratio between the multivalent core (Np₈-PAMAM) and the monovalent stopper (Np-PEG), the size-control obtainable using a bivalent stopper or a more intense grafted core is not described in literature either for the CB[8]-based system or for any type of nanostructured assembly. Hence efforts are made in order to prepare the aforementioned supramolecular system taking advantage of the stabilization provided by a bivalent stopper at the outer shell, instead of monovalent one, or by further crosslinking the internal core by replacing the octavalent core with the hexadeca-valent one. Therefore the first part of this work is focused on the synthesis and characterization of a PEG-based stopper, which contains two naphthol groups, and a PAMAM dendrimer “generation 2”, bearing sixteen naphthol groups. The second part of the work is devoted to the nanoparticles characterization by DLS and SEM and their use as recognition units for the assembly of the SNPs.

The schemes that ideally represent the concept of this work are depicted in figure 2.1 and 2.2.

Figure 2.1 illustrates the SNPs formation by using Np₂-PEG as a stopping agent, while figure 2.2 represents the formation of the supramolecular nanoparticles when Np₁₆-PAMAM is employed as the core.

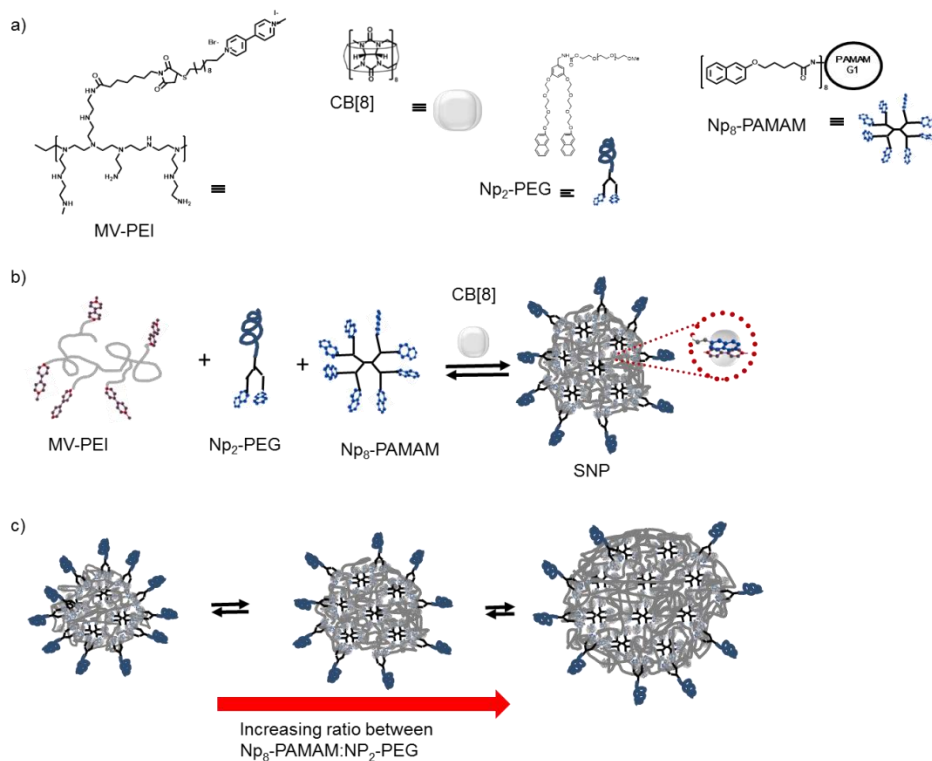


Figure 2.1 Scheme of SNPs formation by using Np₂-PEG as stopper a) Supramolecular building blocks. b) Assembling of these building blocks to give a supramolecular nanoparticle. c) Size-control by adjusting the ratio between Np₈-PAMAM and Np₂-PEG.

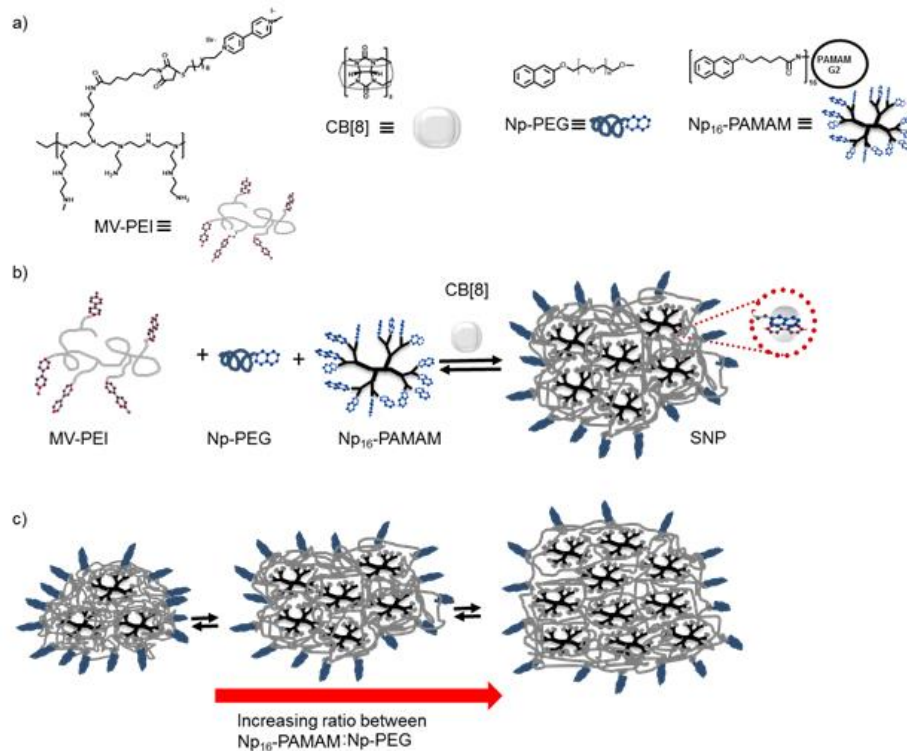


Figure 2.2: Scheme for the SNPs formation by using Np₁₆-PAMAM as core a) Supramolecular building blocks. b) Assembling of these building blocks to give a supramolecular nanoparticle. c) Size-control by adjusting the ratio between Np₁₆-PAMAM and Np-PEG.

3 Experimental

3.1 Chemicals

Starting materials for organic synthesis were purchased from Sigma-Aldrich, Strem Chemicals and were used as received. Poly(amido-amime) “generation 1” (PAMAM G1, MW= 1430) and Poly(amido-amine) “generation 2” (PAMAM G2, MW= 3256) were acquired from Dendritech and used without further purification. Chemical reactions were carried out using analytical grade solvents obtained from Merck and Sigma-Aldrich. Solvents like tetrahydrofuran and diethyl ether were purified by the Mbraun MB-SPS-800 apparatus. Naphthol-PEG (Np-PEG), naphthol-poly(amido-amine) “generation 1” (Np₈-PAMAM), Methyl-4,4-bipyridinium [methyl viologen/ (MV)]-substituted poly(ethylene imine) (MV-PEI degree of substitution: 5 MV units per polymer chain) and 2-naphthol-1-hexanoicacid-pentafluoro-phenolester were synthesized according to the procedure reported in literature.⁵²

Aqueous solutions were prepared in water purified by MilliQ Advantage A10, Millipore R= 18.2 MΩ/cm.

3.2 Equipment

Nuclear Magnetic Resonance (NMR)

¹H-NMR spectra were registered at room temperature on a Varian Bruker 400 MHz with position sample carousel and robotic capability for fully automated operation. Samples were dissolved in deuterated solvents (Cambridge Isotope Laboratories, Inc.).

Mass spectrometry

Synthesized compounds were analyzed with an electrospray ionization (ESI) mass-spectrometer by a micromass LCT from Waters.

Dynamic light scattering (DLS)

Particles size were measured by dynamic light scattering on a Nanotracs by Anaspec operating with a Microtracs Flex operating software, and a Malvern Zetasizer operating with a backscatter detection angle of 173°.

High resolution-Scanning Electron Microscopy (HR-SEM)

Nanoparticles were characterized with a Zeiss Merlin 1550 high resolution scanning electron microscope. Samples were prepared by drop-casting the aqueous solutions on a Formvar coated copper TEM grid, dried overnight and analyzed without further treatment.

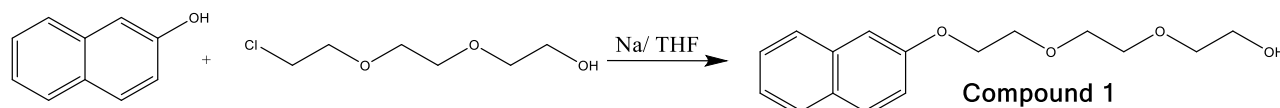
Freeze dry system

N-(3,5-bis(2-(2-(2-(naphthalen-2-yloxy)ethoxy)ethoxy)ethoxy)benzyl)-3-(methoxypolyethylene glycol)propanamide freeze-dried in a Lab Conco, freezezone 4.5.

3.3 Synthesis of the molecules

3.3.1 Synthesis of N-(3,5-bis(2-(2-(2-(naphthalen-2-yloxy)ethoxy)ethoxy)ethoxy)benzyl)-3-(methoxypolyethylene glycol)propanamide (Np₂-PEG)

Synthesis of 2-(2-(2-(naphthalen-2-yloxy)ethoxy)ethoxy)ethanol



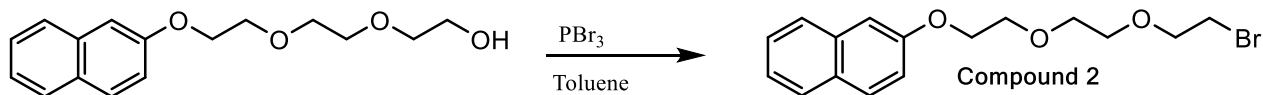
Reaction Scheme 1: Synthesis of 2-(2-(2-(naphthalen-2-yloxy)ethoxy)ethoxy)ethanol

2-Naphthol (4 g, 27.8 mmol; 1 eq) was dissolved in 40 mL of THF and 638 mg of sodium (27.8 mmol; 1 eq) were added to the ice-cooled solution under argon condition. The solution was added drop wise into a second flask filled with 5.76 g of chloro-ethoxy-ethoxy-ethanol (94.2 mmol; 1.23 eq), after sodium was completely dissolved and slowly heated to room temperature. A trace of KI was added to promote Finkelstein halogen exchange. After 12 h of stirring under Argon, the solvent was removed under vacuum and the residue was dissolved in 30 mL of CH₂Cl₂. The unreacted chloro-ethoxy-ethoxy-ethanol was removed by extraction of the organic solution with aqueous HCl (10x100 mL) followed by brine. Before removing the solvent under reduced pressure, the solution was dried over MgSO₄. **Compound 1** was further purified by column chromatography with a gradient eluent from CH₂Cl₂ (100%) to CH₂Cl₂/MeOH (98%:2%), to obtain the pure compound (2.54 g, 33.1% yield).

MS (ESI): calc. for [M+H⁺]: 277.14 g/mol; found: 277.03 g/mol.

¹H-NMR (CDCl₃): δ= 7.77 (q, 3H), 7.46 (t, 1H), 7.36 (t, 1H), 7.20(t, 2H), 4.29 (t, 2H), 3.97 (t, 2H), 3.81-3.65 (m, 9H) ppm.

Synthesis of 2-(2-(2-(2-bromoethoxy)ethoxy)ethoxy)naphthalene



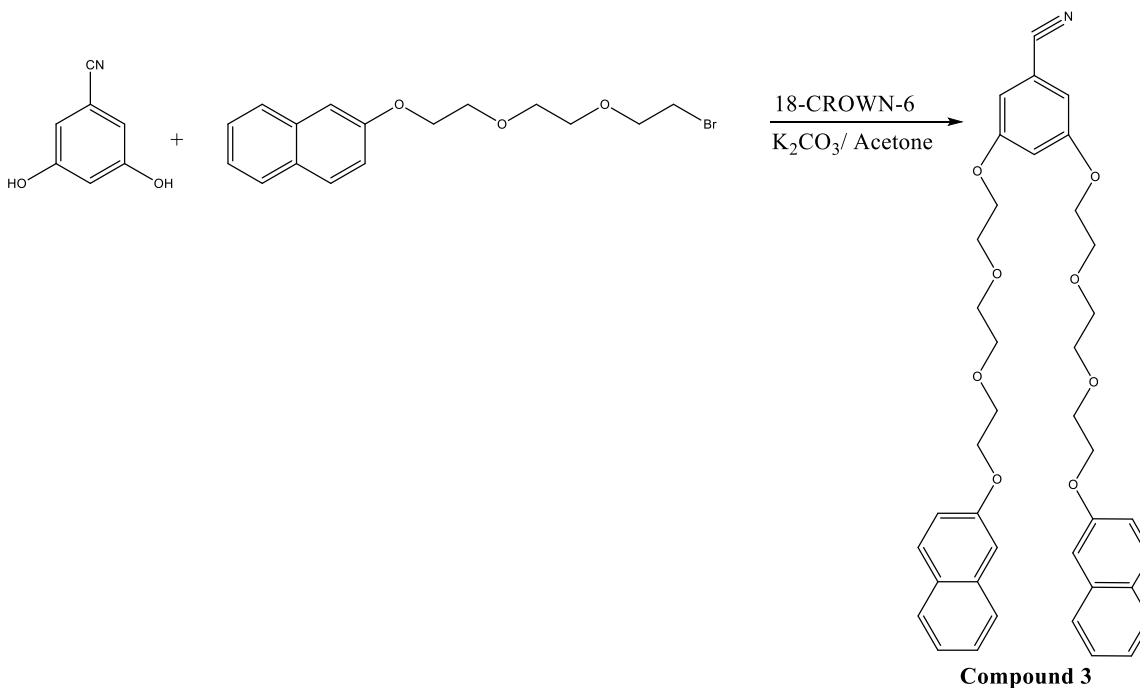
Reaction Scheme 2: synthesis of 2-(2-(2-(2-bromoethoxy)ethoxy)ethoxy)naphthalene

A solution of phosphorous tribromide (1 g, 3.66 mmol, 0.4 eq) and toluene (30 mL) was added drop wise to a cooled (0 °C) solution of toluene (30 mL) and **compound 1** (2.54 g, 9.14 mmol, 1 eq) and stirred overnight at room temperature under argon. The solvent was removed under vacuum and the residue dissolved in a mixture of CH₂Cl₂/H₂O (50/50). The organic layer was washed with water (3x50 mL) and brine (1x50 mL) and dried over MgSO₄. **Compound 2** was further purified by column chromatography with a gradient eluent from CH₂Cl₂ (100%) to CH₂Cl₂/MeOH (98%:2%), to obtain the pure product (1.45 g, 47% yield).

MS (ESI): calc. for [M+H⁺]: 339.23 g/mol; found: 339.059 g/mol and 341.061 g/mol.

¹H-NMR (CDCl₃): δ= 7.75 (q, 3H), 7.45 (m, 2H), 7.19 (t, 2H), 4.29 (t, 2H), 3.97 (t, 2H), 3.87-3.72 (m, 6H), 3.50 (t, 2H) ppm.

Synthesis of 3,5-bis(2-(2-(2-(naphthalen-2-yloxy)ethoxy)ethoxy)ethoxy)benzonitrile



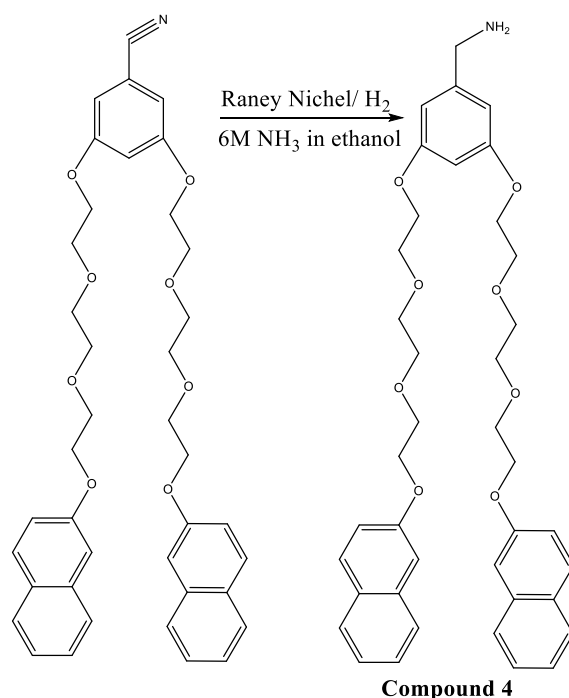
Reaction Scheme 3: synthesis of 3,5-bis(2-(2-(2-(naphthalen-2-yloxy)ethoxy)ethoxy)ethoxy)benzonitrile

2-(2-(2-(2-bromoethoxy)ethoxy)ethoxy)naphthalene (251.5 mg, 0.74 mmol, 2.2 eq) was dissolved in 20 mL of acetone together with 42.8 mg of 3,5-dihydroxybenzonnitrile (0.34 mmol, 1 eq), 18.5 mg of 18-crown-6 (0.071 mmol, 0.21 eq) and 121.4 mg of K_2CO_3 (0.88 mmol, 2.64 eq). The dispersion was refluxed for 72 h under argon. The solvent was evaporated and the residue washed with a mixture of water and diethyl ether (50:50). The aqueous fraction was extracted with diethyl ether (3x30 mL), and the combined organic fraction dried over $MgSO_4$. The solvent was evaporated and the residue purified by a column chromatography (Ethyl acetate/Hexane from 25:75 to 50:50 v/v) to give the **compound 3** (136.2 mg, 59% yield).

MS (ESI): calc. for $[M+H]^+$: 651.74 g/mol; found 652.26 g/mol.

1H -NMR ($CDCl_3$): δ = 7.77 (q, 6H), 7.45 (t, 2H), 7.35 (t, 2H), 7.17 (m, 4H), 6.76 (m, 3H), 4.27 (t, 4H), 4.07 (t, 4H), 3.95 (t, 4H), 3.80-3.76 (m, 12H) ppm.

Synthesis of (3,5-bis(2-(2-(2-(naphthalen-2-loxy)ethoxy)ethoxy)ethoxy)phenyl)methanamine



Reaction Scheme 4: synthesis of (3,5-bis(2-(2-(2-(naphthalen-2-loxy)ethoxy)ethoxy)ethoxy)phenyl)methanamine

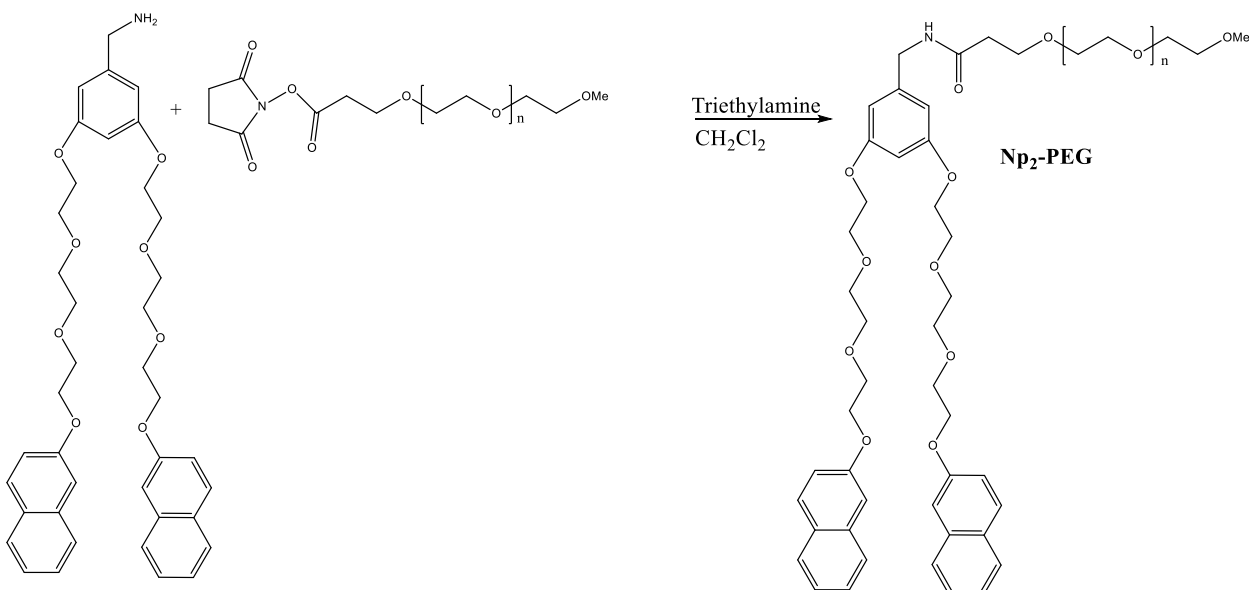
A suspension of **compound 3** (136.2 mg, 0.21 mmol) and a catalytic amount of Ni-Raney was stirred under 10 bar H_2 in 307 mL of 6M ammonia solution in ethanol for 48 h. The suspension was filtered over celite and washed with methanol (1 L) and ethanol. After evaporation of the solvent, the product was dissolved in chloroform and washed with 50 mL of 0.1M NaOH. The water fraction

was washed with chloroform (3x200 mL) and the combined organic fractions were evaporated under reduced pressure to give **compound 4** (112.9 mg, 80.9% yield).

MS (ESI): calc. for $[M+H]^+$: 655.7 g/mol; found 656.68 g/mol.

$^1\text{H-NMR}$ (CDCl_3): δ = 7.66 (q, 6H), 7.36 (t, 2H), 7.26 (t, 2H), 7.11 (t, 4H), 6.39 (d, 3H), 4.18 (t, 4H), 4.02 (t, 4H), 3.77 (m, 18H) ppm.

Synthesis of N-(3,5-bis(2-(2-(2-(naphthalen-2-yloxy)ethoxy)ethoxy)ethoxy)benzyl)-3-(methoxypolyethylene glycol)propanamide (**Np₂-PEG**)



Reaction Scheme 5: synthesis of N-(3,5-bis(2-(2-(2-(naphthalen-2-yloxy)ethoxy)ethoxy)ethoxy)benzyl)-3-(methoxypolyethylene glycol)propanamide (**Np₂-PEG**)

Compound 4 (112.9 mg, 0.172 mmol, 3 eq) was dissolved in 30 mL of CH_2Cl_2 together with 63.8 mg of triethylamine (0.0631 mmol, 1.1 eq) and 286.2 mg of methoxypolyethylene glycol 5000 acetic acid N-succinimidyl ester (NHS-PEG_{5000}) (0.0573 mmol, 1 eq) under argon. The solution was stirred for 72 h at room temperature. The solvent was removed under reduced pressure and the product dissolved in water. The compound was purified by dialysis for 96 hours and then freeze-dried for 48 h.

$^1\text{H-NMR}$ (CDCl_3): δ = 7.67-6.66 (m, 14H), 6.20 (t, 3H), 4.10-3.23 (m, 356H) ppm.

The highly pure **Np₂-PEG** (II), employed for the control experiments described in section 4.3.3, was obtained by repeated precipitation (3 times) of **Np₂-PEG** with dichloromethane and diethyl-ether

$^1\text{H-NMR}$ (CDCl_3): δ = 7.23-6.61 (m, 14H), 6.22 (s, 2H), 5.93 (s, 1H), 3.97-3.23 (m, 334H) ppm

3.3.2 Synthesis of Np₁₆-PAMAM

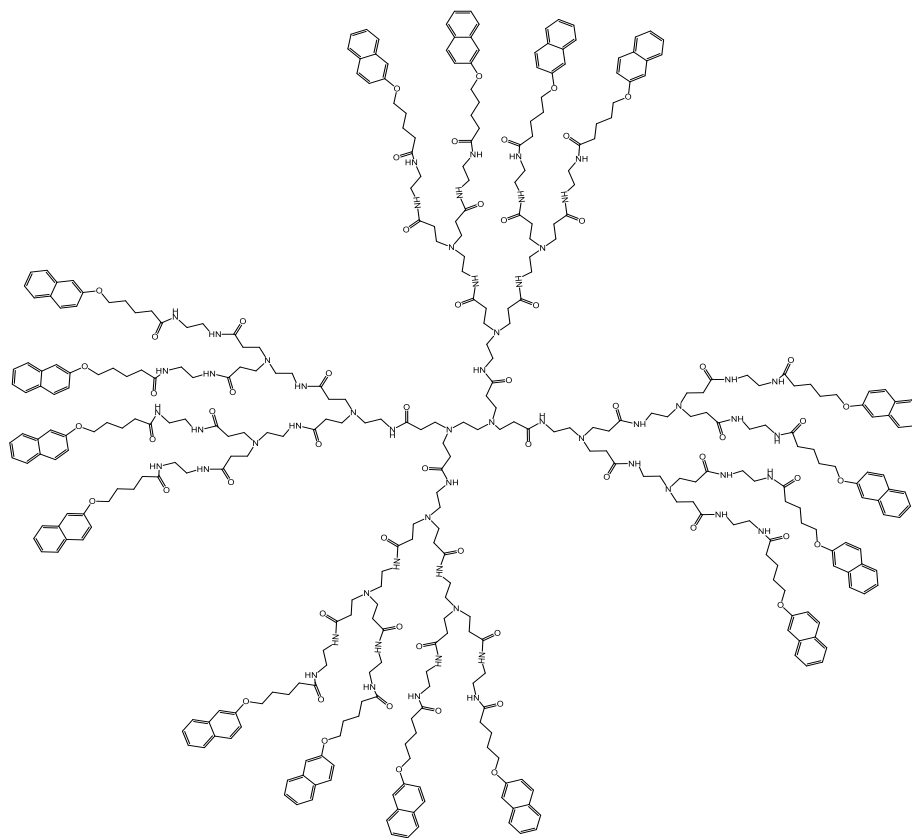
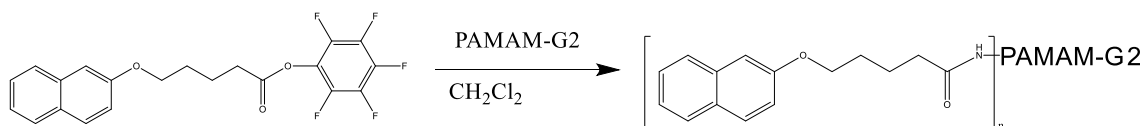


Figure 3.1: Np₁₆-PAMAM.



Reaction Scheme 6: Synthesis of Np₁₆-PAMAM

Poly(amido-amine) (PAMAM) dendrimer “generation 2” stored in methanol solution 20 wt%, (216 mg, 0.0136 mmol; 1 eq) was weighed and the MeOH evaporated. The residue was redissolved in 40 mL of CH₂Cl₂ and 348 mg of 2-naphthol-1-hexanoic acid-pentafluorophenylester (0.085 mmol; 64 eq) was added. The solution was stirred for 72 hours at room temperature under argon atmosphere. The solution was filtered and the solid residue, which contained the desired compound, was purified by repeated precipitation with dichloromethane and hexane.

¹H-NMR (DMSO): δ = 7.95 (d, 44H); 7.77 (s, 47H); 7.41-7.13 (m, 65H); 4.03 (s, 32H); 3.09 (s, 84H); 2.63 (m, 51H); 2.40 (d, 37H); 2.16 (s, 88H); 1.71 (s, 64H) ppm.

3.4 Supramolecular Nanoparticles assembling

3.4.1 Size tunable supramolecular nanoparticles assembled with Np₂-PEG

SNPs were obtained by mixing diluted solutions of the supramolecular building blocks by respecting a molar ratio of 1:1:1. These solutions were prepared by dissolving cucurbit[8]uril (CB[8]), methyl viologen polyethylenimine (MV-PEI) and Np₂-PEG in water while Np₈-PAMAM was dissolved in DMSO, and keeping an overall concentration of these supramolecular recognition units at 0.67 μM . In order to study the influence of the bi-valent stopper on the SNP size tunability, samples with different percentage of naphthol derived from Np₂-PEG and Np₈-PAMAM were prepared, while keeping the concentration of CB[8] and MV-PEI constant. For example, to prepare a solution with an overall volume of 600 μL which has 20% of the naphthol units derived from Np₈-PAMAM and 80% from Np₂-PEG, 300 μL of MV-PEI (0.268 μM) were added to a previously prepared solution of CB[8] (150 μL , 2.688 μM), Np₂-PEG (150 μL , 0.9408 μM) and Np₈-PAMAM (6 μL , 2.52 μM). After mixing the solutions, the sample was stored for at least two days at room temperature before analyzed it with DLS or SEM.

To further understand the behavior of the multivalent stopper, several experiments were carried out in order to expose the system to different external conditions, which are listed below:

Table 3.4.1: Condition used for the assembling of the SNPs by employing Np₂-PEG as stopper

Np ₈ -PAMAM conc.	External cond.	Time in that cond.	Interval before measuring
From 10% to 75%	room temperature	48 hours	48 hours
20%	30°C, 40°C	2 hours	1 hour
20%	Room temp., 30°C, 40°C	48 hours	measured as soon as mixed
20%	sonication	30, 60, 90, 120 min.	1 hour

3.4.2 Size tunable supramolecular nanoparticles assembled with Np₁₆-PAMAM

Supramolecular nanoparticles assembled with Np₁₆-PAMAM were prepared by mixing a solution of methyl viologen polyethylenimine (MV-PEI) to a previously prepared solution of cucurbit[8]uril CB[8], Np-PEG and Np₁₆-PAMAM. The ratio between the three recognition units was varied from the standard 1:1:1 (CB[8]:MV-PEI:Np from PAMAM and PEG) to a 1:1:1:2 (CB[8]:MV-PEI:Np-PEG:Np₁₆-PAMAM respectively). Therefore, also concentration was adapted in order to respect the limit imposed by the ratio; it was done by preparing a solution with an overall volume of 600 μL and

keeping the concentration of MV-PEI and CB[8] constant at 0.67 μM while, for Np-PEG and Np₁₆-PAMAM, it was varied as listed in Table 3.2:

Table3.2: Condition used for the assembling of the SNPs by employing Np₁₆-PAMAM as core.

a: The overall amount of naphthol derives from the sum of 1 mole of naphthol derived from Np-PEG with x mole of naphthol derived from Np₁₆-PAMAM, with x comprises between 0.25 and 2.

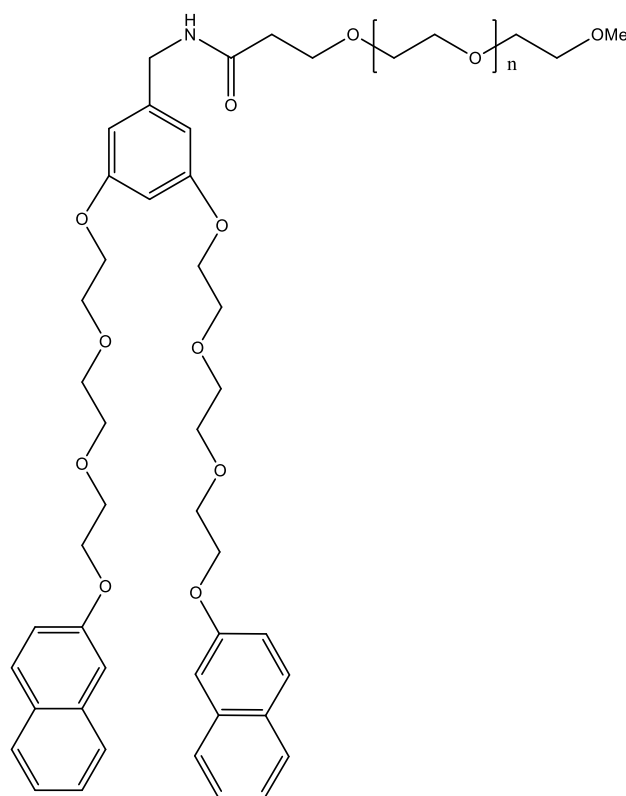
Ratio among recogn. Units	[Np- PEG] (μM)	[Np ₁₆ - PAMAM] (μM)	% Np from Np- PEG	% Np from Np ₁₆ - PAMAM	External cond.	Interval before measure
1:1:1	2,149; 2,15; 1,88	0,42; 0,84; 1,26	90%; 80%; 70%	10%; 20%; 30%	Room Temp.	2 days
1:1:1	2,15	0,84	80%	20%	Room Temp.	Meas. as soon as mixed
1:1:1,25 _a 1:1:1,5 _a 1:1:1,75 _a 1:1:2 _a 1:1:2,5 _a 1:1:3 _a	2,688	1,05 2,1 3,15 4,2 6,3 8,4			Room temp.	2h, 1day, 4 days

After mixing the solutions, the sample was stored for a variable amount of time (see table 3.2) at room temperature before analyzed it with DLS or seven days before analyzed it with SEM.

4 Results and discussion

4.1 Synthesis of Np₂-PEG

In order to evaluate the formation and stability behavior of the supramolecular nanoparticles, in the presence of a multivalent stopping agent, a suitable molecule needs to be synthesized. This molecule contains a triethylene-glycol chain, which acts as a spacer between the guest moieties and the polyethylene glycol units, ensuring to the naphthol units a great mobility and thus favoring them to interact with two, or more, distinct host molecules.

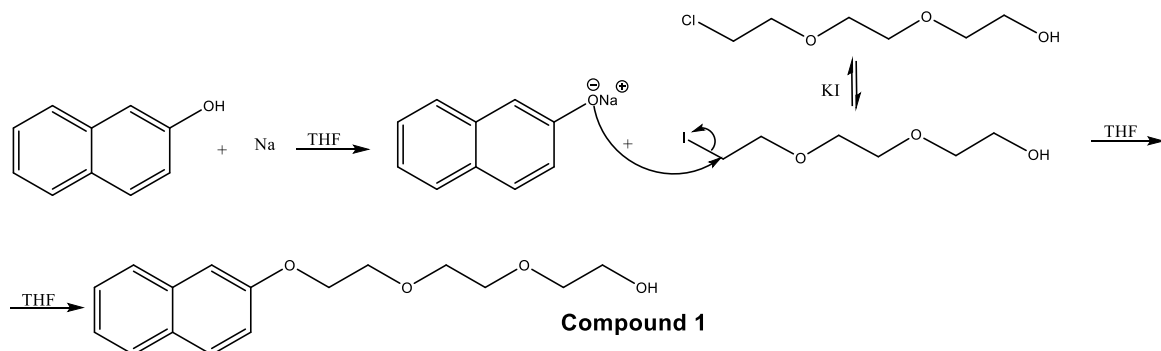


Np₂-PEG

Figure 4.1 N-(3,5-bis(2-(2-(2-(naphthalen-2-yloxy)ethoxy)ethoxy)ethoxy)benzyl)-3-(methoxypolyethylene glycol(5000))propanamide (Np₂-PEG). Guest molecule used in this study as stopping agent

For this purpose, several synthetic steps are required to obtain the target molecule.

4.1.1 Synthesis of 2-(2-(2-(naphthalen-2-yloxy)ethoxy)ethoxy)ethanol



Scheme 7: Reaction mechanism for the formation of 2-(2-(2-(naphthalen-2-yloxy)ethoxy)ethoxy)ethanol. The Williamson's reaction gives the formation of the ether bond whereas the Finkelstein halogen exchange reaction provides the target molecule.

The first step of this synthetic pathway started with the Williamson's reaction between 2-naphthol and chloro-ethoxy-ethoxy-ethanol. The hydroxyl group on the naphthol ring was activated with sodium giving a naphthoxide, which was added to a solution with the halide to produce the desired ether. Traces of KI were also added to speed up the reaction. When KI is added, Finkelstein halogen exchange reaction can take place; therefore the chlorine atom of the chloro-ethoxy-ethoxy-ethanol, can be replaced by iodine, which is a better leaving group and a better nucleophile than Cl. The reaction was performed under Argon, using THF as solvent. The crude product was purified by column chromatography to remove side products, that is from the double conjugated triethylen-glycol.

2-(2-(2-(naphthalen-2-yloxy)ethoxy)ethoxy)ethanol was characterized by $^1\text{H-NMR}$ (figure 4.2) that shows the typical signals ascribable to the naphthol ring, in the region between 7.80 and 7.17 ppm, and to the ethylene glycol moieties, between 4.30 and 3.65 ppm. Integration of these peaks confirmed the mono functionalization of the tryethylen-glycol.

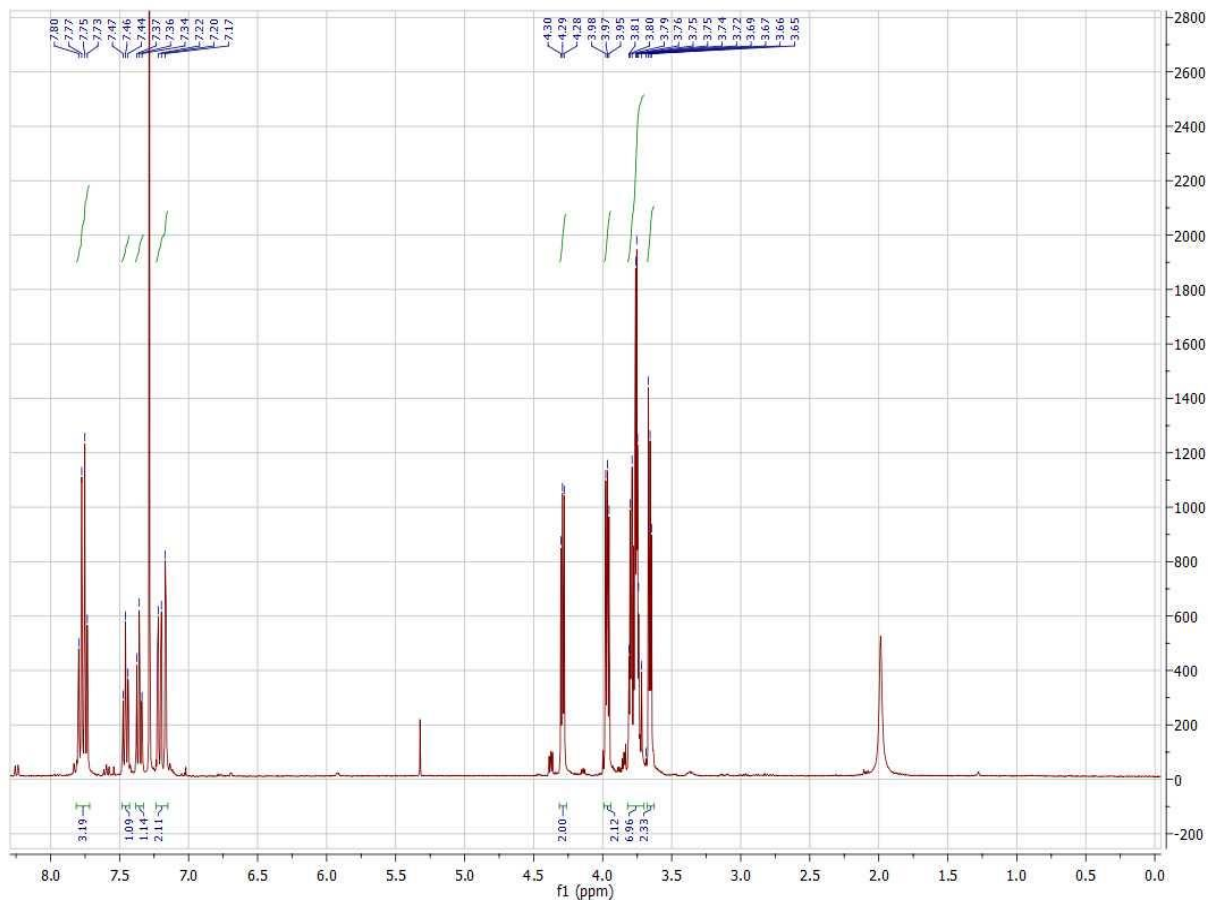
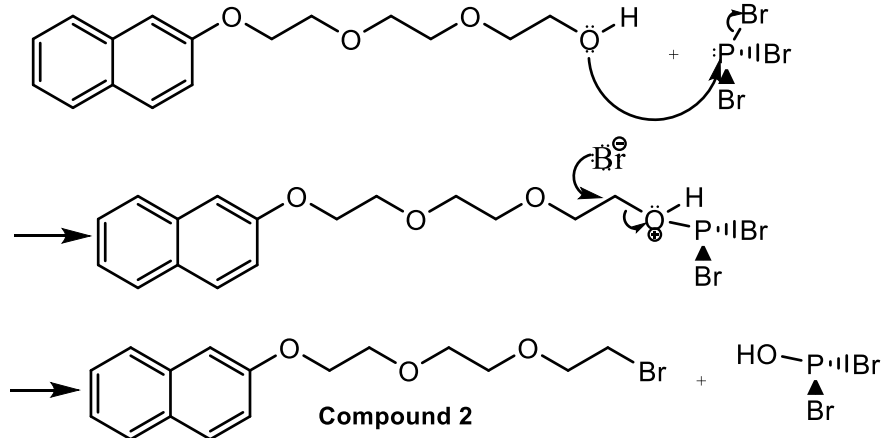


Figure 4.2: $^1\text{H-NMR}$ of 2-(2-(2-(2-(naphthalen-2-yloxy)ethoxy)ethoxy)ethoxy)ethanol

4.1.2 Synthesis of 2-(2-(2-(2-bromoethoxy)ethoxy)ethoxy)naphthalene



Scheme 2: Reaction mechanism of the formation of 2-(2-(2-(2-bromoethoxy)ethoxy)ethoxy)naphthalene

In order to render **compound 1** more reactive, a better leaving group than OH was necessary for the next synthetic step. For this purpose, phosphorous tri-bromide was employed under anhydrous condition and inert atmosphere, which allowed for the formation of the bromide derivative. The crude product was first washed with a mixture of water and dichloromethane to remove the unreacted PBr_3 and its acidic derivative, then subjected to a column chromatography, with a gradient eluent, to obtain the pure compound. In particular the main by-product is obtained from the condensation of two molecules of **compound 1**. The unreacted amount was then removed from the target **compound 2** taking advantage of its lower polarity.

The purity of the **compound 2** was confirmed by $^1\text{H-NMR}$ analysis (figure 4.3). Peaks comprised between 7.55 and 7.22 ppm, whose integrals value is 7, clearly shows the presence of one naphthol ring. Moreover, the peaks in the region between 4.29 and 3.50 ppm indicate the presence of one chain of triethylen-glycol functionalized with bromine, in α to the OH, from 3.69 ppm to 3.50 ppm (integral equal to 2) and confirmed by the peak-shift of the methylene group.

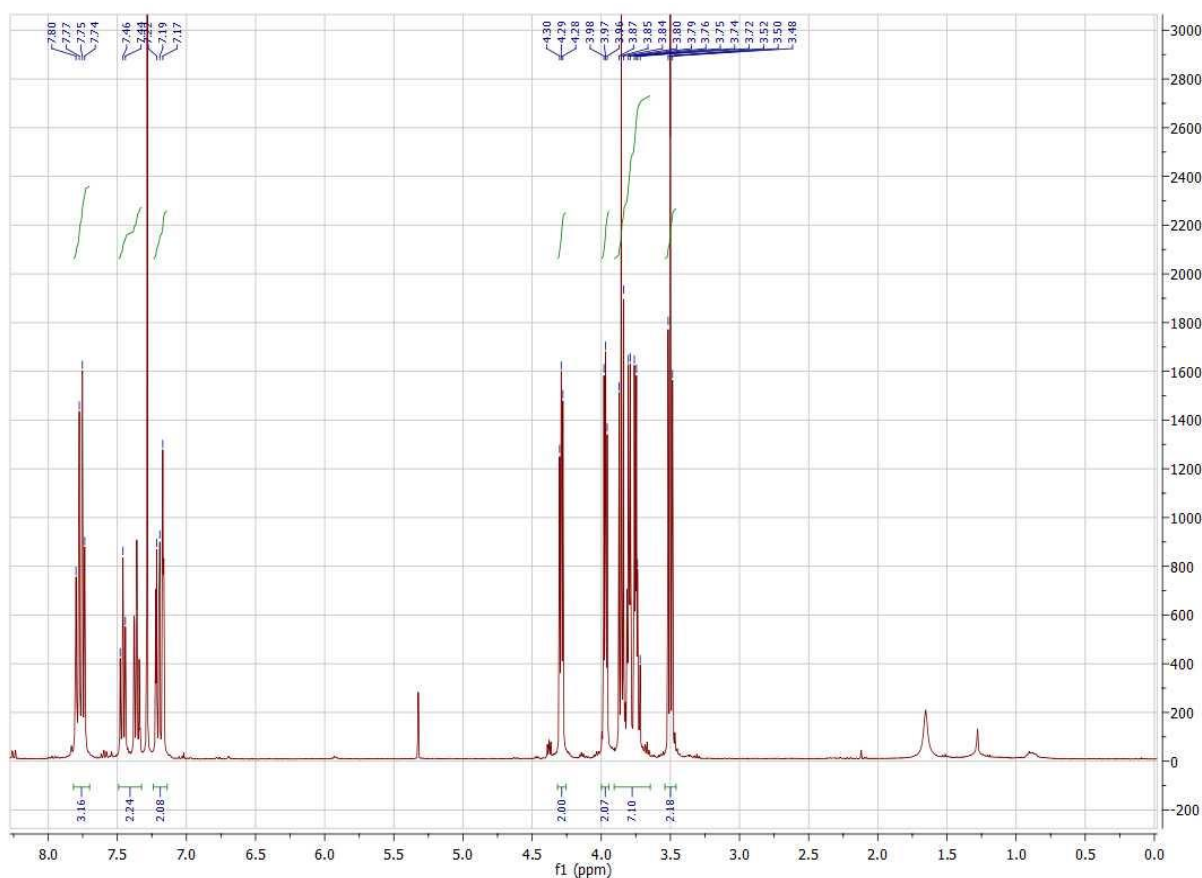
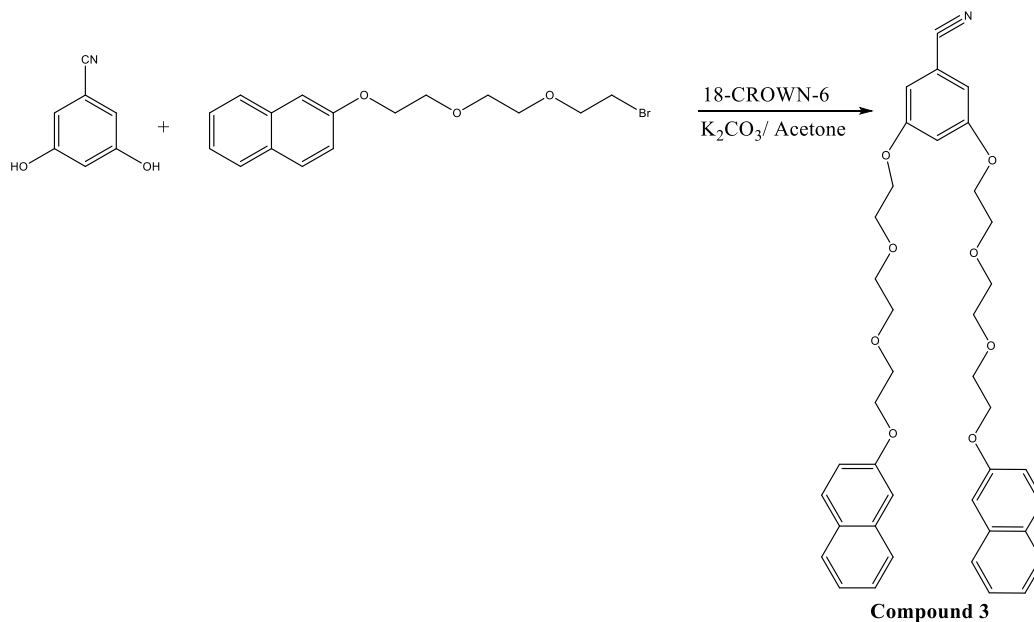


Figure 4.3: $^1\text{H-NMR}$ of 2-(2-(2-(2-bromoethoxy)ethoxy)ethoxy)naphthalene

4.1.3 Synthesis of

3,5-bis(2-(2-(2-(naphthalen-2-



Scheme 8: Reaction mechanism for the formation of 3,5-bis(2-(2-(2-(naphthalen-2-yloxy)ethoxy)ethoxy)ethoxy)benzonitrile. Grafting of two molecules of TEG-functionalized naphthol to a 3,5-dihydroxybenzonitrile by ether-bond formation.

The more reactive **compound 2** is now able to react with the 3,5-dihydroxybenzonitrile through a variation of the Williamson's reaction. In this particular case, the hydroxyl groups are deprotonated by the carbonate anion which is brought in solution by the crown ether⁵⁶, thus allowing also the control of solution pH. The reaction was conducted under anhydrous argon atmosphere and the system was left under reflux condition for 72 hours to increase the yield in the bi-functional compound. The crude product was washed from the water-soluble salts with a mixture of ether and water (50:50). Subsequently **compound 3** was purified from its by-product (residue of unreacted **compound 2** and from the mono-functionalized 3-hydroxy-5-(2-(2-(2-(naphthalen-2-yloxy)ethoxy)ethoxy)ethoxy)benzonitrile) by column chromatography using a mixture of ethyl acetate/hexane (from 25:75 to 50:50 v/v) as eluent.

¹H-NMR analysis confirmed the presence of the desired compound (figure 4.4). Especially peaks in the region between 7.79 and 7.15 ppm, whose integrals values count for 14 protons, reveal the presence of two naphthol rings attached by two chains of triethylen-glycol (confirmed by peaks between 4.28 and 3.94, whose integrals values count for 24 protons) to a phenyl ring (peak at 6.76 ppm, whose integrals values count for 3 protons). However peaks in the region between 1.75 and 0.75 ppm show the presence of some impurities, probably due to oily residue.

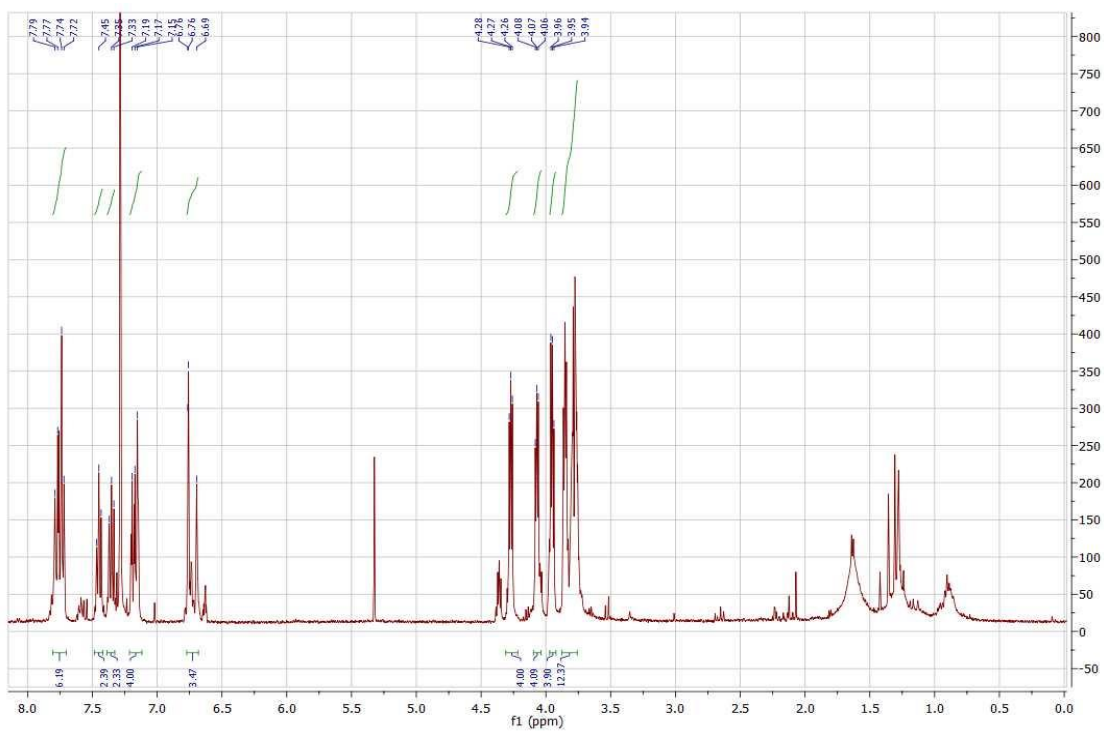
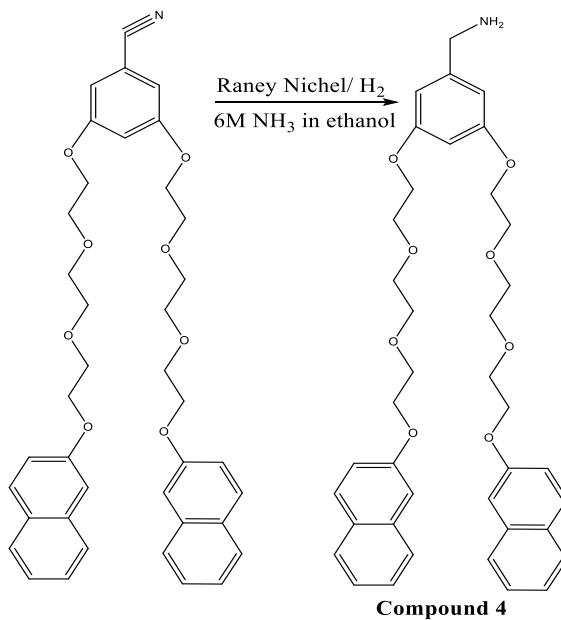


Figure 4.4: ¹H-NMR of 3,5-bis(2-(2-(2-(naphthalen-2-yloxy)ethoxy)ethoxy)ethoxy)benzonitrile

4.1.4 Synthesis of (3,5-bis(2-(2-(2-(naphthalen-2-yloxy)ethoxy)ethoxy)ethoxy)phenyl)methanamine



Scheme 4: Reaction mechanism for the formation of (3,5-bis(2-(2-(2-(naphthalen-2-yloxy)ethoxy)ethoxy)ethoxy)phenyl)methanamine.

The hydrogenation of the nitrile group is an important step which allows polyethylene glycol to be grafted on the (3,5-bis(2-(2-(2-(naphthalen-2-loxy)ethoxy)ethoxy)ethoxy)phenyl)methanamine.

Compound 3 was mixed with a catalytic amount of Nickel-Raney in a solution of Ammonia 6M in ethanol, 10 bar of hydrogen and left for 48 hours. The solution was filtered over celite with ethanol to separate it from the solid catalyst. The crude product was then dissolved in chloroform and washed with NaOH before obtain **compound 4** as pure product.

$^1\text{H-NMR}$ analysis confirmed the presence of the desired product. Peaks between 7.70 and 7.06 ppm confirmed the presence of two naphthol rings (whose integrals value is equal to 14 protons); peaks between 4.19 and 3.68 ppm, whose integrals value count for 26 protons, indicate the presence of two naphthol chains bonded to a phenol ring (peak at 6.39, integral equal to 3). Even if peaks of the secondary amine are not visible, because hidden by the peaks of the tryethylene glycol chains, the presence of the two protons bonded on a nitrogen atom is confirmed by the integrals values of those peaks between 3.87 and 3.68 ppm. These peaks count for 18 protons, two more protons than those expected from two chains of tryethylene glycol. Therefore, these two protons may be ascribed to protons bonded to the nitrogen atom.

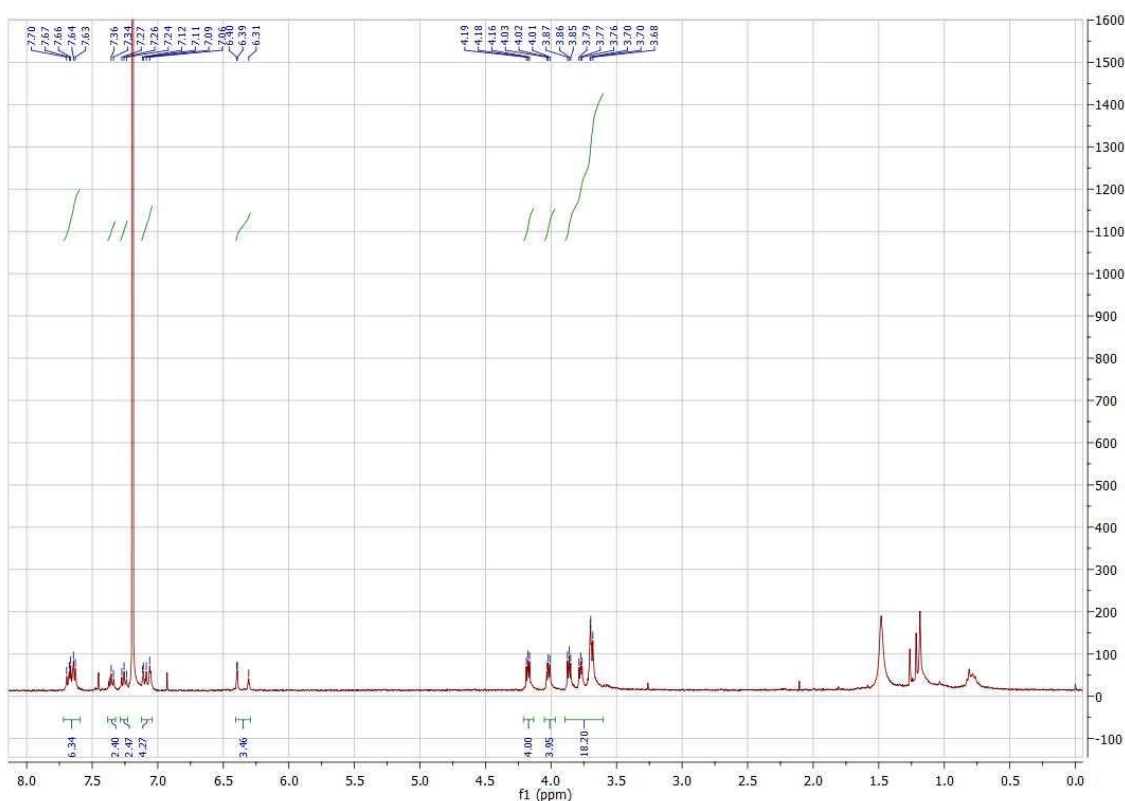
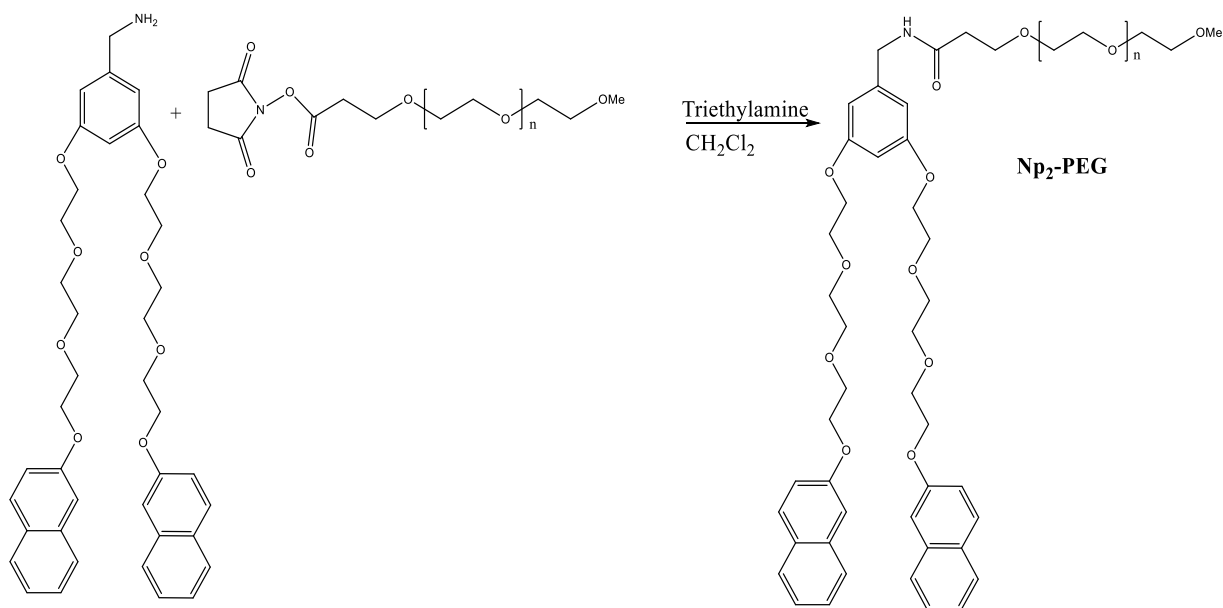


Figure 4.5: $^1\text{H-NMR}$ of (3,5-bis(2-(2-(2-(naphthalen-2-loxy)ethoxy)ethoxy)ethoxy)phenyl)methanamine

4.1.5 N-(3,5-bis(2-(2-(2-(naphthalen-2-yloxy)ethoxy)ethoxy)ethoxy)benzyl)-3-(methoxypolyethylene glycol)propanamide (Np₂-PEG)



Scheme 5: Reaction mechanism for the formation of N-(3,5-bis(2-(2-(2-(naphthalen-2-yloxy)ethoxy)ethoxy)ethoxy)benzyl)-3-(methoxypolyethylene glycol)propanamide (Np₂-PEG). Amide bond formation between **compound 4** and NHS-PEG₅₀₀₀.

The last step of the synthetic pathway leads to the formation of the divalent stopper Np₂-PEG and involved the amide bond formation between **compound 4** and methoxypolyethylene glycol 5000 acetic acid N-succinimidyl ester (NHS-PEG₅₀₀₀). The amine group, acting as a nucleophile, attaches the electrophilic carbon, on the NHS-PEG₅₀₀₀, while the succinimide group promotes the reaction thanks to its good leaving group characteristics. The reaction was run at room temperature, under anhydrous condition, for 72 hours using an excess of **compound 4**. The solvent was removed and the crude product dissolved in water. Dialysis was performed to purify the compound from unreacted **compound 4**. The pure compound was then dried by freeze-drying.

¹H-NMR analysis confirmed the functionalization of **compound 4** to give Np₂-PEG (figure 4.6). Peaks between 7.27 and 6.25 ppm confirmed the presence of two naphthol rings (integrals equal to 14); peaks at 6.20 ppm, whose integrals count for 3 protons, show the presence of a phenyl ring. Moreover peaks between 4.10 and 3.23 ppm show the presence of PEG units. However, peaks between 1.14 and 0.72 ppm show the presence of some impurities (probably due to some oily residue), which persisted even after the purification treatment.

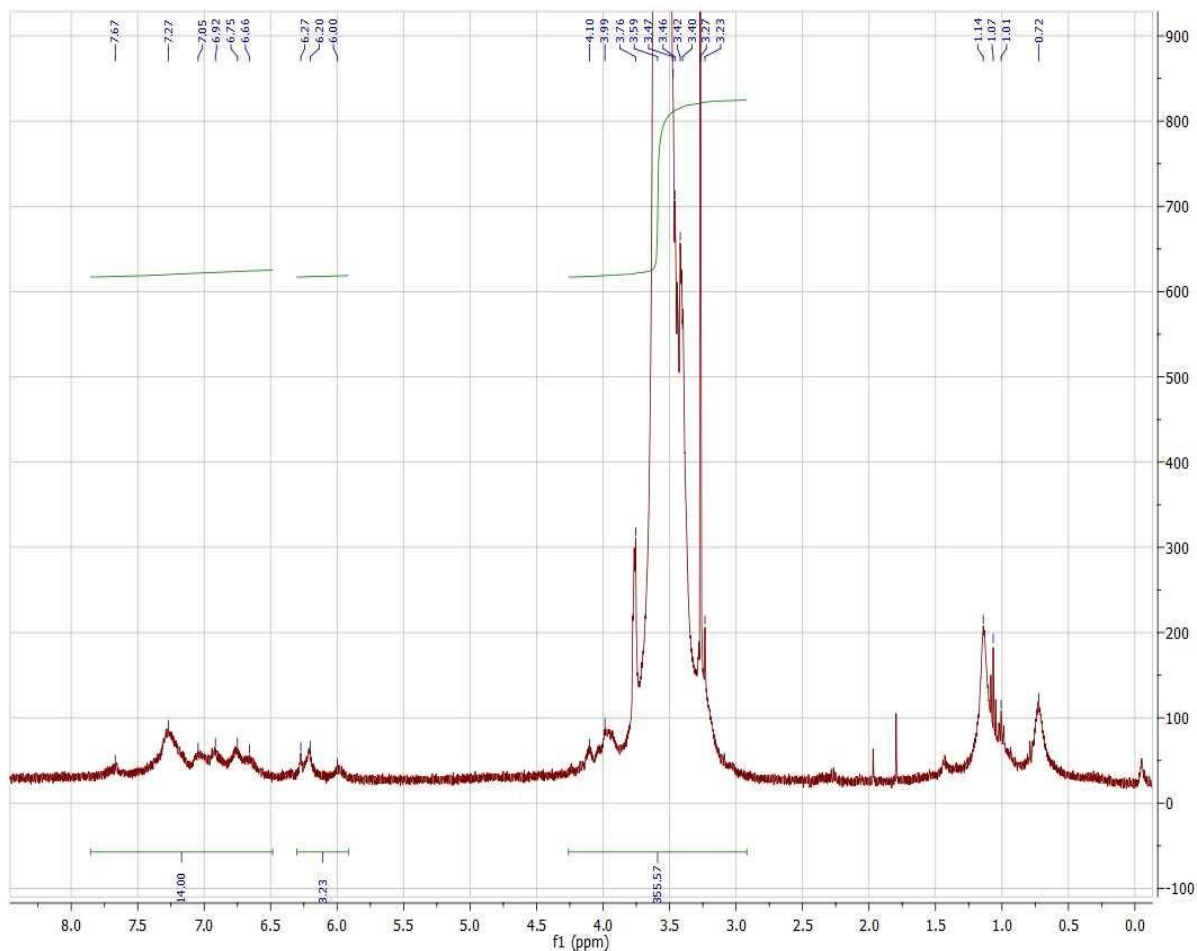


Figure 4.6: ¹H-NMR of N-(3,5-bis(2-(2-(2-(naphthalen-2-yloxy)ethoxy)ethoxy)ethoxy)benzyl)-3-(methoxypolyethylene glycol)propanamide (Np₂-PEG).

Even if these impurities were present in a negligible concentration, a previously synthesized Np₂-PEG with higher purity (renamed as: “Np₂-PEG (I)”) was then employed for the assembling. ¹H-NMR confirmed the higher purity of this stopper (figure 4.7). It is clear a reduction of those peaks comprised 0.2 and 2 ppm

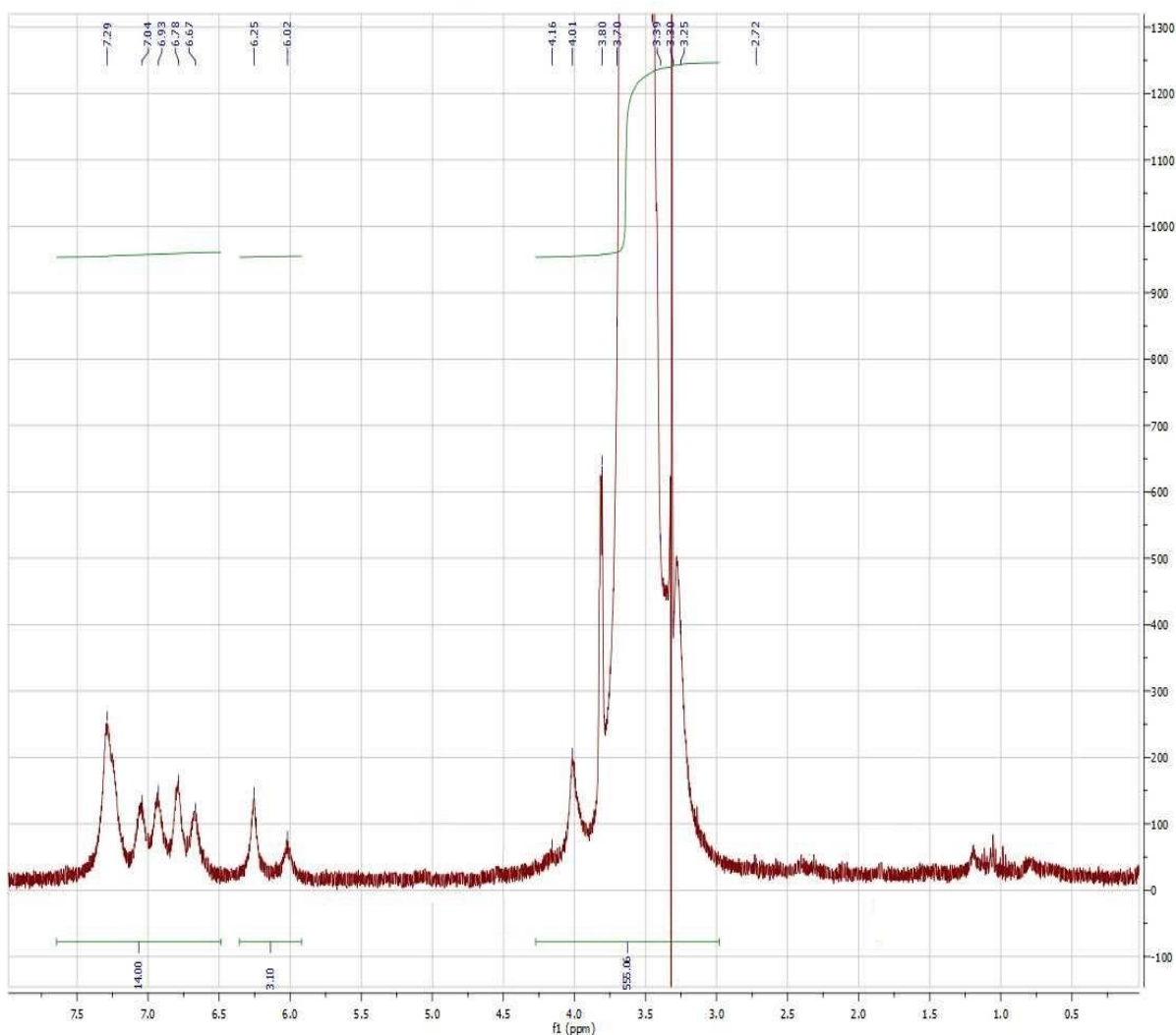


Figure 4.7: ¹H-NMR of the Np₂-PEG (I) previously synthesized

As a further proof that these impurities do not affect the formation of the SNPs, nanoparticles were also assembled by using a batch of Np₂-PEG which was further purified by repeated precipitation with dichloromethane and diethyl ether (renamed as “Np₂-PEG (II)”). Its purity was confirmed by ¹H-NMR analysis (figure 4.8). In comparison with the other two spectra (figure 4.6 and 4.7) those peaks attributable to the oily residue are not present anymore, while it is present only a small peak belonging to the residue diethyl ether.

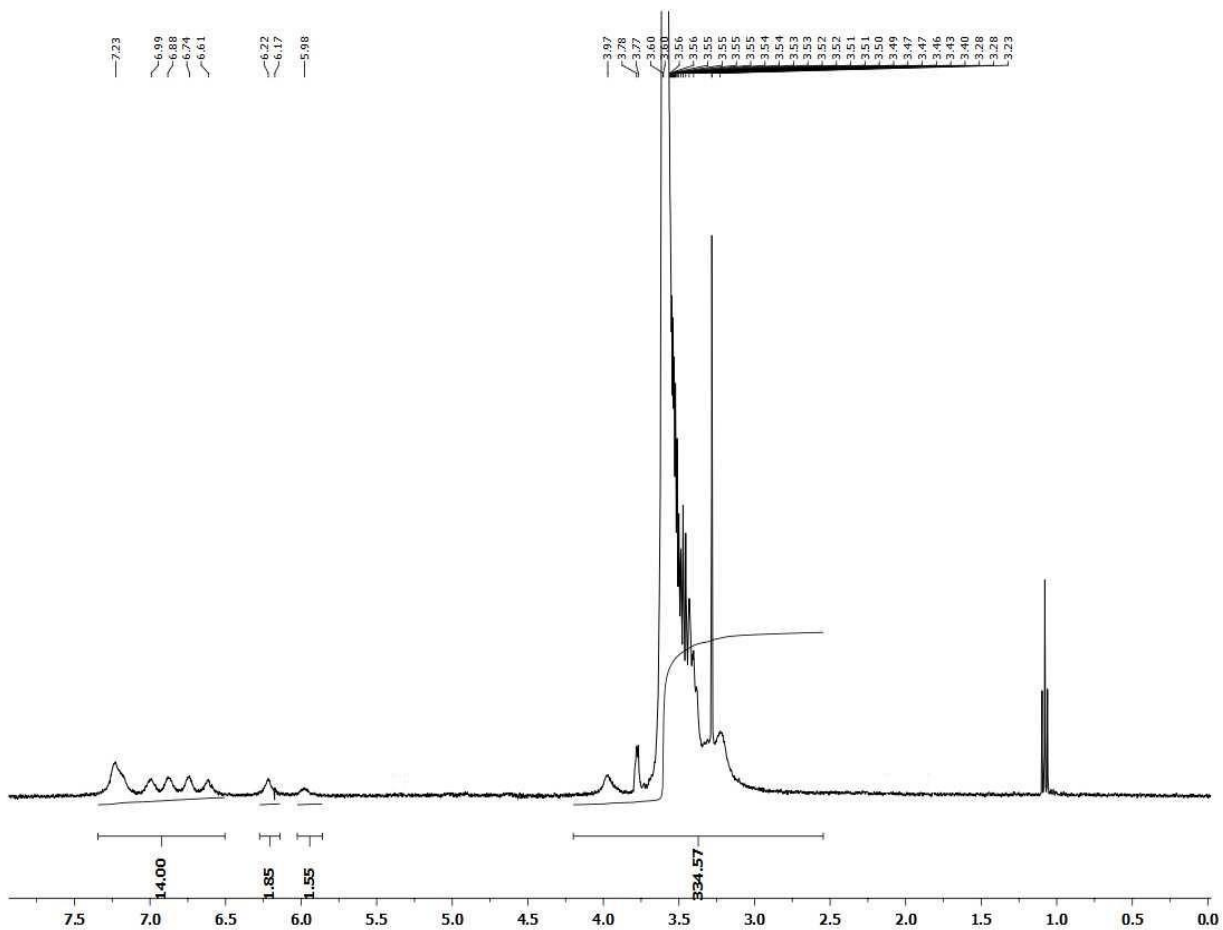
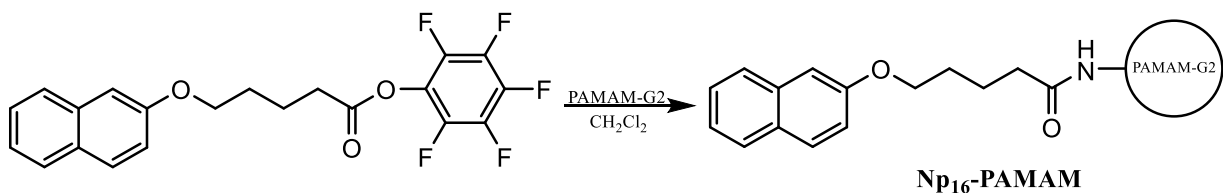


Figure 4.8: $^1\text{H-NMR}$ of $\text{Np}_2\text{-PEG}$ after repeated precipitation with diethyl ether and dichloromethane.

4.2 Synthesis of $\text{Np}_{16}\text{-PAMAM}$



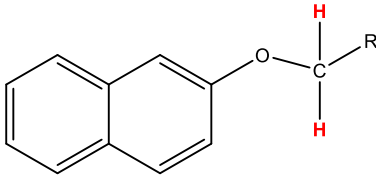
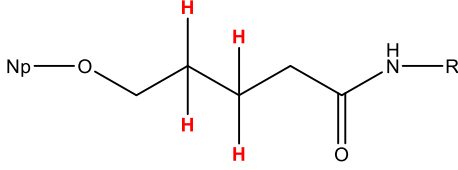
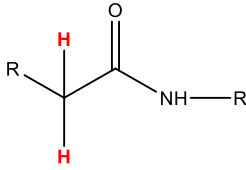
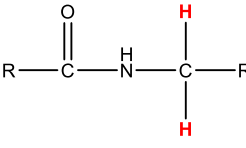
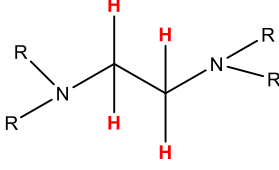
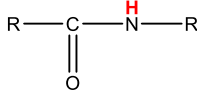
Scheme 6: Reaction mechanism for the formation of $\text{Np}_{16}\text{-PAMAM}$

With regard to describe the behavior of the $\text{CB}[8]$ -assembled SNPs, *i.e.* when the traditional $\text{Np}_8\text{-PAMAM}$ was replaced by a more interacting grafted dendrimer, an appropriate molecule needs to be synthesized. Therefore PAMAM dendrimer “generation 2”, dissolved (20 wt%) in methanol, was weighed and methanol evaporated. Subsequently, it was dissolved in CH_2Cl_2 with perfluorophenyl 5-(naphthalen-2-yloxy)pentanoate.

To overcome the problems arising from the steric hindrance of the amino groups on the dendrimer, the reaction was left under argon for 72 hours. The crude product was then purified by repeated precipitation with diethyl ether and hexane.

$^1\text{H-NMR}$ analysis (figure 4.9) confirmed the complete functionalization of the dendrimer with 16 naphthol groups. It can be seen from peaks between 7.77 and 7.13 ppm whose integral counts for 112 protons *i.e.* 16 naphthol rings mono-functionalized. Other peaks present in the NMR spectra confirm the presence of the PAMAM dendrimer generation 2. For simplicity they are summarized in table 4.1.

Table 4.1: $^1\text{H-NMR}$ analysis for Np_{16} -PAMAM

Functional group	ppm	Number of protons (integrals)
	4.03	32
	1.71	64
	2.16	88
	2.33/2.63	88
	3.09	84
	7.96-7.89	44

Peaks between 2.52 and 2.50 ppm may be ascribed to the solvent (DMSO) while peak at 3.34 ppm are attributed to the water absorbed by DMSO.

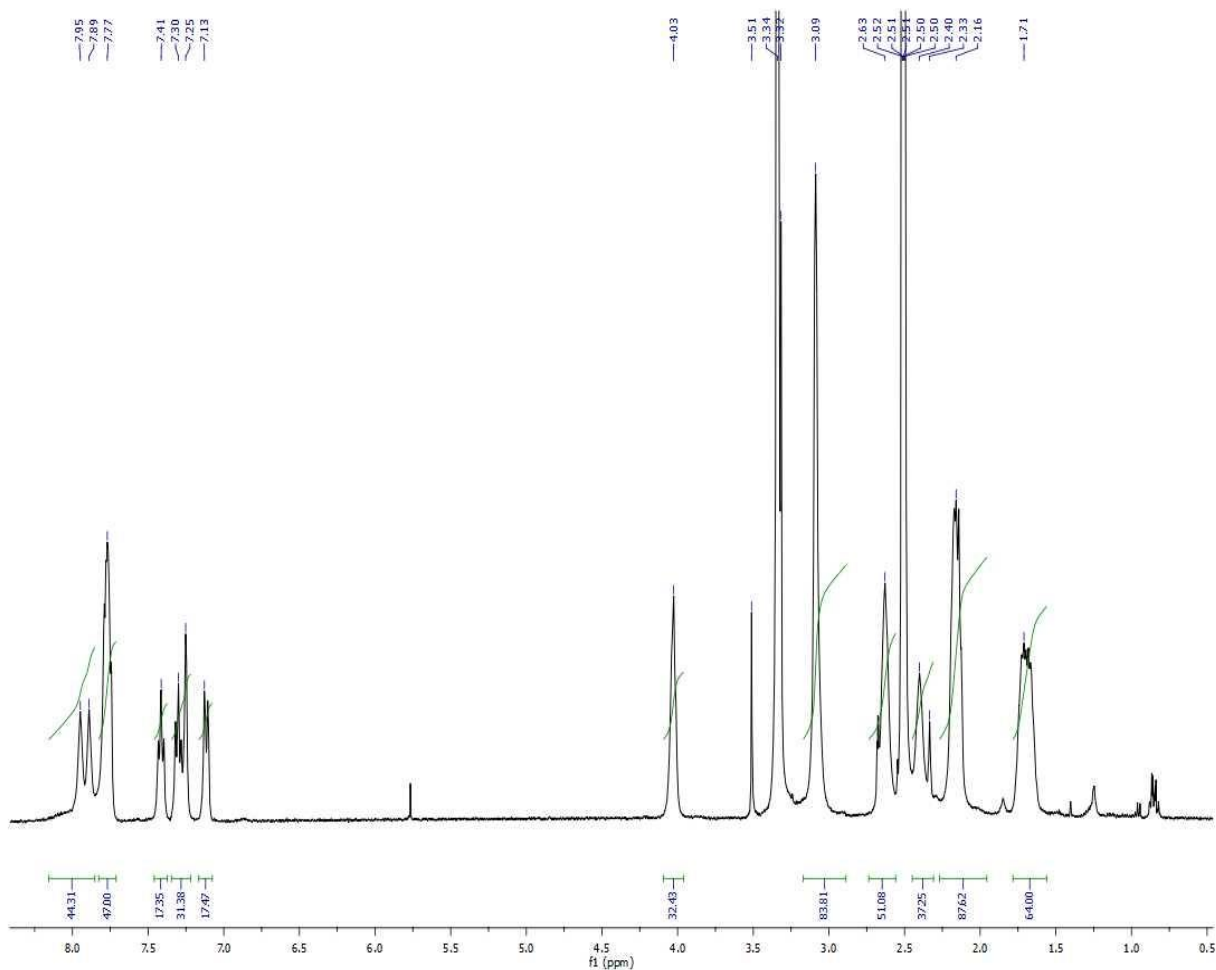


Figure 4.9: ¹H-NMR of the Np₁₆-PAMAM

4.3 Preparation of supramolecular nanoparticles through the assembling with the multivalent Np₂-PEG

Cucurbit[nurils (CB[n]) form a class of macrocyclic molecules, which have been recently employed as molecular recognition units thanks to their ability to give supramolecular complex by hydrophobic or ion-dipole interactions.³⁴

Methyl-viologen (MV²⁺) and naphthol derivatives arrange into a charge transfer complex which can be hosted into the CB[8] cavity, giving a ternary complex, thus forming supramolecular

nanoparticles. A control over the size of these nanoparticles was already proven to be obtainable by simply tuning the ratio between the stopper (Np-PEG) and the cross-linker agent (Np₈-PAMAM).⁵² Based on these results, nanoparticles assembled with Np₂-PEG as stopping agent were prepared by mixing an aqueous solution of methyl viologen polyethyleimine (MV-PEI) to a previously prepared solution of CB[8], Np₂-PEG and Np₈-PAMAM. The overall concentration of the three molecular recognition units was 0.67 μM, keeping constant the ratio of the three supramolecular recognition units CB[8]/MV/Np to 1:1:1, in order to evaluate the size control of the bivalent Np₂-PEG.

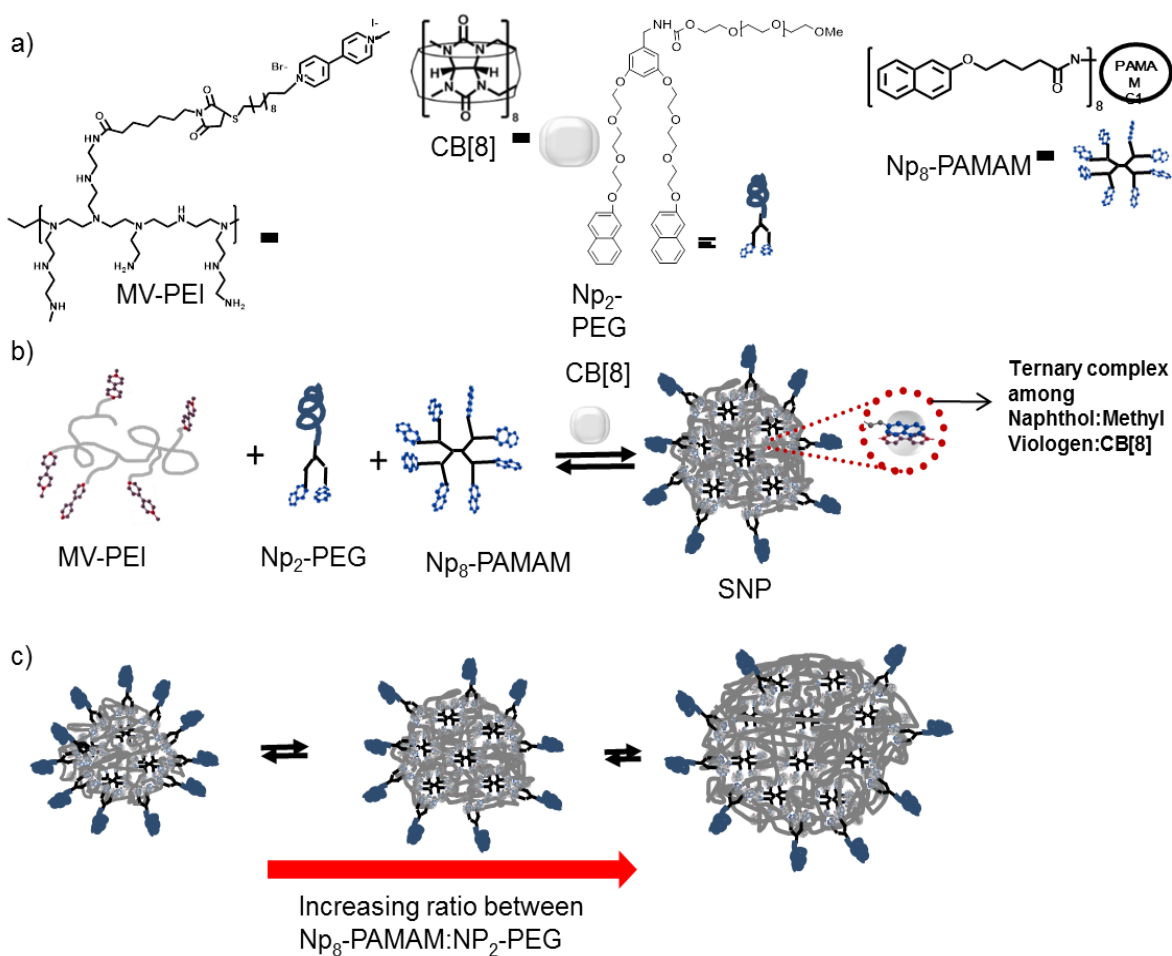


Figure 4.10: Scheme for SNPs formation using Np₂-PEG as stopper a) Supramolecular building blocks. b) Assembling of these building blocks to give a supramolecular nanoparticle. c) Size-control by controlling the ratio between Np₈-PAMAM and Np₂-PEG.

4.3.1 Size control given by the relative concentration of Np₂-PEG

In order to study the influence that the bi-valent stopper has on the size-tunability of the SNPs, samples with different percentage of naphthol derived from Np₂-PEG (I) and Np₈-PAMAM were prepared, while the overall concentration of naphthol present in the solution was kept constant. For this reason the ratio between Np₂-PEG (I):Np₈-PAMAM was varied from 90%:10% to 25%:75%. Particles thus obtained were analyzed by dynamic light scattering (DLS). Scanning electron microscopy (SEM) analysis was also performed to some of these samples with the purpose of obtaining an overview of the shape and size of the nanoparticles.

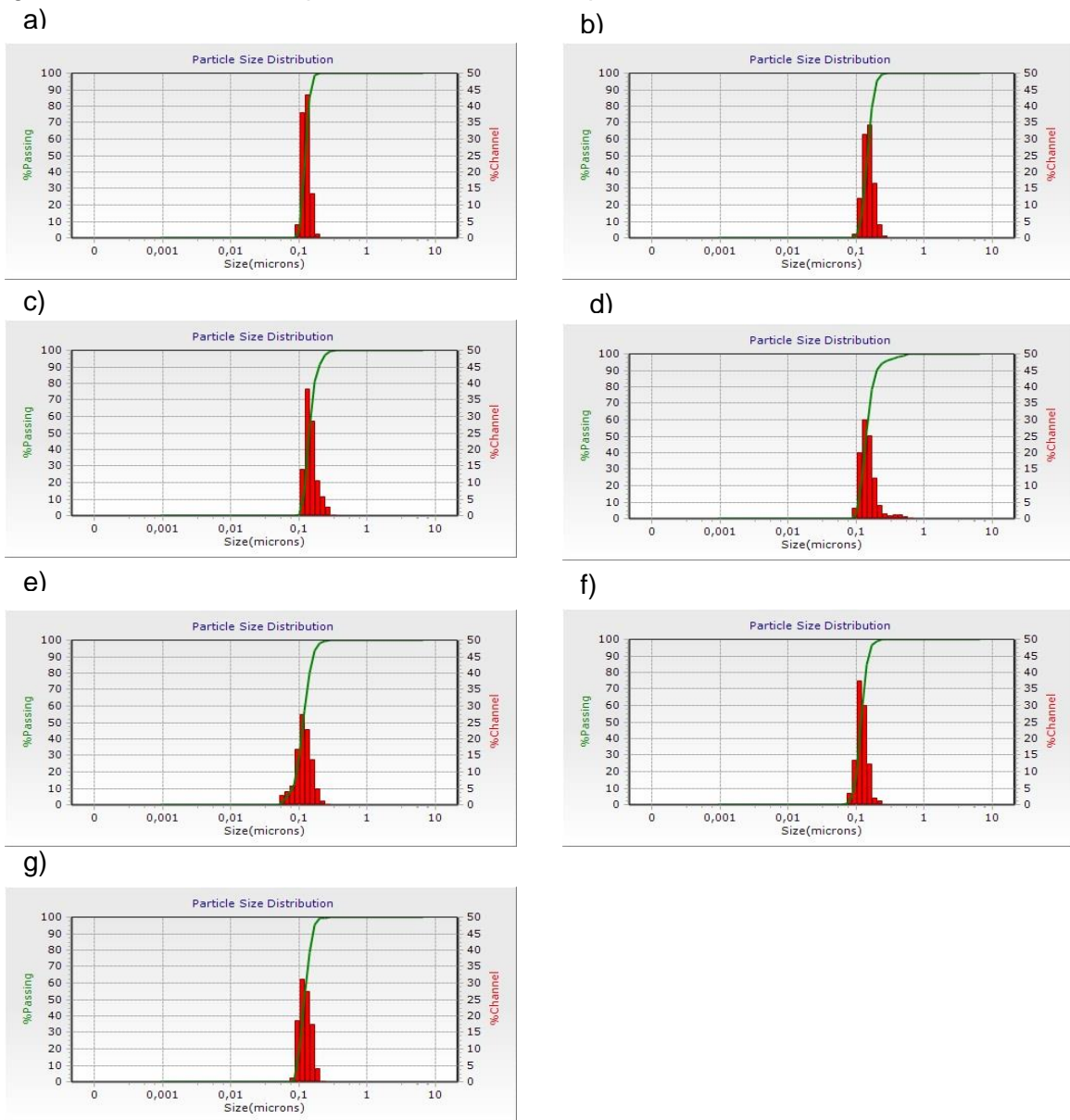


Figure 4.11: Dynamic light scattering (DLS) plots for samples with different percentage of naphthol derived from Np₂-PEG (I) and Np₈-PAMAM: a) 90%:10%: b) 80%:20%: c) 70%:30%: d) 40%:60% and a) 75%:25%.

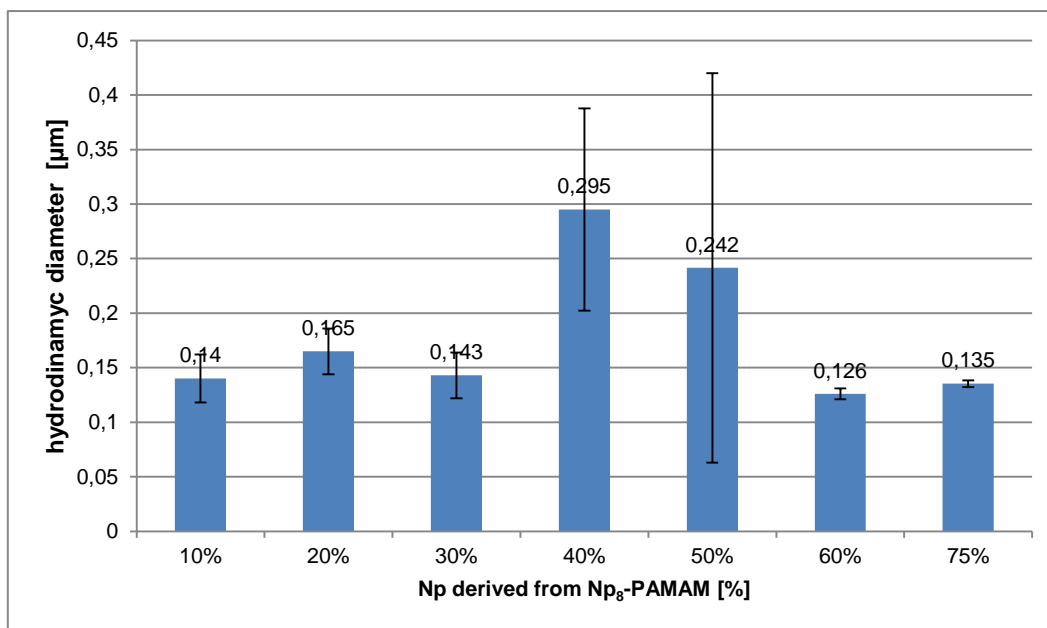


Figure 4.12: Hydrodynamic diameter of the supramolecular nanoparticles based on the DLS data average

DLS measurements (figure 4.11) were performed on these samples 48 hours after their preparation as a function of system composition, *i.e.* varying the relative amount of naphthol coming from Np₈-PAMAM and Np₂-PEG (I). The time interval is required in order to allow the system to reach the equilibrium and form stable particles. These measurements confirmed that nanoparticles are formed when CB[8], MV-PEI, Np₈-PAMAM and Np₂-PEG (I) are mixed together. While size-tunability was already proven for those particles assembled with the monovalent Np-PEG as stopping agent³⁴, this new system, in which the bi-valent Np₂-PEG should work as stopping agent, does not show the same control on the nanoparticles size. Here, an increase of the hydrodynamic diameter, when the relative concentration of Np₈-PAMAM increase, is not shown anymore. This is clearly noticeable from figure 4.12 in which the average hydrodynamic diameter evaluated by DLS was plotted against system composition.

Particles size ranges from 126 ± 5 nm, when the relative percentage of naphthol derived from Np₈-PAMAM is the 60% of the total, to 295 ± 93 nm, when the percentage of naphthol derived from Np₈-PAMAM is 40%.

To further understand the behavior of this system, HR-SEM measurements were performed on these samples (figure 4.13). These images show that by increasing the relative percentage of the dendrimer, a layer (probably made by the excess of it) starts to form. This layer appears as a dark-grey spots, which surround the nanoparticles leading to formation of poorly defined and aggregated particles. This layer also seems to trap the newly formed nanoparticles, reducing their mobility and

preventing the attainment of the equilibrium, giving as final result big particles aggregated and trapped inside this layer. This phenomenon becomes noticeable when the relative percentage of Np_8 -PAMAM exceeds 20% (figure 4.13c) and the more the amount of Np_8 -PAMAM increases, the more this layer becomes thick leading to formation of aggregated particles. This is more appreciable from figure 4.13d and figure 4.13e. In figure 4.13d particles were assembled using a relative percentage of Np_8 -PAMAM of 40%, it is visible the formation of big aggregates made of two or more particles collapsed together. When the relative percentage of dendrimer was 75%, small particles are formed again (figure 4.13e). This phenomenon may be attributed to an excessive reduction of the diffusivity of the CB[8], MV-PEI and Np_2 -PEG, through a densely “crosslinked” layer of Np_8 -PAMAM, due to the high amount of dendrimer present in solution.

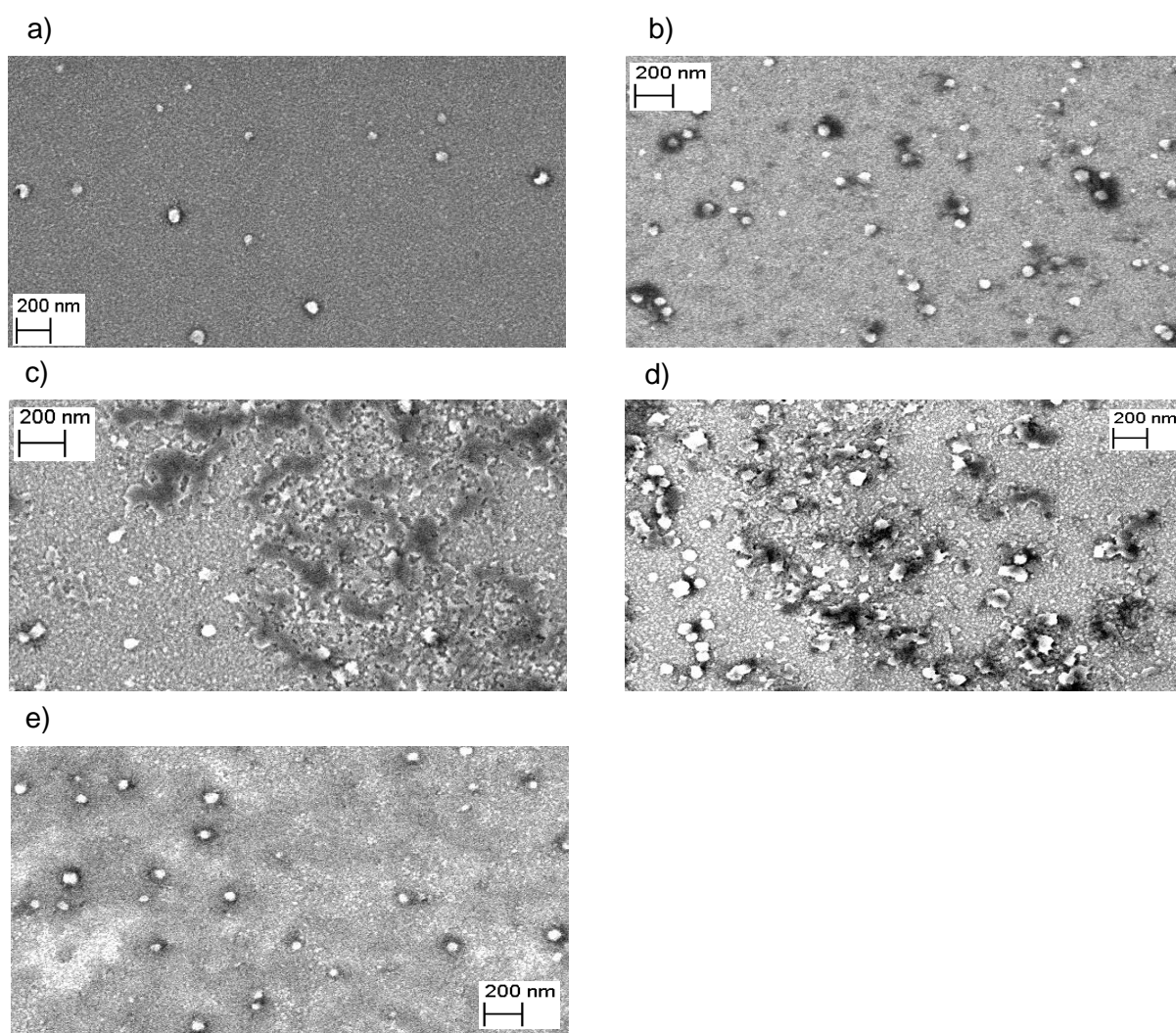


Figure 4.13: SEM images for the system with different percentage of naphthol derived from Np_8 -PAMAM and Np_2 -PEG (I). Naphthol derived from Np_8 -PAMAM: a) 10%; b) 20%; c) 30%; d) 40% and e) 75%.

As noticeable from figure 4.14a, nanoparticles change their size in relation to the percentage of Np_8 -PAMAM used. These size range from a mean diameter of 56 ± 11 nm to 75 ± 21 nm, which are in disagreement with the data obtained from DLS measure, figure 4.14b. This discrepancy between data obtained by DLS measurements and those obtained from SEM analysis may be attributed to the sampling design. While the laser of the DLS machine is able to detect all particles, even the bigger ones that maybe were precipitated due to an increase in their mass. Samples for SEM were prepared by taking an aliquot of solution, which probably did not contain the heaviest particles that were going to settle on the bottom of the tube, thus possibly giving a very large data gap between SEM and DLS. However, due to a lack of time it was not possible to repeat the SEM measures by improving the sampling stage.

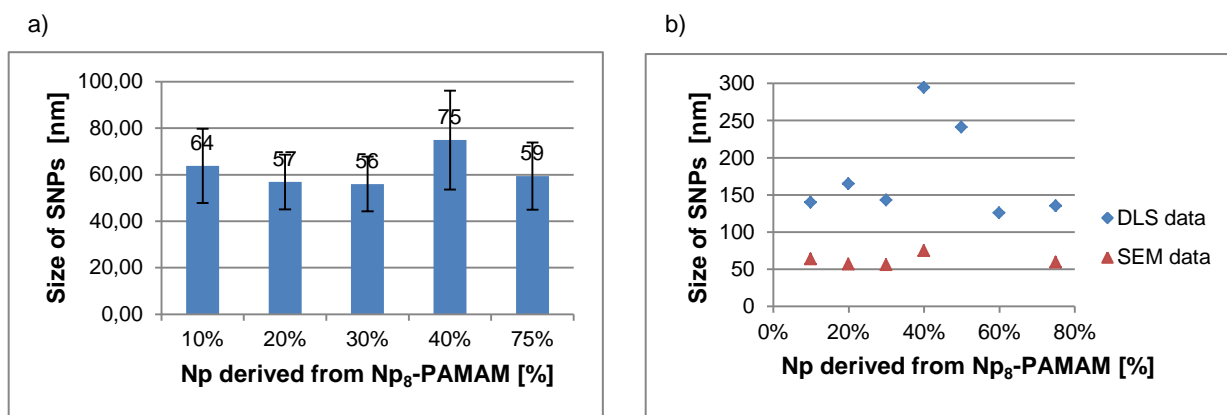


Figure 4.14: a) size of the supramolecular nanoparticles based on hr-SEM data average. b) SNPs diameter observed by DLS (♦) or SEM (▲).

As visible in the following sections, tests were carried out on particles assembled using a relative percentage between Np_8 -PAMAM and Np_2 -PEG (I) of 20%:80%. This percentage was chosen since the stopper and the core are assumed to be in the optimal ratio to prevent aggregation of the nanoparticles just formed. At the same time, this percentage should ensures proper crosslinking, which would not be possible if a lower or higher amount of dendrimer was used

4.3.2 Size control obtainable by altering the external condition

Of fundamental importance is the equilibrium on which this system is based. Even if supramolecular chemistry is in general based on weak interactions, ternary complexes and charge transfer interactions make an exception by exhibiting one of the stronger interactions. This is possible due to the ion-dipole interactions between the electron-deficient MV^{2+} and the electron-rich naphthol, which have been proven to have binding constants in the range of 10^{11} - 10^{13} M^{-1} .⁵⁷ The high stability of this complex implies that high energies are necessary for the reversible

disassembly of the supramolecular recognition units, therefore long times are required before obtaining stable nanoparticles upon repeated self-assembly/disassembly cycles. Therefore, the external conditions of the investigated system were varied by providing extra energy through a sonication treatment, or an increase of the temperature during the assembly stages, in order to perturb this equilibrium.

In all the tests, the relative concentration of Np_8 -PAMAM was fixed to 20% as it was assumed that with this relative percentage the amount of naphthol derived from the dendrimer and that derived from the stopper were in the best ratio to produce stable particles. The external conditions followed the scheme depicted in table 3.1.

4.3.2.1 Response of the system to sonication

Due to the formation of the dendritic layer, which reduces the diffusion of the supramolecular building blocks, sonication was applied to favor the dispersion of these building blocks. Therefore four samples, containing 20% of naphthol derived from Np_8 -PAMAM and the other 80% resulted from Np_2 -PEG (I), were subjected to a sonication treatment. These samples were exposed to ultrasonic waves for a variable time, ranging from 30 to 120 minutes, and then left one hour to stand at room temperature otherwise DLS measurements were not reproducible. DLS analysis was then performed to evaluate the influence of sonication on the hydrodynamic diameter.

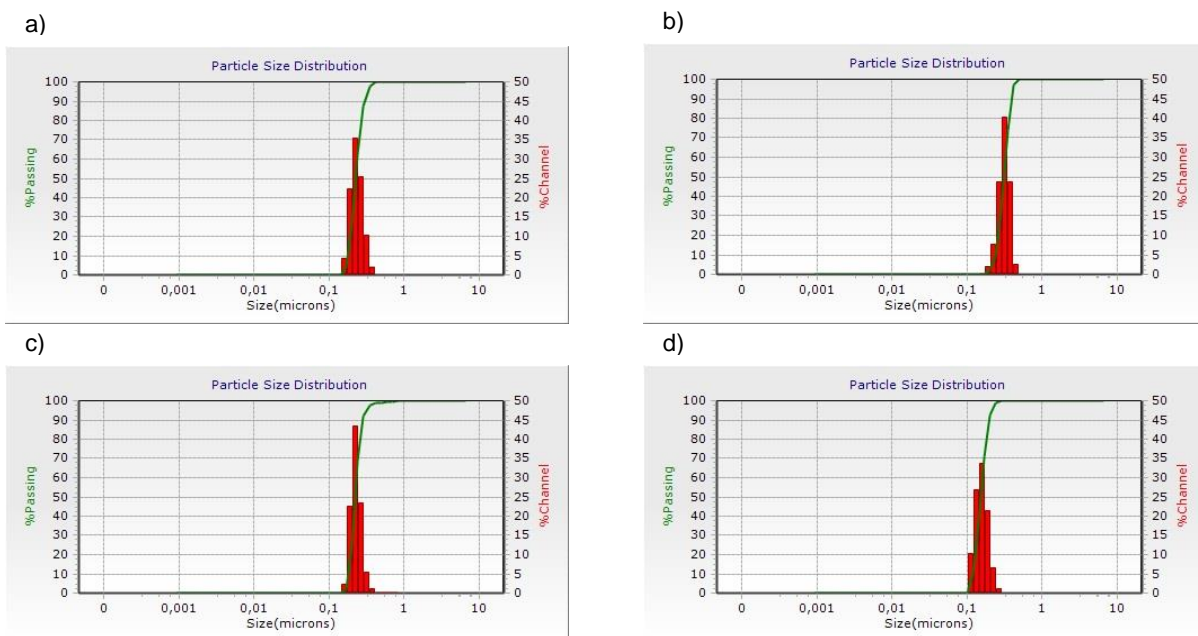


Figure 4.15: DLS plots for samples subjected to a sonication treatment for a) 30 minutes; b) 60 minutes; c) 90 minutes and d) 120 minutes.

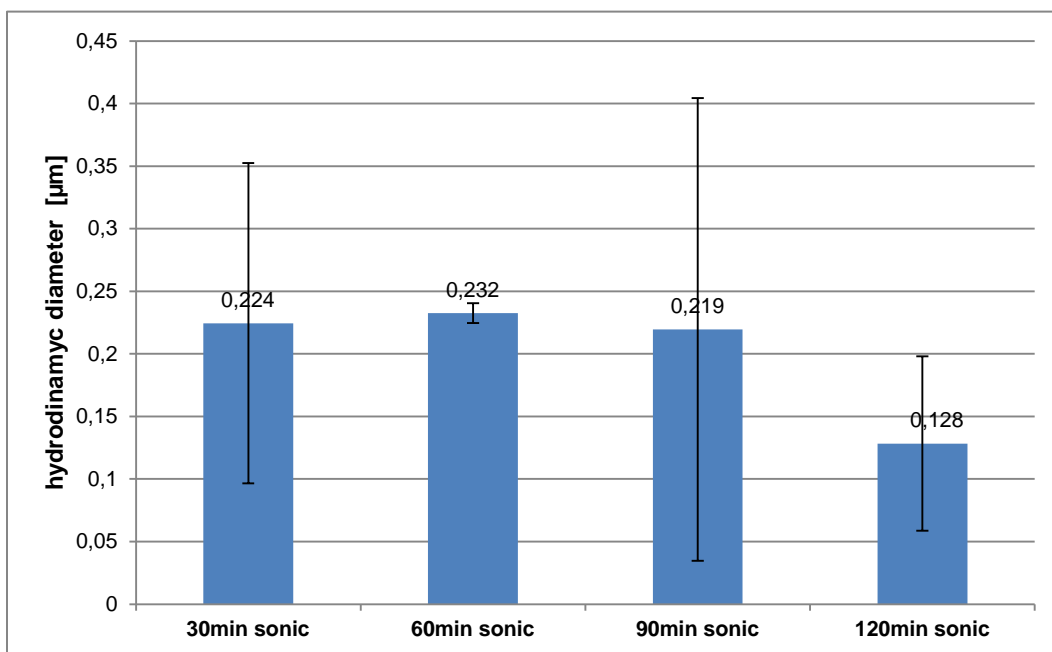


Figure 4.16: Hydrodynamic diameter of the supramolecular nanoparticles based on the DLS data average as a function of the sonication time.

The system just assembled was subjected to a sonication treatment and particles were observable even after one hour from the treatment (figure 4.15). By comparing data reported in figure 4.16, especially when the system was sonicated for 120 minutes, with data in figure 4.12, for a concentration of Np_8 -PAMAM of 20%, a decrease in size of the nanoparticles occurred after sonication (128 ± 70 nm vs. 165 ± 21 nm). However, from the mean data reported in figure 4.16, it can be noted that these particles present a broad standard deviation. This may be related to a failed achievement of the equilibrium which leads to the aggregation of the nanoparticles. Therefore, this treatment seems not able to supply the energy necessary to disassemble and reassemble the supramolecular recognition units, hence stable nanoparticles were not formed

4.3.2.2 Response of the system when assembled at higher temperatures

Temperature was also proven to affect the formation of all supramolecular systems. For this CB[8]-based system in particular it was demonstrated that the formation of nanoparticles occurs faster at higher temperatures because, after a first formation of the ternary complex, further assembly and disassembly steps are required to get well-defined particles⁵² and high temperatures speed up the association and dissociation mechanism.

Samples containing 20% of Np_8 -PAMAM and the 80% of Np_2 -PEG (I) were exposed at 30 °C or 40 °C for two hours and then allowed to rest one hour at room before DLS measurements (figures 4.17a and 4.17b).

The mean data obtained from DLS (figure 4.17c) showed a reduction in size of the SNPs, in comparison to those samples with the same composition but assembled at room temperature. This phenomenon is more appreciable when the temperature reaches 40 °C. A reduction of the standard deviation is also noticeable in figure 4.17c, suggesting that temperature may speed up the assembly and disassembly steps, thus leading to a faster formation of well-defined particles.

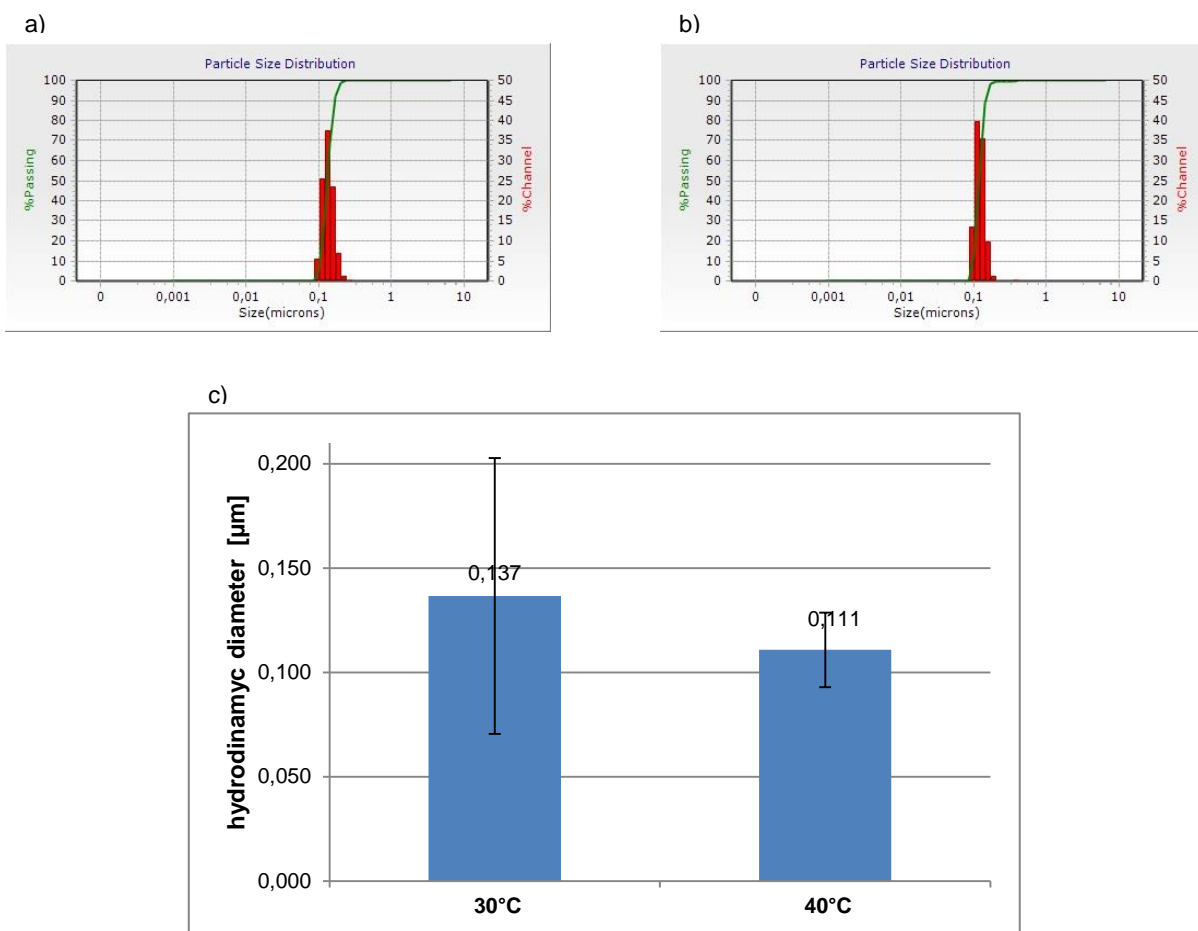


Figure 4.17: DLS plots for particles subjected to a temperature of 30 °C(a) and 40 °C (b) for two hours. c) plot of the hydrodynamic diameter based on DLS data average

Based on these results obtained after only 2 hours of treatment, the assembly behavior was monitored for 48 hours, carrying out time-dependent DLS measurements at room temperature, 30 °C and 40 °C (figure 4.18).

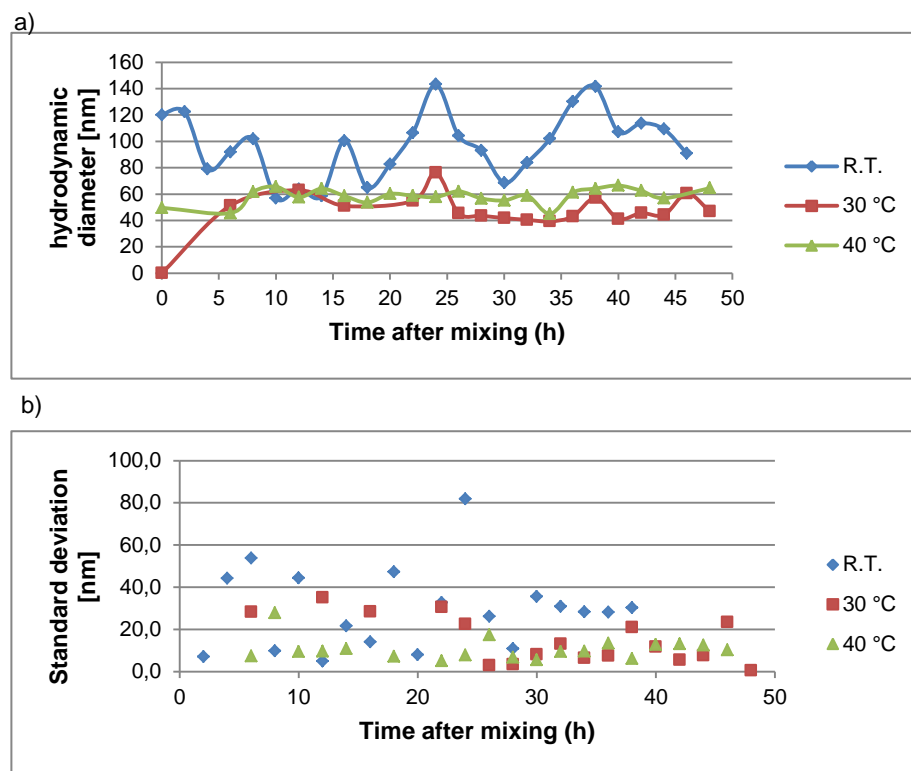


Figure 4.18: Time dependent DLS measurements. a) hydrodynamic SNPs diameter averaged over three measurements and b) corresponding standard deviation.

Graphs illustrated in figure 4.18 show that after two hours from the assembling particles assembled at both 30 °C or 40 °C are smaller in comparison with those particles subject at the same temperatures for two hours and then allowed to rest one hour at room temperature (figure 4.17). This phenomena might be ascribed to having left the particles at room temperature for one hour. Therefore, the energy supplied by increasing the temperature was lost preventing the disassembly/reassembly mechanism. Moreover, graphs in figure 4.18 describe the behavior in time of the system at different temperatures. At room temperature SNPs sizes vary in a broad range showing particles with a mean hydrodynamic diameter of 101 ± 36 nm. This broad range points out that the equilibrium is still underway even after 48 hours. When the supramolecular recognition units are assembled at 30°C, particles size fluctuates in a narrower range but this range still results in a broad standard deviation (figure 4.18b) which indicates that even if an increase of temperature possibly improves the formation of SNPs by speeding up the destruction and recreation of the ternary complex, the energy thus supplied is not enough to get stable and well-defined particles. By contrast, the sample assembled at 40 °C shows stable particles size (61 ± 13 nm) even 5 hours after samples preparation (figure 4.18a), presenting a narrow standard deviation in comparison with

the samples assembled at either R.T. or 30 °C. These results proved that the presence of a divalent stopper leads to a greater demand of energy to obtain stable particles, than that required when a monovalent stopper was used. This may be ascribed to the presence of multivalent interactions established between the bivalent stopper, the CB[8] and the MV-PEI. These multivalent interactions add their energy demand to the already high-energy request for the assembly and disassembly of the ternary complex. Assembly and disassembly of SNPs, which is the crucial step to obtain stable particles, may therefore be accelerated by increasing temperature. This result proved that stable and well-defined particles might be obtained when the energy barrier, generated by the ternary complex and the multivalent interactions, is overcome by working at higher temperatures.

4.3.3 Influence of the impurities present in the Np₂-PEG on the nanoparticles formation

As already stated above (section 4.1.5), nanoparticles were also assembled by using a stopping agent, which contained smaller amounts of impurities, to prove that these impurities do not affect the formation of the nanoparticles. Two control experiments were carried out by employing Np₂-PEG (II) highly purified as stopping agent. Firstly, nanoparticles were assembled at room temperature. Their hydrodynamic diameter was measured after 2 days from the assembling, in order to let them reach the equilibrium, by DLS.

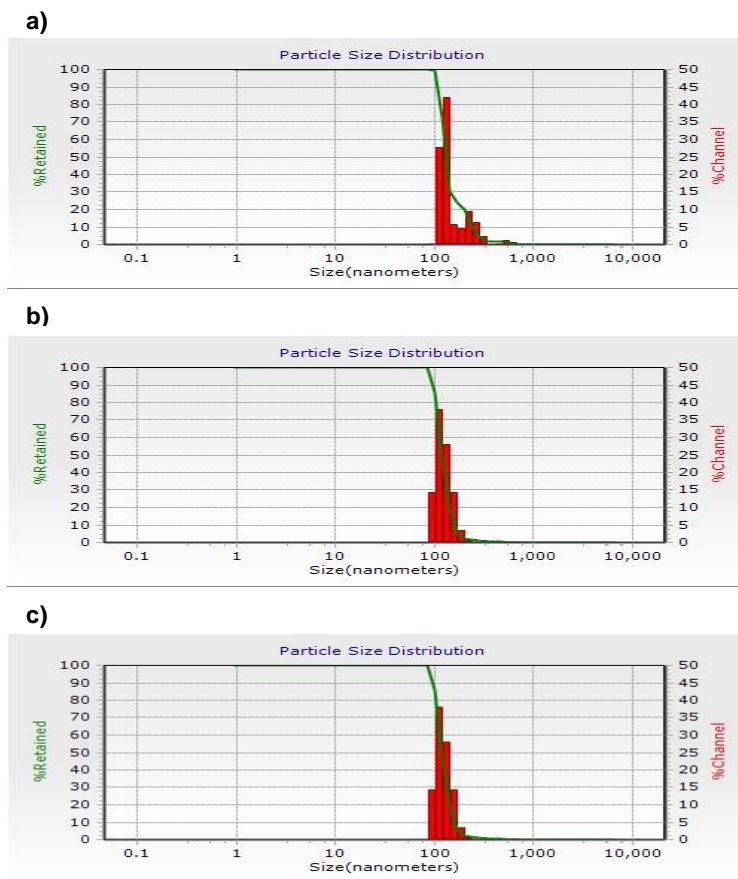


Figure 4.19: Dynamic light scattering (DLS) plots for samples with different percentage of naphthol derived from Np_2 -PEG (II) and Np_8 -PAMAM: a) 90%:10%; b) 80%:20% and c) 70%:30%

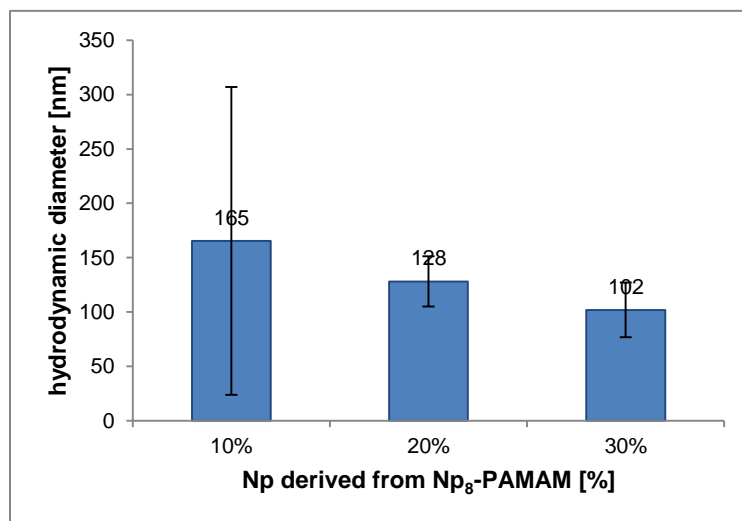


Figure 4.20: Hydrodynamic diameter of the supramolecular nanoparticles based on the DLS data average.

Figure 4.19 and 4.20 show the hydrodynamic diameter of these particles. It is worth noticing the similarity in size between those particles, as depicted in figure 4.11 and 4.12. Moreover, both particles show no size tunability, with comparable huge standard deviation, sign that no improvement was produced on the system.

The second control experiment was carried out in order to evaluate the influence of the highly pure Np₂-PEG (II) when particles are formed at higher temperature. Particles were assembled by using a relative percentage of naphthol coming from Np₈-PAMAM of the 20% of the total, consequently the relative percentage of Np₂-PEG (II) was 80%. The assembling was carried out by exposing the supramolecular recognition units at 40 °C for two hours. After two hours, the system was cooled down to room temperature and DLS measurements were performed on it.

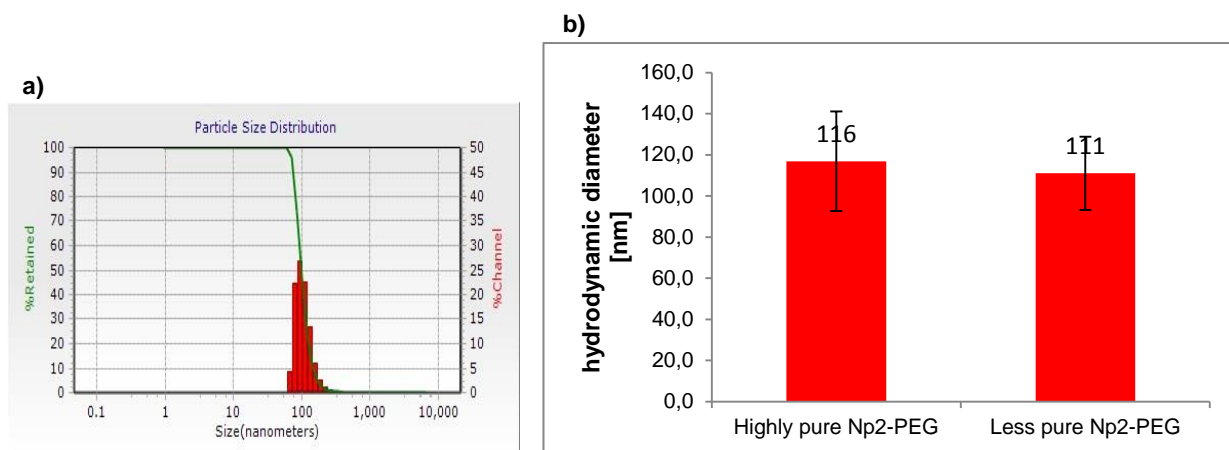


Figure 4.21: a) DLS plot for sample assembled at 40 °C with a relative percentage of naphthol derived from Np₂-PEG (II) and Np₈-PAMAM of 80%:20%. b) comparison graph of the size of particles, obtained after an exposure of 2 hours at 40 °C, between samples assembled with highly pure Np₂-PEG (II) and less pure Np₂-PEG (I).

These data (figure 4.21) shows that even if particles assembled at 40 °C have smaller size, in comparison with those particles assembled at room temperature, no significant variations occurred by using the less pure Np₂-PEG (I) (figure 4.21b). This result further proves that the higher purity of the Np₂-PEG (II) used in these experiments was not crucial in the system assembling, suggesting once again that temperature is the only parameter which can really improve the formation of stable and well-defined nanoparticles.

4.4 Supramolecular nanoparticles assembled with Np₁₆-PAMAM

In the CB[8]-based supramolecular nanoparticles Np₈-PAMAM acts as “core” by cross-linking the supramolecular structure, thus leading to the formation of the particles.

While polyamido-amine dendrimer “generation 1” (PAMAM G1) functionalized with 8 units of naphthol was already proven to be able to shape well-defined particles, allowing a control over the size by simply tuning the mixing ratio between the core and the stopping units.⁵² The same properties have not been investigated yet by a more interactive grafted core. On this purpose, polyamido-amine dendrimer “generation 2” (PAMAM G2) functionalized with 16 naphthol units was employed as the core, while the stopper used for the assembling of the CB[8]-based nanoparticles was the monovalent Np-PEG in order to study the effect of the increased valency on the core

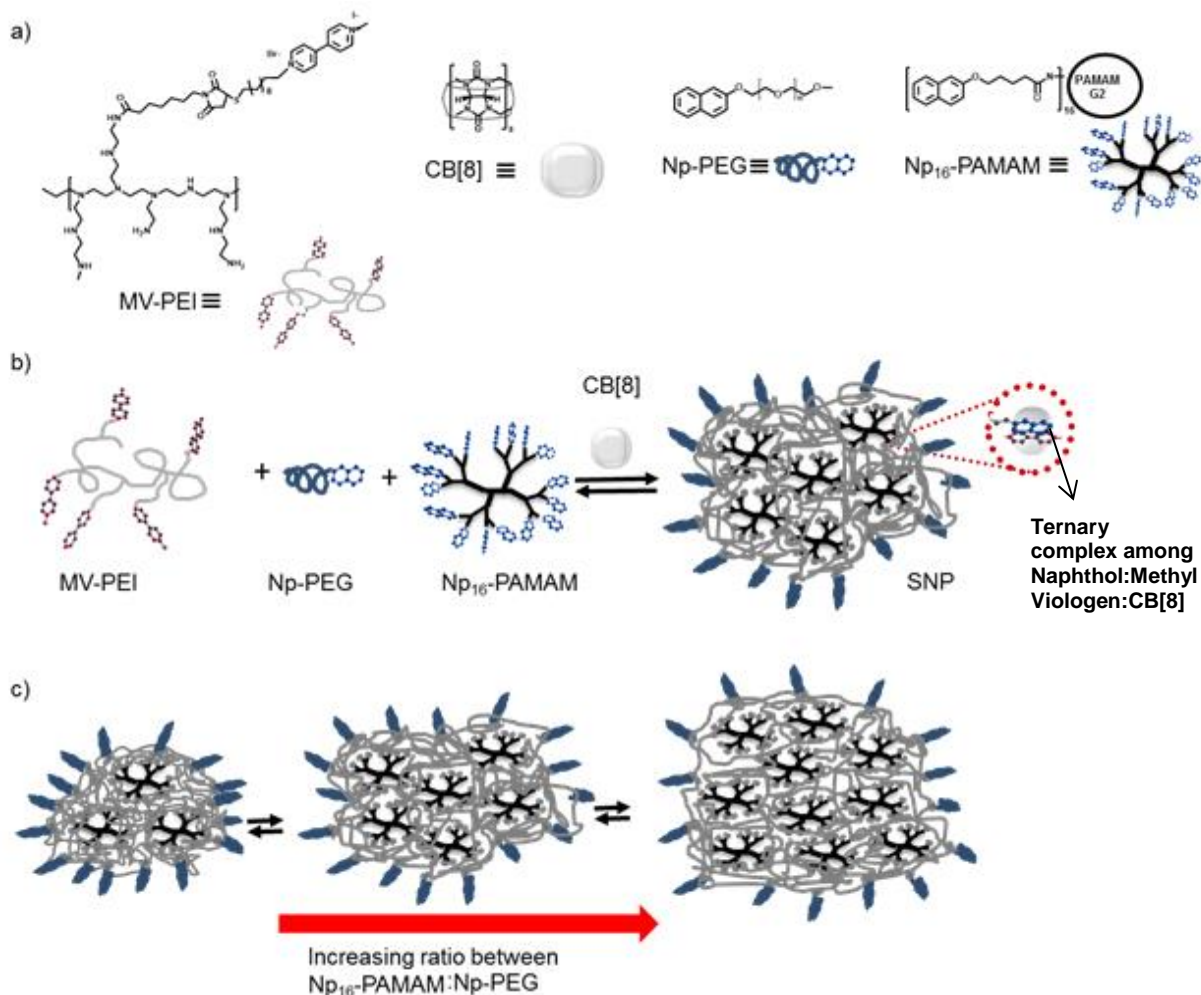


Figure 4.22: Scheme for SNPs formation using Np₁₆-PAMAM as core a) Supramolecular building blocks. b) Assembly of these building blocks to give a supramolecular nanoparticle. c) Size-control by controlling the ratio between SNP Np₁₆-PAMAM and Np-PEG.

4.4.1 Size control through the relative concentration of Np₁₆-PAMAM

The effect over nanoparticles size control was investigated when the relative percentage between the new core (Np₁₆-PAMAM) and the stopper (Np-PEG) was varied, while the ratio among the three supramolecular recognition units was kept constant to 1:1:1. The size tunability was investigated when the relative percentage of naphthol derived from Np₁₆-PAMAM was varied in a range between 10% and 30%. DLS measurements were performed to evaluate the size control over the SNPs thus assembled.

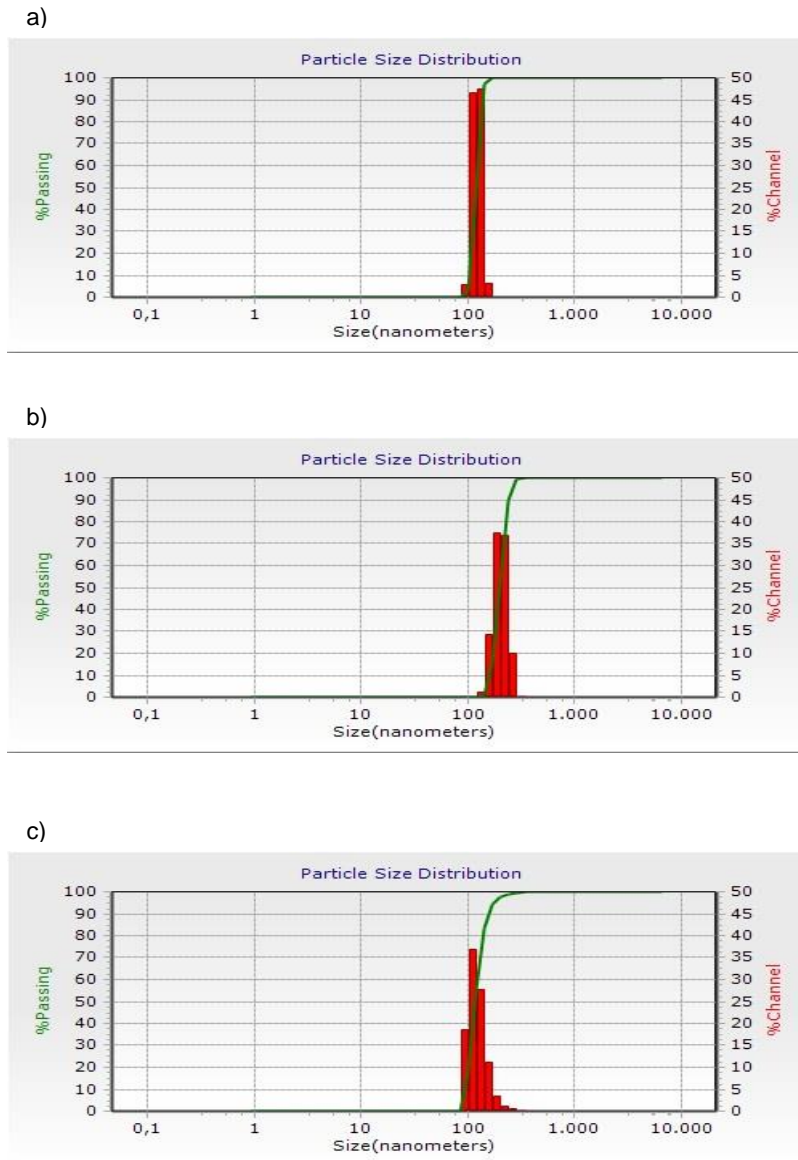


Figure 4.23: Dynamic light scattering (DLS) plots for samples with different percentage of naphthol derived from Np-PEG and Np₁₆-PAMAM: a) 90%:10%; b) 80%:20% and c) 70%:30%

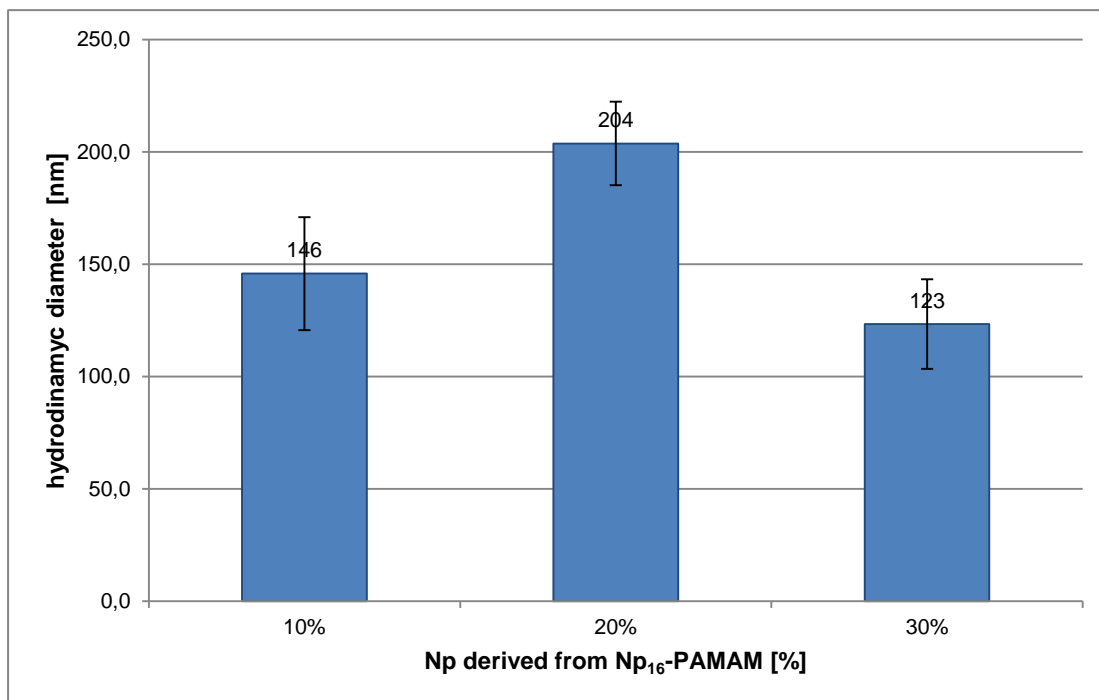


Figure 4.24: Hydrodynamic diameter of the supramolecular nanoparticles based on the DLS data average.

Nanoparticles assembled with the bigger dendrimer Np₁₆-PAMAM are expected to have bigger sizes than those assemblies with the smaller Np₈-PAMAM.

DLS measurements (figure 4.23) confirmed that SNPs may be formed when the octavalent core, based on the Np₈-PAMAM, is replaced by an hexadeca-valent core constituted by Np₁₆-PAMAM. However, even if nanoparticles are formed, a control over the size of these nanoparticles is not shown. Figure 4.24 makes a better idea by depicting the hydrodynamic diameter of these particles. It can be noted that when the relative percentage of Np₁₆-PAMAM increases from 10% to 20% particle size increases from 146 ± 25 nm to 204 ± 18 nm. Nevertheless, when the percentage of Np₁₆-PAMAM rises again from 20% to 30% the hydrodynamic diameter of the nanoparticles drops to 123 ± 20 nm.

As for the system which employs Np₈-PAMAM as core, this system is based on the equilibrium between the assembly and disassembly stages of the supramolecular recognition units (figure 4.22b). Therefore the formation of SNPs was studied by time-dependent DLS measurements, on samples assembled with a relative percentage of Np₁₆-PAMAM of 20%, as it was assumed to be the optimal ratio for the production of stable nanoparticles, in order to monitor the assembly behavior in time when Np₁₆-PAMAM was employed as core.

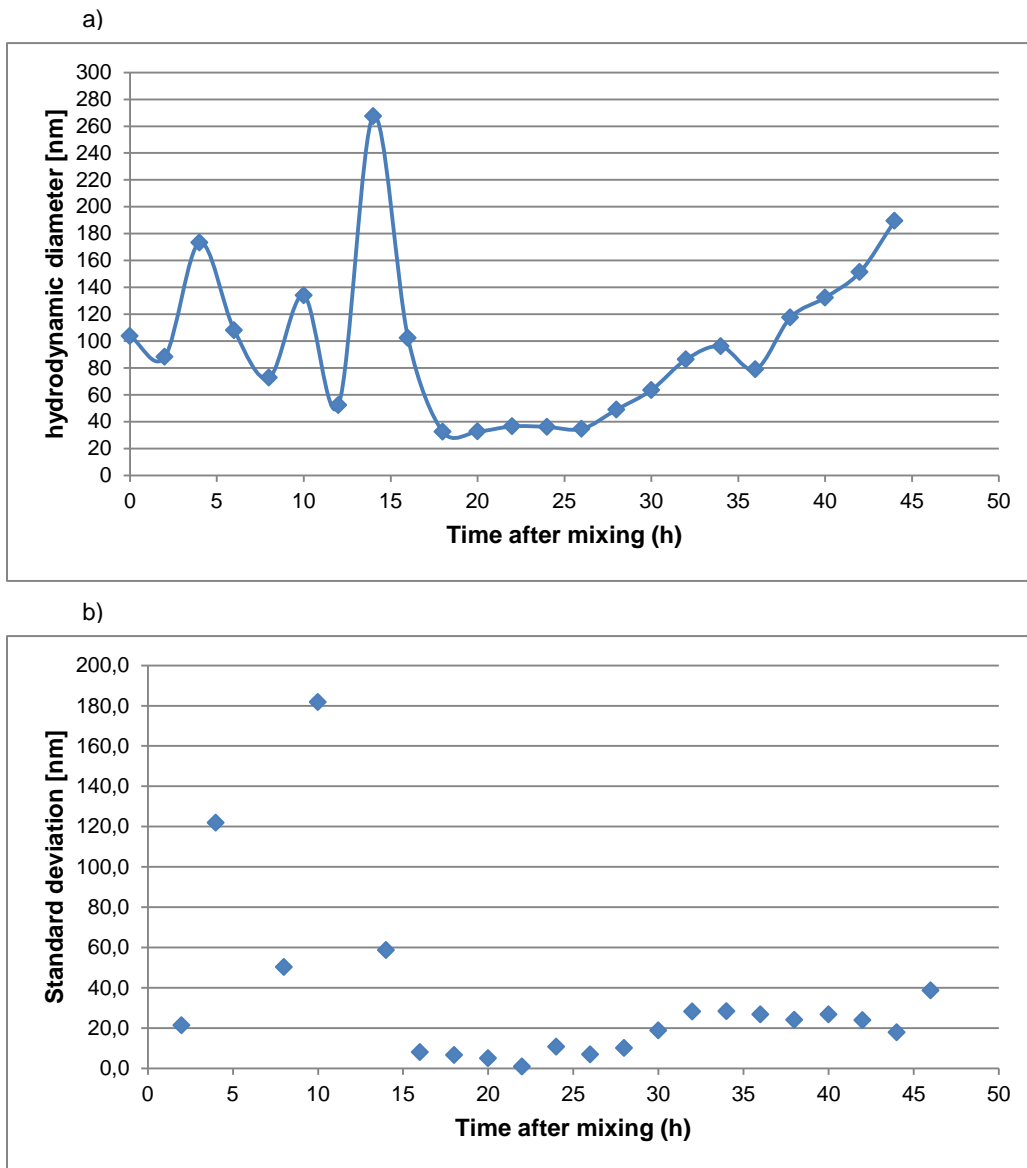


Figure 4.25: Time-dependent DLS data for particles assembled with a relative percentage of Np₁₆-PAMAM of 20%. a) hydrodynamic SNPs diameter averaged over three measurements and b) corresponding standard deviation.

Figure 4.25 shows the behavior of the system with time. During the first 15 hours particles size fluctuates in a broad range, *i.e.* from 52 to 270 nm, since the system is still far from reaching the equilibrium. After almost 17 hours from the assembling these particles begin to stabilize. However, it can be noted that particles increase their dimension during time, reaching an average size of 170 nm, in accordance with data obtained for those particles employing the same amount of Np₁₆-PAMAM (figure 4.23b and 4.24), possibly indicating that aggregation was taking place. However, these plots clearly show that the system was not able to reach the equilibrium even after 48 hours.

This may be attributed to the dendrimer and the increased amount of multivalent intermolecular connections. As for the stopper, an increase of the valency leads to a greater energy barrier to overcome for the formation of stable nanoparticles. This barrier cannot be overcome by working at room temperature but, due to a lack of time, further experiments at higher temperature were not performed.

To have a better overview on this system, SEM analysis was performed on samples containing 10%, 20% and 30% of naphthol derived from Np₁₆-PAMAM and prepared following the procedure described in chapter 3.2.

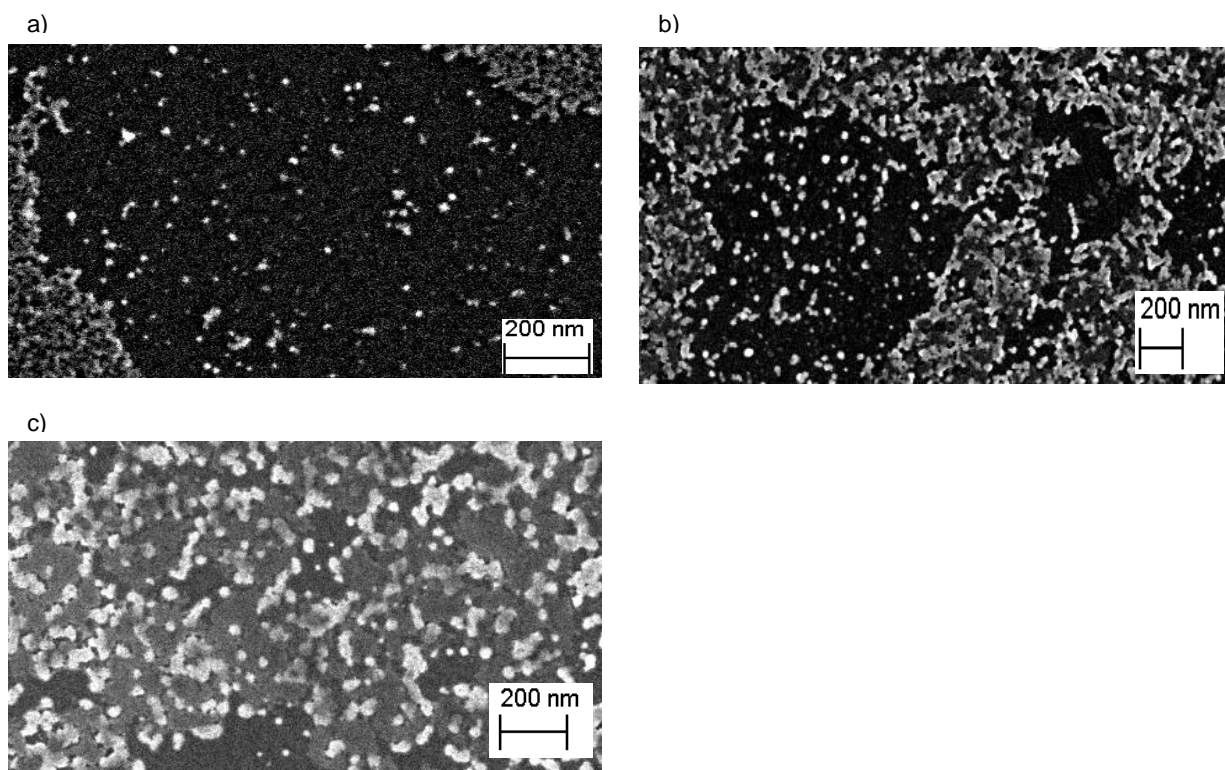


Figure 4.26: SEM images for the system with different percentage of naphthol derived from Np₁₆-PAMAM: a) 10%; 20%; c) 30%

Figure 4.26a shows particles formed when the relative percentage of Np₁₆-PAMAM used was 10%. Here distinct particles, with an average diameter of 28 ± 20 nm, are surrounded by a layer of material and other particles which start to aggregate. When the percentage of Np₁₆-PAMAM reaches 20% (figure 4.26b) distinct particles are less visible while bigger aggregates are present. Figure 4.26c shows SEM image for samples with a relative percentage of dendrimer of 30%. Here distinct particles are not visible anymore, but aggregates, formed by several particles stuck together, are present.

From these images a layer, probably made by an excess of dendrimer, seems to trap the nanoparticles reducing their mobility and the diffusivity of the supramolecular recognition units. It might also be assumed that some of the particles shown are simply micelles formed by PEG during the drying of the sample. By combining the data obtained from DLS measurements and those obtained from SEM images, is possible to assume that the presence of this layer leads to an increase of the energy demand even higher than that required for the assembly and disassembly of the ternary complex made by naphthol:methyl-viologen:CB[8]. Therefore, the attainment of the equilibrium is prevented at room temperature and no well-defined particles can be obtained.

4.4.2 Size control by adjusting the ratio among the supramolecular recognition units

The presence of Np₁₆-PAMAM facilitates the formation of more intermolecular cross linking, which prevents the stability of the particles and lead to the aggregation of the supramolecular nanoparticles. To avoid this problem, the overall concentration of the stopper was increased by changing the ratio among the supramolecular recognition units. In particular, the ratio was changed from 1:1:1 (CB[8]:MV²⁺:Np, with naphthol coming from Np-PEG and Np₁₆-PAMAM) to 1:1:1:X (where X is comprised between 0.25 and 2, and it represents the molar ratio among CB[8]:MV²⁺:Np-PEG:Np₁₆-PAMAM). By changing the molar ratio among the recognition units, a higher and constant amount of stopper was thus ensured to the system in order to guarantee higher shielding property to the nanoparticles. Conversely, the amount of Np₁₆-PAMAM was varied in order to evaluate the size tunability of the system.

Samples were prepared by following the procedure described in section 3.4.2. Their hydrodynamic diameter was evaluated by DLS measurements. Their behavior with time was also monitored by DLS measurements after 2 hours, 1 day and 4 days from the assembling process.

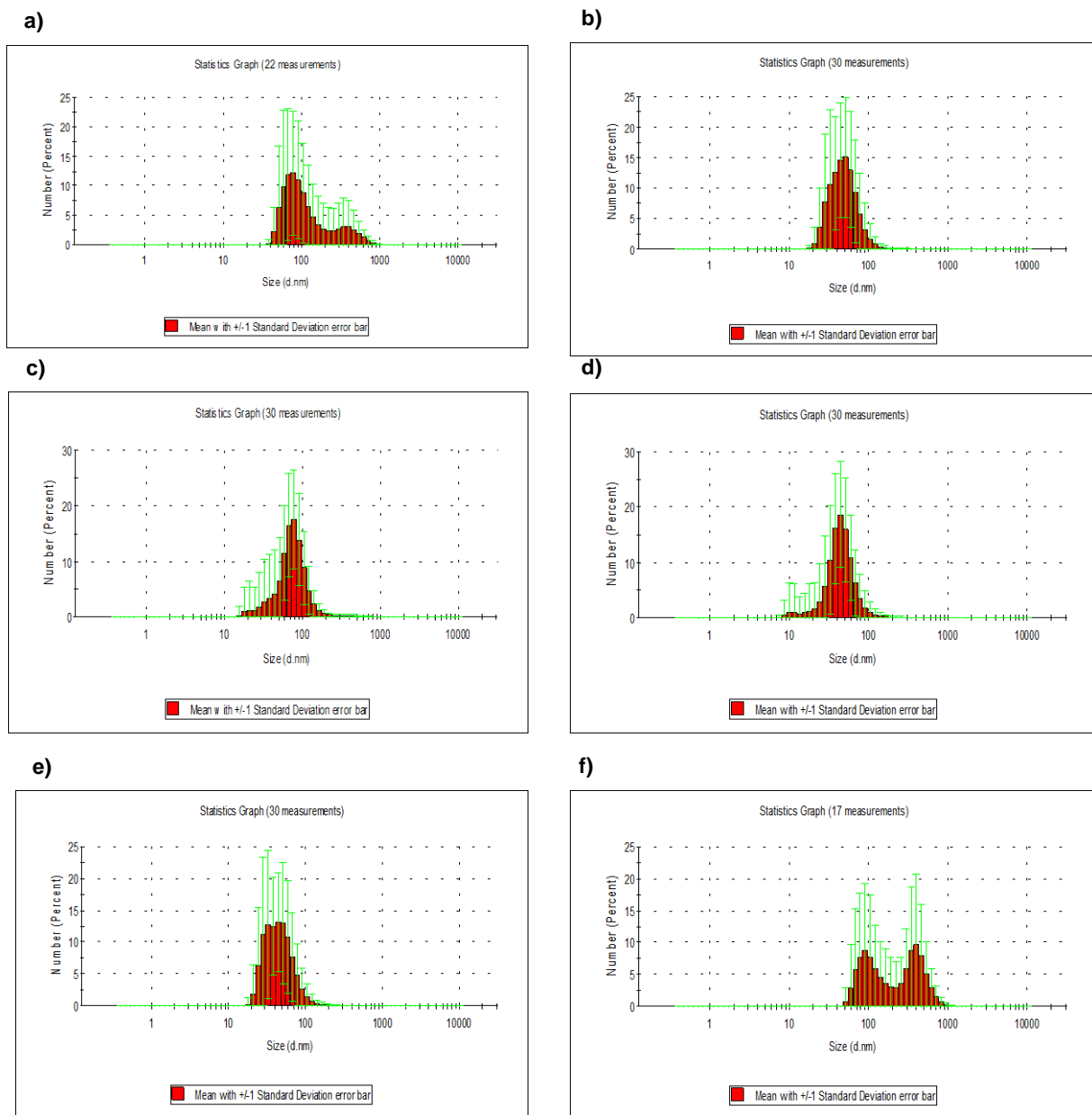


Figure 4.27: Dynamic light scattering (DLS) plots for samples with different ratio among CB[8]:MV²⁺:Np-PEG:Np₁₆-PAMAM: a) 1:1:1:0.25; b) 1:1:1:0.5; c) 1:1:1:0.75; d) 1:1:1:1; e) 1:1:1:1.5; f) 1:1:1:2. Measurements performed after 2 hours from the assembling

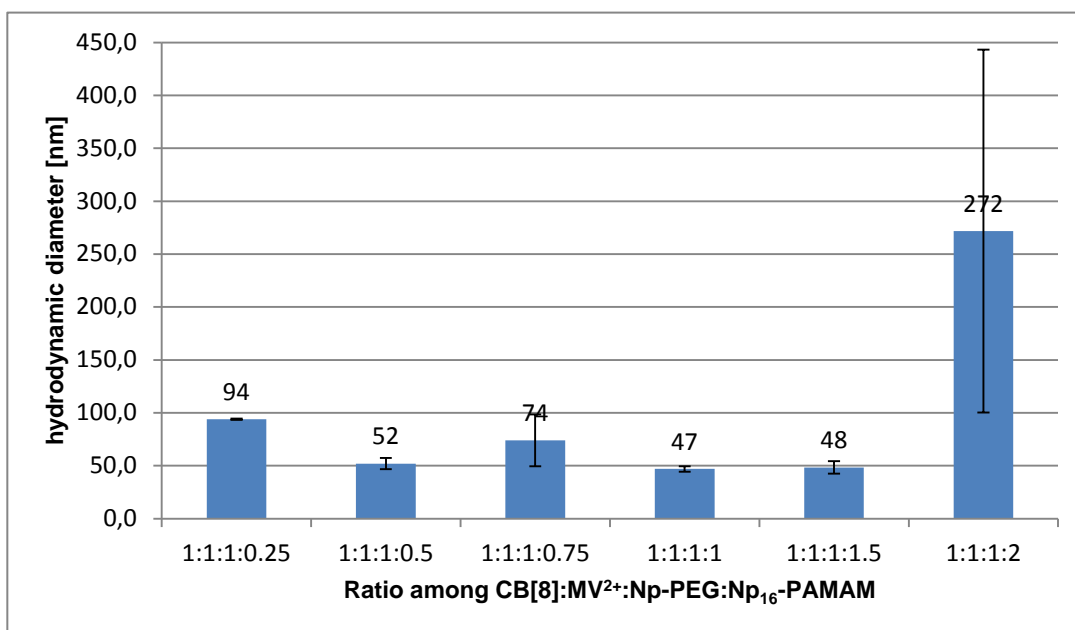


Figure 4.28: Hydrodynamic diameter of the supramolecular nanoparticles based on the DLS data average after 2 hours from the assembling.

Figures 4.27 and 4.28 show that nanoparticles are present after only 2 hours from the assembling. Even if a trend of the nanoparticles size is not shown, a clear reduction of the dimension is visible (except for that sample with a ratio among the recognition units of 1:1:1:2) in comparison with samples assembled by respecting the traditional ratio of 1:1:1 (figures 4.23 and 4.24), where the naphthol content is the sum of the naphthol coming from the stopper and that coming from the dendrimer. These data demonstrate that by increasing the amount of the stopper the particles are better shielded, thus leading to a reduction of their size. However, when the ratio was 1:1:1:2 (*i.e.* when the amount of naphthol was no longer the sum of that coming from the dendrimer and the stopper, but when it was divided keeping constant to 1 the amount of naphthol coming from the stopper and varying the amount of naphthol coming from the dendrimer), the amount of dendrimer exceeded the amount of stopper. Therefore cross-linking could take place, generating aggregation among the nanoparticles.

Data depicted in figure 4.27 and 4.28 were obtained after only 2 hours from the assembling, so the system may be assumed to be out the equilibrium state because not enough time has been granted for the assembling and disassembling steps of the recognition units. To evaluate the SNPs when the time elapsed between the assembling and the measurements was higher, DLS analysis were performed after 1 day and after 4 days.

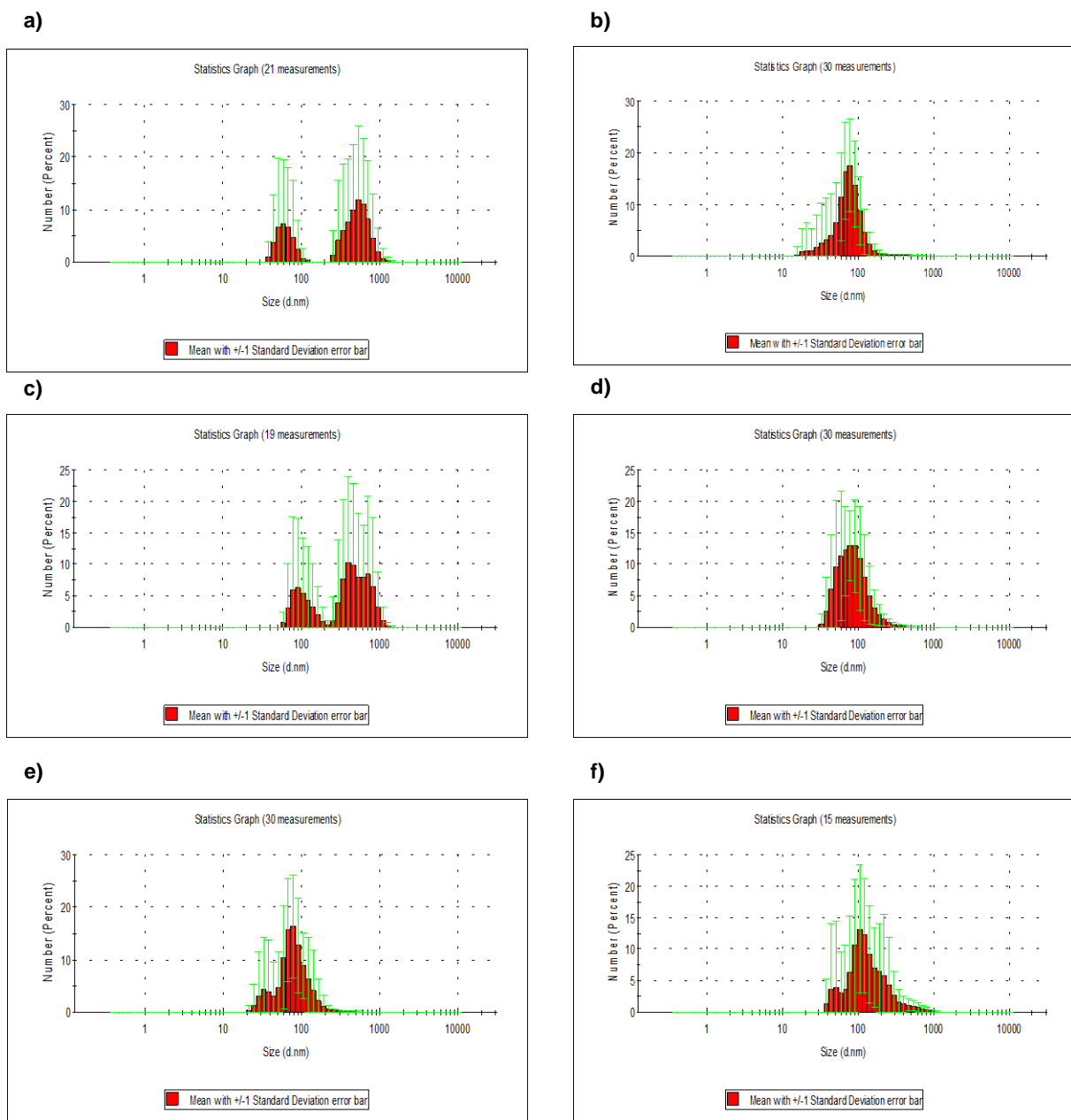


Figure 4.29: Dynamic light scattering (DLS) plots for samples with different ratio among CB[8]:MV²⁺:Np-PEG:Np₁₆-PAMAM: a) 1:1:1:0.25; b) 1:1:1:0.5; c) 1:1:1:0.75; d) 1:1:1:1; e) 1:1:1:1.5; f) 1:1:1:2. Measurements performed after 1 day from the assembling

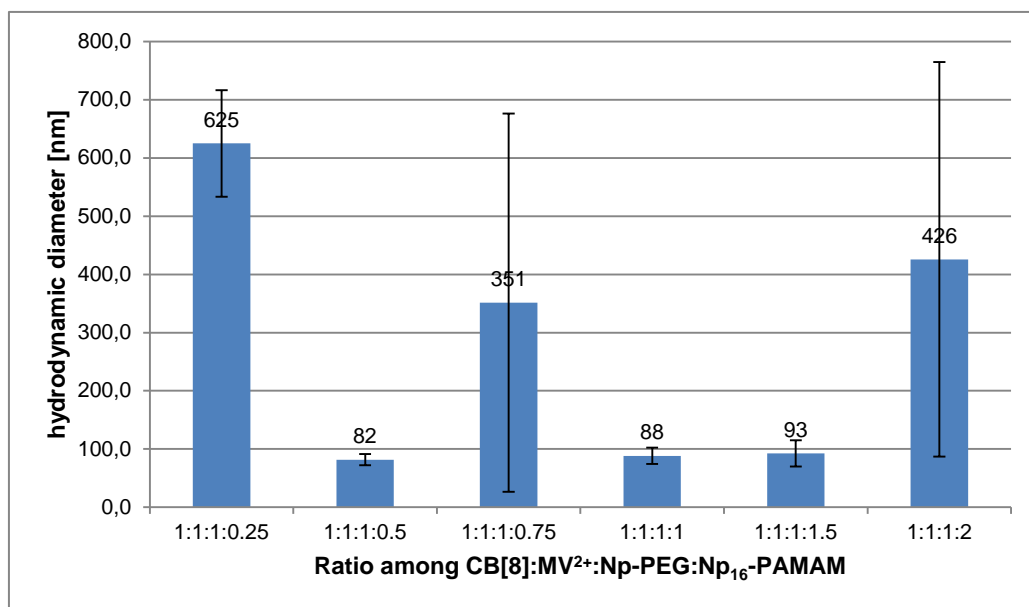


Figure 4.30: Hydrodynamic diameter of the supramolecular nanoparticles based on the DLS data average after 1 day from the assembling

Figures 4.29 and 4.30 show data obtained after 1 day from the assembling process. It is clear that particles increased their size after 1 day, confirming the hypothesis that after 2 hours the equilibrium was not reached yet. Notably, particles obtained with composition ratio between 1:1:1:0.5 and 1:1:1:1.5 (figure 4.30) show a size trend. This behavior implies that a control over the size of the SNPs might be possible by tuning the amount of the core. The higher concentration of the stopper employed in this system, compared to that which adopts the 1:1:1 ratio among the supramolecular recognition units, ensures high covering of the nanoparticles, thus preventing their uncontrolled aggregation. Therefore, when the amount of core increases particles do not aggregate and, within certain limits, a good control of their size is achieved.

Conversely, when the amount of core, or stopper, was too high (particles assembled with a ratio of 1:1:1:2 and 1:1:1:0.25 respectively) excessive cross linking, or a destruction of the network take place, respectively. The large size and broad standard deviation for those particles assembled by using a ratio among CB[8]:MV²⁺:Np-PEG:Np₁₆-PAMAM of 1:1:1:0.75 was attributed to DLS machine failure.

To ensure to the system enough time to achieve the equilibrium, samples were analyzed after 4 days from the assembling by DLS analysis. Data obtained are shown in figure 4.31 and 4.32

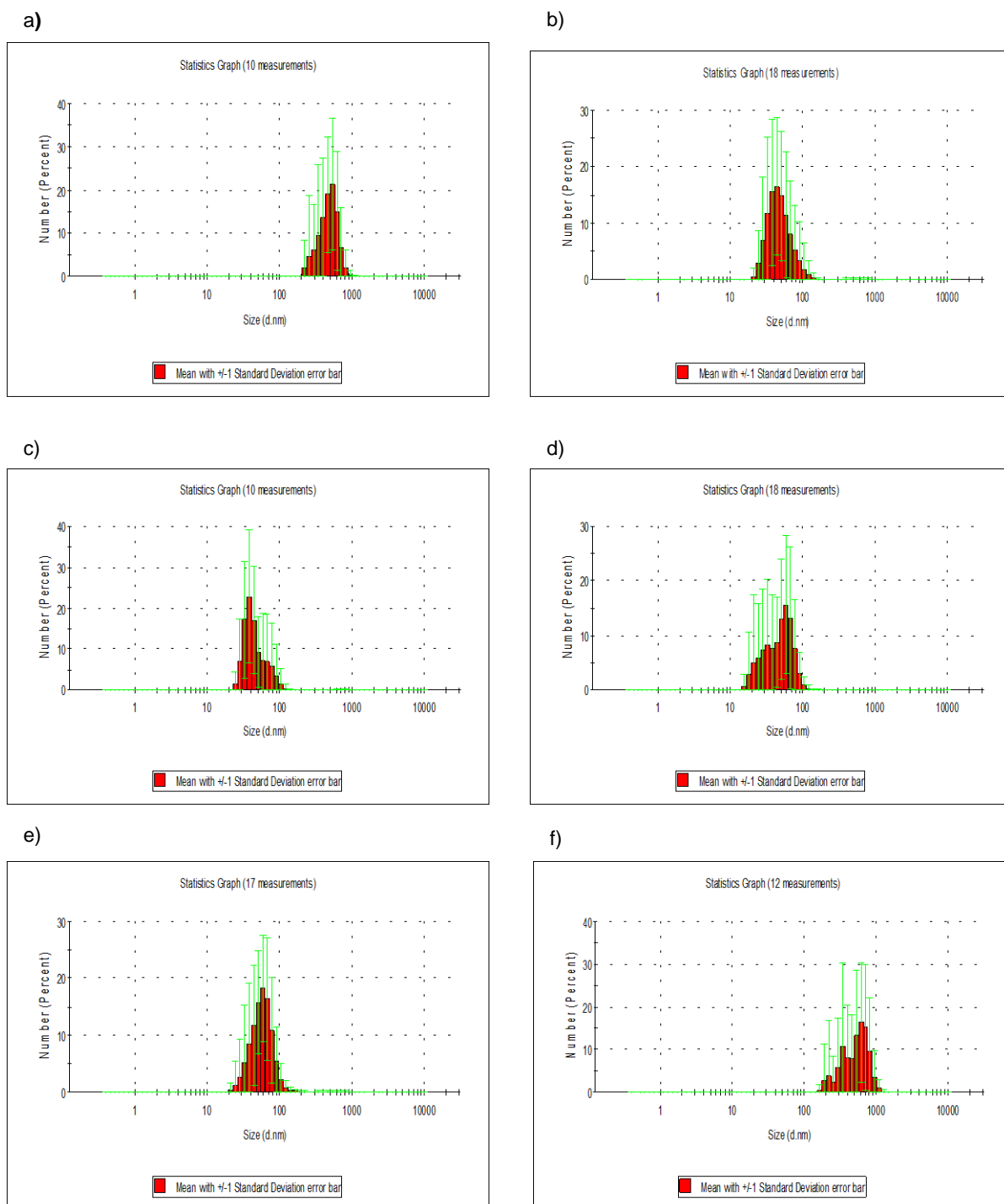


Figure 4.31: Dynamic light scattering (DLS) plots for samples with different ratio among CB[8]:MV²⁺:Np-PEG:Np₁₆-PAMAM: a) 1:1:1:0.25; b) 1:1:1:0.5; c) 1:1:1:0.75; d) 1:1:1:1; e) 1:1:1:1.5; f) 1:1:1:2. Measurements performed after 4 days from the assembling.

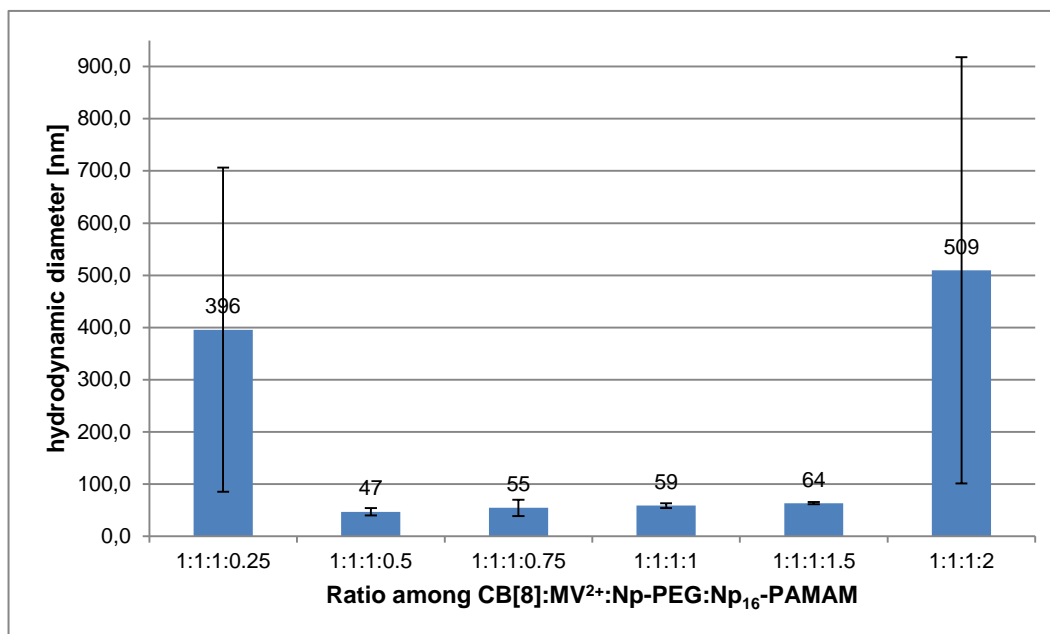


Figure 4.32: Hydrodynamic diameter of the supramolecular nanoparticles based on the DLS data average after 4 days from the assembling.

Data depicted in figure 4.32 shows that nanoparticles size, in comparison with those obtained after 1 day from the assembling, decreased. This may be ascribed to an enhanced disassembly and reassembly of the supramolecular recognition units, which gives higher stability to the nanoparticles and leads to well-defined SNPs. What is also noticeable is that the size-trend outlined after one day from the assembling (figure 4.30) is now confirmed. This proves the hypothesis that by employing a molar ratio among CB[8]:MV²⁺:Np-PEG:Np₁₆-PAMAM in a range between 1:1:1:0.5 and 1:1:1:1.5 the concentration of the stopper and the core are in a good ratio for the formation of nanoparticles characterized by a small hydrodynamic diameter, a narrow standard deviation and also with the possibility to tune the size of the SNPs. The prevalence of the stopper (Np-PEG), and its monovalent character, ensures good shielding of the nanoparticles. Therefore, a control over the size of the nanoparticles may be obtained by simply playing on the ratio of the supramolecular recognition units. As for the assembling after 1 day, when the amount of stopper, or core, is too high, particles are not well shaped (figure 4.31 and 4.32). If the amount of core exceeds in a way too high the amount of stopper, intermolecular cross linking occurs, thus forming large size aggregates. By contrast if the amount of stopping units is too high they destroy the network and the formation of well-defined nanoparticles is not possible.

SNPs thus obtained were also analyzed by SEM microscopy after 7 days from the assembling process in order to have a broader view of their behavior.

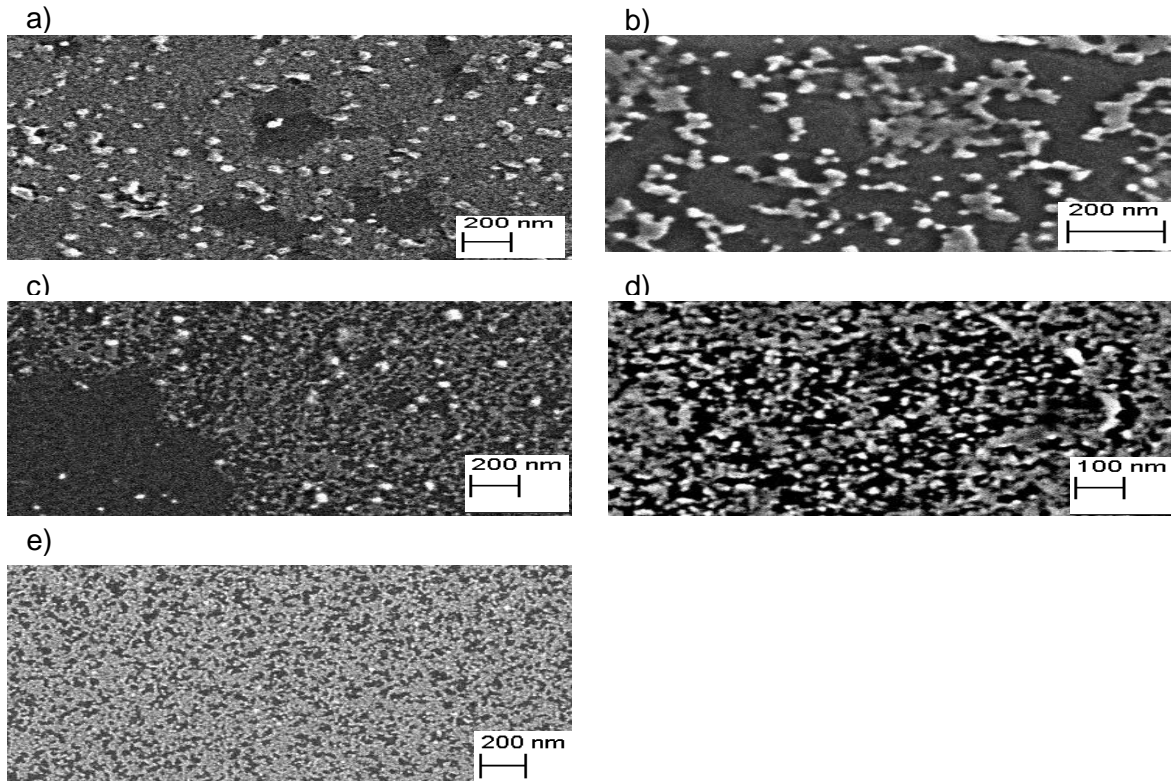


Figure 4.33: SEM images for samples with different molar ratio among CB[8]:MV²⁺:Np-PEG:Np₁₆-PAMAM: a) 1:1:1:0.25; b) 1:1:1:0.5; c) 1:1:1:0.75; d) 1:1:1:1; e) 1:1:1:2.

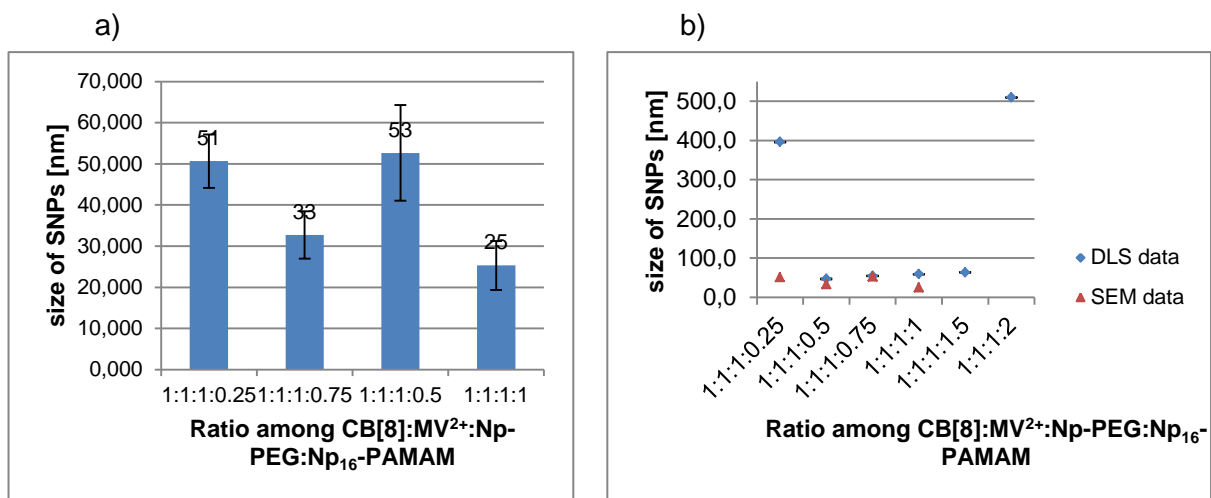


Figure 4.34: a) size of the supramolecular nanoparticles based on hr-SEM data average. b) SNPs diameter observed by DLS (◆) or SEM (▲).

Figures 4.33a and 4.33e show particles after 7 days from the assembling procedure with a molar ratio among the supramolecular recognition units of 1:1:1:0.25 and 1:1:1:2. It indicates that an excess of stopper or dendrimer, respectively, is present. As already stated, if too much stopper, or core, is present in solution is not possible to obtain stable and well defined nanoparticles due to an irregular formation of intermolecular cross-linking. In figure 4.33a white spots are visible. While the smaller spots might be attributed to micelles formed by drying out SEM sample, the bigger ones might be associated to SNPs. These nanoparticles look mostly aggregated and not well-defined. This aggregation may also explain the huge discrepancy between DLS and SEM data (figure 4.34b). Albeit the laser of the DLS was able to measure even these particles, SEM samples were prepared by taking an aliquot of the solution from the top of it. Most likely, this aliquot did not contain the bigger particles which were precipitated. The same could happen for sample depicted in figure 4.33e. Here an excess of core is present (white-grey stains). Therefore particles are aggregated and mostly of them precipitated, so that they were not included in the sample analyzed at the microscope. Figures 4.33b and 4.33c show particles assembled with a ratio among CB[8]:MV²⁺:Np-PEG:Np₁₆-PAMAM of 1:1:1:0.5 and 1:1:1:0.75 respectively. In both pictures free nanoparticles are visible even if some PEG residue (dark-grey stains) and micelles are still present. Here particles size is in a good agreement with that obtained by DLS measurements (figure 4.34b). Picture 4.33d shows particles assembled with a molar ratio among the recognition units of 1:1:1:1. Even if some free particles are still visible, a layer, probably made by the excess of core (grey stains) is taking place and seems to trap these nanoparticles. By comparing data obtained by SEM and those obtained by DLS is visible that they are not in a good accordance (59 ± 5 nm vs. 25 ± 6 nm) and it is probably due to the sampling method. Therefore, for this reason particles assembled with a molar ratios among CB[8]:MV²⁺:Np-PEG:Np₁₆-PAMAM of 1:1:1:1.5 were not measured by SEM.

5 CONCLUSIONS AND OUTLOOK

In this work, novel CB[8]-based supramolecular nanoparticles based on the ternary complex formation among CB[8]:MV²⁺:Np were assembled, and the influence of the multivalency over the size-tunability was studied. A bivalent stopper and a more intense grafted core, based on a poly amido-amine (PAMAM) "generation 2", were firstly synthesized and then employed as recognition units and the effects of their enhanced valency was investigated. The bivalent stopper (Np₂-PEG) was synthesized by binding naphthol molecules to a triethylene spacer followed by grafting two of these obtained molecules to a benzene ring, which was then reacted with a PEG₅₀₀₀. However, due to some oily residue, this Np₂-PEG has not been used as supramolecular building block and it was replaced by the previously synthesized and highly pure Np₂-PEG (I). Conversely, the more intense grafted core Np₁₆-PAMAM was obtained by the complete functionalization of the PAMAM dendrimer "generation 2" with 16 units of naphthol through amide bond formation.

The size-tunability of the supramolecular nanoparticles, assembled with the bivalent stopper, was studied by varying the relative molar percentage between Np₂-PEG and Np₈-PAMAM. DLS and SEM measurements have shown that a control over the size of the nanoparticles is not possible by only changing the molar percentage between the two naphthol recognition units. In fact, the only change of the molar percentage between the naphthol units leads to the formation of irreproducible and aggregated nanoparticles. Contrary, the increased valency of the stopper induces the formation of more stable ternary complexes, thus preventing the disassembly and reassembly of the four supramolecular building blocks. Therefore, well-defined particles cannot be formed due to the high energy required to reach the thermodynamic equilibrium. However, the preliminary experiments carried out at higher temperature have shown that by increasing the temperature up to 40 °C, particles characterized by less aggregation, increased stability and smaller hydrodynamic diameter (61 ± 13 nm compared to 165 ± 21 nm of those particles assembled at room temperature) are formed. These results will stimulate the design of new experiments, taking advantages of the assembling at higher temperature. In particular, it would be interesting to prove if a control over the size of the supramolecular nanoparticles can be obtained when the assembling is carried out at higher temperature and the relative percentage among the supramolecular recognition units is changed. This would lead to a production of nanoparticles with a wide spectra of size which are easy to assemble and with an enhanced stability provided by the increased valency of the system.

The studies about the increased valency in the core of the nanoparticles have shown that by employing a more intense grafted core intermolecular crosslinking are favored, thus leading to the

formation of aggregated and not well-defined nanoparticles. By respecting the 1:1:1 ratio among MV^{2+} :CB[8]:Np-PEG/Np₁₆-PAMAM, required for the formation of the ternary complex, the amount of the stopper is not enough to control the intermolecular network formation, favored by the increased valency of the core. However, DLS and SEM measurements proved that a control over the crosslinking is possible when the ratio among the supramolecular recognition units is changed from the traditional 1:1:1 to the newly 1:1:1:X, where X represents the amount of Np₁₆-PAMAM and is comprised between 0.25 to 1.5. By employing this ratio an higher coverage of the nanoparticles was obtained, whereas an increase in the amount of dendrimer leads to an increase of the nanoparticles size from 47 nm to 64 nm. Therefore, the size of the supramolecular nanoparticles can be effectively modulated by controlling the molar ratio among the supramolecular building blocks.

Moreover, it would be attractive to improve the disassemble and drug release mechanism. Recently, Huskens *et al.* has developed an UV/light-based mechanism to reversibly assemble and disassemble CB[8]-based nanoparticles based on the formation of the ternary complex with azobenzene instead of naphthol.⁵³ These results will open the possibility to evaluate if this mechanism may also works on a system characterized by an higher overall valency. This would make nanoparticles that, in addition to a greater stability, offer the possibility to be easily and reversibly assembled and disassembled, thus becoming an interesting vector for drug delivery.

Once optimized their assembly and stability with time, these supramolecular systems will surely serve as innovative and smart encapsulating agents of drugs, proteins and genes.

REFERENCES

1. J.-M. Lehn, *journal of inclusion phenomena*, 1988, 351-396.
2. J. S. Lindsey, *New J. Chem.*, 1991, **15**, 153-180.
3. G. M. Whitesides, J. P. Mathias and C. T. Seto, *Molecular self-assembly and nanochemistry: a chemical strategy for the synthesis of nanostructures*, DTIC Document, 1991.
4. J. L. A. Jonathan W. Steed, ed. Wiley, 2009.
5. J. K. M. S. Christopher A. Hunter, *J. Am. Chem. Soc.*, 1990, 5525-5534.
6. D. A. D. Jennifer C. Ma, *Chem. Rev.*, 1997, 1303-1324.
7. Y. H. Ko, Kim, E.; Hwang, I.; Kim, K., *Chemical communications*, 2007, 1305-1315.
8. G. V. Oshovsky, D. N. Reinhoudt and W. Verboom, *Angewandte Chemie International Edition*, 2007, **46**, 2366-2393.
9. A. N. Kim A. Sharp, Richard Friedman, Barry Honig, *Biochemistry*, 1991, **30**, 9686-9697.
10. S. J. Loeb and J. A. Wisner, *Angewandte Chemie International Edition*, 1998, **37**, 2838-2840.
11. W. J. Lees, A. Spaltenstein, J. E. Kingery-Wood and G. M. Whitesides, *J. Med. Chem.*, 1994, **37**, 3419-3343.
12. L. K. BIRGIT BENDEBY, CORINE SANDSTRO M, *j. incl. phenom. macrocycl. chem.*, 2004, 173-181.
13. J. Szejtli, *Chem. Rev.*, 1998, **1743-1753**.
14. N. G. Hădărugă, *Chemistry Central Journal*, 2012, **6**, 16.
15. S. Bhatia, M. Dimde and R. Haag, *MedChemComm*, 2014, **5**, 862-878.
16. A. Mulder, J. Huskens and D. N. Reinhoudt, *Organic & biomolecular chemistry*, 2004, **2**, 3409-3424.
17. C. W. C. Jason E Gestwicki, Laura E Strong, Karolyn A Oetjen, Laura L Kiessling, *J. Am. Chem. Soc.*, 2002, **124**, 14922-14933.
18. Daniel Pagé and R. Roy, *Bioconjugate Chem.*, 1997, **8**, 714-723.
19. D. J. Cram, *J. incl. phenom.*, 1988, **6**, 397-413.
20. J. J. Lundquist and E. J. Toone, *Chem. Rev.*, 2002, **102**, 555-578.
21. S.-K. C. Mathai Mammen and G. M. Whitesides, *Angew Chem Int Ed*, 1998, **37**, 2754-2794.
22. A. Schont and E. Freire, *Biochemistry*, 1989, **28**.
23. L. Mandolini, *Advances in Physical Organic Chemistry APL*, 1987, **22**, 1.
24. M. D. Camara-Campos Amaya, Hunter Christopher A., Turega Simon, *Journal of the American Chemical Society*, 2009, **131**, 18518-18524.
25. S. L. Cockroft and C. A. Hunter, *Chemical Society Reviews*, 2007, **36**, 172-188.
26. R. Behrend, E. Meyer and F. Rusche, *Justus Liebigs Annalen der Chemie*, 1905, **339**, 1-37.
27. W. A. Freeman, W. L. Mock and N. Y. Shih, *Journal of the American Chemical Society*, 1981, **103**, 7367-7368.
28. L. Jae, S. Wook Samal, N. Selvapalam, H.-J. Kim and K. Kim, in *Accounts of Chemical Research*, American Chemical Society, 2003, vol. 36, pp. 621-630.
29. J. Kim, I.-S. Jung, S.-Y. Kim, E. Lee, J.-K. Kang, S. Sakamoto, K. Yamaguchi and K. Kim, *Journal of the American Chemical Society*, 2000, **122**, 540-541.
30. M. V. Rekharsky and Y. Inoue, *Chemical reviews*, 1998, **98**, 1875-1918.
31. W. L. Mock and N. Y. Shih, *The Journal of Organic Chemistry*, 1986, **51**, 4440-4446.
32. W. Mock, in *Supramolecular Chemistry II — Host Design and Molecular Recognition*, ed. E. Weber, Springer Berlin Heidelberg, 1995, vol. 175, pp. 1-24.
33. J. Lagona, P. Mukhopadhyay, S. Chakrabarti and L. Isaacs, *Angewandte Chemie*, 2005, **44**, 4844-4870.
34. J. h. Hee-Joon Kim, Woo Sung Jeon, Eunsung Lee, Jaheon Kim, Shigeru Sakamoto, Kentaro Yamaguchi, Kimoon Kim in *Angew. Chem. Int. Ed.*, 2001, vol. 40, pp. 1526-1529.

35. U. Rauwald, F. Biedermann, S. Deroo, C. V. Robinson and O. A. Scherman, *The Journal of Physical Chemistry B*, 2010, **114**, 8606-8615.
36. W. S. Jeon, H.-J. Kim, C. Lee and K. Kim, *Chemical communications*, 2002, 1828-1829.
37. S. M. Moghimi, A. C. Hunter and J. C. Murray, *Pharmacological reviews*, 2001, **53**, 283-318.
38. H. Maeda, J. Wu, T. Sawa, Y. Matsumura and K. Hori, *Journal of controlled release*, 2000, **65**, 271-284.
39. S.-D. Li and L. Huang, *Molecular pharmaceuticals*, 2008, **5**, 496-504.
40. M. C. Woodle and D. D. Lasic, *Biochimica et Biophysica Acta (BBA)-Reviews on Biomembranes*, 1992, **1113**, 171-199.
41. Y. Sadzuka, S. Hirotsu and S. Hirota, *Cancer letters*, 1998, **127**, 99-106.
42. F. Yuan, *Seminars in radiation oncology*, 1998.
43. J. N. Moreira, R. Gaspar and T. M. Allen, *Biochimica et Biophysica Acta (BBA)-Biomembranes*, 2001, **1515**, 167-176.
44. A. A. Gabizon, *Cancer investigation*, 2001, **19**, 424-436.
45. M. O'Brien, N. Wigler, M. Inbar, R. Rosso, E. Grischke, A. Santoro, R. Catane, D. Kieback, P. Tomczak and S. Ackland, *Annals of oncology*, 2004, **15**, 440-449.
46. M. R. Ranson, J. Carmichael, K. O'Byrne, S. Stewart, D. Smith and A. Howell, *Journal of Clinical Oncology*, 1997, **15**, 3185-3191.
47. K. M. Laginha, S. Verwoert, G. J. Charrois and T. M. Allen, *Clinical cancer research*, 2005, **11**, 6944-6949.
48. H. Wang, S. Wang, H. Su, K. J. Chen, A. L. Armijo, W. Y. Lin, Y. Wang, J. Sun, K. i. Kamei and J. Czernin, *Angewandte Chemie International Edition*, 2009, **48**, 4344-4348.
49. K. J. Chen, M. A. Garcia, H. Wang and H. R. Tseng, *Supramolecular nanoparticles for molecular diagnostics and therapeutics*, Wiley Online Library, 2012.
50. E. M. M. Del Valle, *Process Biochemistry*, 2004, **39**, 1033-1046.
51. H. Wang, K.-J. Chen, S. Wang, M. Ohashi, K.-i. Kamei, J. Sun, J. H. Ha, K. Liu and H.-R. Tseng, *Chemical communications*, 2010, **46**, 1851-1853.
52. C. Stoffelen and J. Huskens, *Chemical communications*, 2013, **49**, 6740-6742.
53. C. Stoffelen, J. Voskuhl, P. Jonkheijm and J. Huskens, *Angewandte Chemie*, 2014.
54. F. Tian, D. Jiao, F. Biedermann and O. A. Scherman, *Nature communications*, 2012, **3**, 1207.
55. M. Gaumet, A. Vargas, R. Gurny and F. Delie, *European journal of pharmaceuticals and biopharmaceutics : official journal of Arbeitsgemeinschaft fur Pharmazeutische Verfahrenstechnik e.V.*, 2008, **69**, 1-9.
56. S. K. Banerjee, B. D. Gupta and K. Singh, *Journal of the Chemical Society, Chemical Communications*, 1982, 815-816.
57. A. Gonzalez-Campo, M. Brasch, D. A. Uhlenheuer, A. Gomez-Casado, L. Yang, L. Brunsveld, J. Huskens and P. Jonkheijm, *Langmuir : the ACS journal of surfaces and colloids*, 2012, **28**, 16364-16371.